CHARACTERIZATION OF MOLECULAR INTERACTIONS AND ORGANIZATION IN SOLUTION AND INTERFACIAL SYSTEMS

By

Christine Ella Hay

A DISSERTATION

Submitted to
Michigan State University
in partial fulfillment of the requirements
for the degree of

Chemistry – Doctor of Philosophy

2014

ABSTRACT

CHARACTERIZATION OF MOLECULAR INTERACTIONS AND ORGANIZATION IN SOLUTION AND INTERFACIAL SYSTEMS

By

Christine Ella Hay

Liquid solutions and liquid-liquid interfaces are the media for numerous chemical reactions, where the local environments are conducive to interactions and exchanges. As a means of broadening our understanding of the molecular organization in liquid solutions and in proximity to phase boundaries, we report on the rotational diffusion dynamics of probe molecules in increasingly complex systems. Neat liquids represent the simplest systems interrogated. In our first study, we measure the induced orientational anisotropy function, R(t), using time-correlated single photon counting of two chromophores, resorufin and 6-(N-(7-nitrobenz-2-oxa-1,3-diazol-4-yl)amino)hexanoic acid (NBDHA) in water and in N-octyl-2-pyrrolidone (NOP). Our data show distinctly different anisotropy decays in aqueous solution compared to NOP solutions, and taken in the context of the Chuang and Eisenthal model, this indicates a change in effective rotor shape swept out by the solute's rotation. The similarity in the behavior of the two different chromophores in these solvent systems points to solvent-solvent interactions and local organization as the dominant factors in mediating motional dynamics.

By adding varying concentrations of electrolyte to aqueous and NOP systems, the rotational diffusion dynamics of the anionic chromophore, resorufin, are altered as a result of interaction with electrolyte cations. In aqueous solutions containing lithium perchlorate (LiClO₄), resorufin exhibits a single exponential anisotropy decay as was the case in pure water, however, reorientation times are dependent on electrolyte concentration. In contrast to the observed behavior of resorufin in pure NOP, where bi-exponential decay occurs, we observe a

single exponential anisotropy decay for resorufin in NOP with the addition of non-aqueous electrolyte. For resorufin in NOP, the reorientation time constant increases with increasing electrolyte concentration, consistent with formation of a complex between the resorufin anion and the electrolyte cation.

Elucidating the local organization near phase boundaries compared to bulk solutions represents a more complex problem to interrogate. We use a TCSPC confocal imaging instrument to obtain depth-resolved fluorescence lifetime and anisotropy decay data for lissamine rhodamine B sulfonyl chloride (LRSC) in NOP saturated with water and in ethylene glycol (EG) supported on a glass surface. The fluorescence anisotropy data of LRSC in NOP and EG as a function of distance from NOP|glass and EG|glass interfaces reveal a gradient spanning tens of micrometers from the NOP|glass interface into the NOP phase, and no corresponding gradient in EG. From these data, we assert there is a compositional heterogeneity in the form of water nano-droplets in the NOP phase, where water molecules solvate LRSC. NOP is miscible with small amounts of water allowing for the presence of water inclusions in solution, while phase separation occurs for sufficiently high water concentrations.

By forming a liquid-liquid interface composed of water and NOP supported on glass, we observe both compositional and dielectric gradients. We report on spatially resolved fluorescence lifetime and anisotropy decay time constant data of LRSC in the NOP phase near the liquid-liquid (NOP|water) interface and the liquid-solid (NOP|glass) interface. These data reveal a micron-scale position-dependent molecular environment characterized by an anisotropy decay gradient as a function of distance from the NOP|glass interface. In addition, the presence of a fluorescence lifetime gradient normal to the NOP|water interface indicates the existence of a gradient in the concentration of water nano-droplets.

ACKNOWLEDGMENTS

This dissertation is the culmination of work that could not have been completed without the contributions of others. I want to take this opportunity to thank those involved in my graduate career. First and foremost, I would like to thank my research advisor, Dr. Gary Blanchard, for his guidance, support, generosity, and optimism. I would also like to thank our collaborator, Dr. Frank Marken, of the University of Bath, UK for his insight and suggestions. I want to express gratitude to Dr. Dana Spence, Dr. Greg Swain, and Dr. David Weliky for serving on my dissertation advisory committee.

My fellow Blanchard group members have been an essential part of my graduate studies and research. I would like to thank the following former and current Blanchard research group members for their advice, support, and friendship: Dr. Benjamin Oberts, Dr. Monika (Domińska) Ngowe, Dr. Heather Pillman, Dr. Margaretta (Dimos) Koster, Dr. Douglas Gornowich, Dr. Iwan Setiawan, Chen Qiu, Fredy Pratama, Stephen Baumler, Xiaoran Zhang, and Hannah Mize.

Finally, I would like to express thanks to my friends in the MSU Chemistry Department and the MSU Forensic Chemistry Program, as well as my Master's research advisor, Dr. Ruth Waddell Smith for their support during my time at MSU. I would like to give a special thanks to my family for their encouragement, love, and support.

TABLE OF CONTENTS

LIST OF TABLES	vii
LIST OF FIGURES	viii
Chapter 1	1
Introduction	1
1.1 Significance and Research Objective	1
1.2 Literature Review	
REFERENCES	
Chapter 2	
Solvent-Dependent Changes in Molecular Reorientation Dynamics: The Role of S	olvent-Solvent
Interactions	
2.1 Introduction	21
2.2 Experimental Methods	24
2.3 Results and Discussion	27
2.4 Conclusions	43
REFERENCES	44
Chapter 3	48
The Effects of Electrolyte Concentration on the Rotational Dynamics of Resorufin	48
3.1 Introduction	48
3.2 Experimental Methods	53
3.3 Results and Discussion	
3.4 Conclusions	67
REFERENCES	
Chapter 4	72
Detection and Characterization of a Liquid Solid Interfacial Compositional Gradie	
Nano-Droplets in Wet N-Octyl-2-Pyrrolidone	
4.1 Introduction.	
4.2 Experimental Methods	
4.3 Results and Discussion	
4.4 Conclusions	
REFERENCES	
Chapter 5	103
Characterization of Liquid Liquid Solid Multi-Interfacial Compositional Gradients	
5.1 Introduction	
5.2 Experimental Methods	
5.3 Results and Discussion	
5.4 Conclusions	
REFERENCES	120

Chapter 6	
Conclusions	
6.1 Conclusions	
6.2 Future Directions	126
REFERENCES	

LIST OF TABLES

Table 2.1	Calculated changes in permanent dipole moment, $\Delta\mu$, upon excitation for the chromophores resorufin and NBDHA in solvents water and NOP
Table 2.2	Comparison of reorientation dynamics of resorufin ⁴⁸ and NBDHA ⁴⁵ in selected solvents
Table 2.3	Anisotropy decay time constants, τ_{OR} , and Cartesian components of the average rotational diffusion constants, D, for resorufin and NBDHA in water and in NOP 38
Table 3.1	Reorientation times, τ_{OR} , of resorufin in neat NOP and NOP with various concentrations of TBAB or TOAB electrolytes
Table 3.2	Reorientation times, τ_{OR} , of resorufin in water and various concentrations of LiClO ₄ (aq)
Table 4.1	Estimated number of water molecules surrounding LRSC (model prediction for number of waters, <i>n</i>). ^a
Table 5.1	Fluorescence lifetime, τ_{fl} , (ps) of LRSC as a function of depth into the NOP phase of a NOP water system and distance from the NOP water interface
Table 5.2	Fluorescence anisotropy decay time constants, τ_{OR} , (ps) of LRSC as a function of depth into the NOP phase of a NOP water system and distance from the NOP water interface

LIST OF FIGURES

Figure 1.1	Structure of N-octyl-2-pyrrolidone (NOP)
Figure 1.2	Time-resolved fluorescence lifetime decay for resorufin in aqueous solution. The best fit line (red) is a one-component exponential decay function
Figure 1.3	(a) Parallel (black) and perpendicular (red) emission transients and (b) orientational anisotropy function, R(t), for resorufin in aqueous solution. The best fit line (red) is a one-component exponential decay function.
Figure 2.1	Structures of (a) resorufin sodium salt and (b) NBD hexanoic acid (NBDHA) shown with Cartesian <i>x</i> and <i>y</i> axes for clarity
Figure 2.2	Time-correlated single photon counting (TCSPC) instrument
Figure 2.3	Normalized absorption and emission spectra of (a) NBDHA in water and (b) NBDHA in NOP
Figure 2.4	Normalized absorption and emission spectra of (a) resorufin in water and (b) resorufin in NOP
Figure 2.5	(a) Orientational anisotropy function, R(t), plotted as a function of time for resorufin in water. (b) R(t) as a function of time for NBDHA in water. The data are fitted to single exponential decays.
Figure 2.6	(a) Orientational anisotropy function, R(t), plotted as a function of time for resorufin in NOP. (b) R(t) as a function of time for NBDHA in NOP. The data are fitted to two-component exponential decays.
Figure 2.7	Three-dimensional shape representing the volume swept out when a long-axis polarized chromophore (a) rotates about the <i>x</i> -axis as a prolate rotor and (b) rotates about the <i>z</i> -axis as an oblate rotor
Figure 3.1	Structures of non-aqueous electrolytes, (a) tetrabutylammonium bromide (TBAB) and (b) tetraoctylammonium bromide (TOAB), with hydrodynamic volumes of 299 ų and 571 ų, respectively
Figure 3.2	Illustration of the resorufin anion reorienting as an oblate rotor with diffusion primarily about the <i>z</i> -axis in neat NOP and sweeping out a volume representative of a prolate rotor after formation of a complex with a tetrabutyl- or tetraoctylammonium cation.
Figure 3.3	Reorientation time of the reorienting moiety as a function of electrolyte concentration (log_{10} scale) for resorufin in TBAB/NOP (filled circles) and TOAB/NOP (open circles). Error bars represent \pm 1 standard deviation

Figure 3.4	Normalized (a) absorption and (b) emission spectra of resorufin in neat NOP (black), 10^{-3} M TOAB (red), 10^{-2} M TOAB (blue), and 10^{-1} M TOAB (green)
Figure 3.5	Reorientation time as a function of electrolyte concentration (log_{10} scale) for resorufin in aqueous LiClO ₄ . Errors bars represent \pm 1 standard deviation 64
Figure 3.6	Normalized (a) absorption and (b) emission spectra of resorufin in water (black), 5×10^{-3} M LiClO ₄ (red), 10^{-2} M LiClO ₄ (blue), 5×10^{-2} M LiClO ₄ (green), and 10^{-1} M LiClO ₄ (orange).
Figure 4.1	Structures of (a) lissamine rhodamine B sulfonyl chloride (LRSC) and (b) N-octyl-2-pyrrolidone (NOP)
Figure 4.2	Time-resolved fluorescence lifetime and anisotropy imaging instrument with time-correlated single photon counting (TCSPC) detection
Figure 4.3	Schematic of sample and optical excitation/collection configuration for NOP glass and EG glass interfaces. (NOP glass interface shown.)
Figure 4.4	Dependence of LRSC in NOP fluorescence lifetime (\bullet) and anisotropy decay time constant (\circ) on distance from the glass interface. The line drawn through the fluorescence lifetime data is intended as a guide to the eye. The glass support was cleaned with piranha solution and rinsed with water prior to use. Refer to Fig. 4.3 for the experimental configuration and the x , y , z coordinate designation
Figure 4.5	Dependence of LRSC in NOP fluorescence lifetime (\bullet) and anisotropy decay time constant (\circ) on distance from the glass interface. The line drawn through the fluorescence lifetime data is intended as a guide to the eye. The glass support was cleaned using UV-generated ozone and rinsed with ethanol prior to use. Refer to Fig. 4.3 for the experimental configuration and the x , y , z coordinate designation
Figure 4.6	Dependence of LRSC in EG fluorescence lifetime (\bullet) and anisotropy decay time constant (\circ) on distance from the glass interface. The line drawn through the fluorescence lifetime data (solid) and the anisotropy decay data (dashed) are intended as guides to the eye. The glass support was cleaned using piranha solution and rinsed with water prior to use. Refer to Fig. 4.3 for the experimental configuration and the x y , z coordinate designation.
Figure 4.7	(a) Calculated number of water molecules in the immediate proximity of LRSC as a function of distance from the NOP glass interface, for the interface cleaned with piranha solution and water (●) and cleaned with ethanol and UV-generated ozone (○). (b) Calculated diameters of the reorienting entities containing the chromophore and the number of water molecules indicated in (a), as a function of distance from the NOP glass interface
Figure 4.8	Normailzed absorption spectra of LRSC in water (black), LRSC in dry NOP (red), LRSC in NOP after equilibration with water (blue), and LRSC in NOP after extraction from water (green).

Figure 4.9	Dynamic light scattering (DLS) data showing the size distribution of water nano-droplets present in wet NOP after exposure to water (•) and dry NOP (o), showing the absence of species in the same size range as the water nano-droplets. For all DLS measurements no chromophore was present
Figure 5.1	Schematic of sample and optical excitation/collection configuration for NOP water glass interface
Figure 5.2	Time-resolved images of partitioning of LRSC initially deposited into the aqueous phase (bottom) and migrating into the NOP phase (top). In each image, the cuvette on left contains LRSC and the cuvette on the right is NOP water with no chromophore to demonstrate the existence of the phase separation
Figure 5.3	(a) Reorientation time and (b) calculated number of water molecules as a function of distance from the NOP $ $ glass interface. Refer to Fig. 5.1 for the experimental configuration and the x , y , z coordinate designation
Figure 5.4	(a) Reorientation time and (b) calculated number of water molecules as a function of distance from the NOP water interface. Refer to Fig. 5.1 for the experimental configuration and the x , y , z coordinate designation
Figure 5.5	(a) Fluorescence lifetime as a function of distance from the NOP glass interface for three different distances from the water interface. (b) Fluorescence lifetime as a function of distance from the NOP water interface for six different distances from the NOP glass interface. Experimental error bars representing the standard deviation are shown for each data point. Refer to Fig. 5.1 for the experimental configuration and the x , y , z coordinate designation
Figure 5.6	(a) Dielectric constant as a function of distance from the NOP glass interface for three different distances from the water interface. (b) Dielectric constant as a function of distance from the NOP water interface for six different distances from the NOP glass interface. Refer to Fig. 5.1 for the experimental configuration and the <i>x</i> , <i>y</i> , <i>z</i> coordinate designation

Chapter 1

Introduction

1.1 Significance and Research Objective

The formation of liquid interfaces dates back to the origins of life on Earth and continues to impact many aspects of modern life. Early liquid-liquid interfaces were the site of photochemical reactions allowing light harvesting to take place in primitive cells¹ and are still incorporated into energy conversion devices today, while liquid-solid interfaces, which are also ubiquitous in nature, are utilized in the making sensors and microscale devices.² Biological cell membranes, which have fluid properties similar to a liquid-liquid interface and surfaces that behave more akin to a liquid-solid interface, represent a well-studied interfacial system and function as the site of many chemical reactions necessary for cell function including a majority of energy conversion processes in living organisms.³ Liquid-liquid interfaces can take on many structural forms depending on the physical properties at work. For example, partially miscible and immiscible liquids can form emulsions or colloidal suspensions of structured liquids that are utilized in industrial products, such as detergents, paints, and cosmetics. Liquid interfaces including liquid-air, liquid-liquid, and liquid-solid are present in both simple and complex systems and play a vital role in many chemical processes, such as chemical separations, phase transfer catalysis, drug delivery, and charge transfer at electrode surfaces.

From a fundamental perspective, a liquid interface can be used to study the unique properties of interfaces that allow them to function as reaction centers.⁴⁻⁷ Central to the function of an interface is the structure and dynamics occurring in the interfacial region. Macroscopic properties of interfaces, such as surface tension at liquid-solid interfaces, have been widely studied, however, the microscopic properties of interfaces have been more difficult to ascertain.⁸

In the study of an interfacial system, knowledge about both sides of the system is important. For a liquid interface, this knowledge begins with understanding interactions and dynamics within the liquid phase.

Fluorescence spectroscopy is sensitive to microenvironments in liquid solutions and, therefore, is particularly useful for the study of solvation phenomena. Rotational diffusion measurements made by time-resolved fluorescence spectroscopic techniques provide a means of measuring the dynamic motion of a probe molecule and elucidating properties of the local organization in the solution. Through the use of optical spectroscopic techniques, a molecular scale understanding of solution phase, solute-solvent and solvent-solvent, interactions is sought to increase our knowledge of the liquid phase as a means to have greater control over chemical processes, such as heterogeneous catalysis and ion transfer reactions.

The objective of the research presented here is to gain a better fundamental understanding of the molecular organization in solution phase media and in interfacial systems. The goals of this research project are to use time-resolved fluorescence spectroscopy to study the local environment of probe molecules in neat solutions, in solutions containing additives in the form of electrolytes, and finally in proximity to liquid-solid and liquid-liquid interfaces. The liquid-liquid and liquid-solid phase boundaries, as well as the three phase boundary formed between the two interfaces are of particular interest for photochemical and photoelectrochemical reactions involving ion transfer.

The solvent systems used throughout this research are water and N-octyl-2-pyrrolidone (NOP). Both water and NOP exhibit unique solvation properties and form a liquid-liquid interface at room temperature. Three fluorescent probe molecules are used as solutes in these studies; resorufin sodium salt, 6-[N-(7-nitrobenz-2-oxa-1,3-diazol-4-yl)amino] hexanoic acid

(NBDHA), and lissamine rhodamine B sulfonyl chloride (LRSC). More detailed descriptions of the probe molecules are presented in the subsequent chapters, while the remainder of this chapter focuses on relevant research highlighting studies on solvation and liquid interfaces.

1.2 Literature Review

Physical properties of liquids have been studied for centuries and advancements in measurement techniques have allowed researchers to delve in progressively greater depth into the complexity of liquid solutions. Both experimental and theoretical techniques have enhanced the field by showing how nano- and microscale interactions affect macroscale properties. This review focuses on optical spectroscopic techniques used for the study of intermolecular interactions as a means to understand solvation phenomena in liquid solutions and in interfacial systems. Prior to a review of significant research, a brief introduction to the liquid phase is necessary.

The liquid phase is governed by interactions between its components. In a neat liquid, the interactions are homogeneous in nature, whereas in solutions composed of a solute and a solvent, where the solvent is the major component, interactions occur between dissimilar molecules. In both cases intermolecular interactions between solvent-solvent and/or solute-solvent play a deterministic role in the physical properties of the liquid. The theory describing the behavior of liquids lies between kinetic gas theory and solid state physics and is not as well understood as either of these phases. 10

Macroscopic descriptions of solvents are based on physical properties including boiling point, density, and surface tension among others, however, the individual, interacting solvent molecules do not behave as a macroscopic continuum. Molecular scale solvent properties, such as dipole moment and electronic polarizability provide a better description of the range of

processes operating at the microscopic level.¹⁰ Microscale solvent properties along with the extent of solvent-solvent interactions lead to the distinctive organization found in solvents like water. Liquid water forms dynamic three-dimensional hydrogen bonded networks, whereas nonpolar solvents, such as hydrocarbons, are less structured due to their relatively weak solvent-solvent interactions.¹¹ The nature of the solvent-solvent and solute-solvent interactions is important for a molecular scale understanding of the solvation of solutes. The molecular interactions occurring in solutions can be divided into two broad classes; specific interactions, where interactions occur between specific sites of interacting molecules, such as hydrogen bonding, and non-specific interactions, which include van der Waals, as well as dipole-dipole interactions.⁹ The interactions between dissimilar molecules, also referred to as cohesion forces, originate from Coulombic forces between the nuclei and electrons of adjacent atoms and are either attractive or repulsive in nature.¹² It is these interactions that create the framework that controls a solute's local environment in solution, while also affecting adsorption and/or other structural arrangement at phase boundaries.

Molecular rotation in liquid solutions provides a means for determining the extent of intermolecular interaction. In order to gauge the dependence of rotational motion on intermolecular interaction, time-resolved fluorescence spectroscopy is used to measure the rotational diffusion dynamics of fluorescent probe molecules. The time-scale of fluorescence is on the order of nanoseconds (10⁻⁹ s), which is sufficient time for interaction with other molecules in solution. Molecular interaction during the excited state lifetime of a fluorescing species leads to such phenomena as quenching 14-17 and solvent relaxation, while the relatively long duration of the excited state lifetime of the probe molecule allows for measurement of rotational diffusion via time-resolved measurements. ²¹

Our understanding of rotational diffusion in liquid solutions is based on hydrodynamic theory and the foundation of this theory is the Debye-Stokes-Einstein (DSE) model.²² The DSE model (Eq. 1.1) relates the orientational relaxation time, τ_{OR} , of spherical rotors in continuum solvents to the viscosity of the medium (η), the thermal energy of the system (k_BT), and hydrodynamic volume of a rotating probe (V).²²

$$\tau_{OR} = \frac{\eta V}{k_B T} \tag{1.1}$$

Researchers have used this theory to describe rotational diffusion in systems ranging from neat liquids to biological cell mimics. There are limitations to the DSE model and additional modifications have been included to account for frictional interactions and the ellipsoidal shape of non-spherical rotors.^{23,24} Deviations from the predictions of the DSE model can be exploited as indicators of strong solute-solvent interactions in the form of electrostatic interactions and/or hydrogen bonding.²⁵⁻²⁷ Frictional interactions between the solvent and the solute described in terms of "slip" and "stick" boundary conditions define the limits within the DSE model and are related to the strength of interaction or drag experienced by the rotating solute. The slip limit, proposed Hu and Zwanzig, ²³ implies a solute rotates without frictional interactions with solvent molecules and the torque experienced by the solute is only that required to displace the solvent molecules within the volume swept out by the rotating solute.²⁸ Alternately, the stick limit implies greater frictional interaction between the solute and the solvent molecules making up the solvation shell, which causes drag on the solute, slowing the rotational motion.²⁸ Most studies cite good agreement with hydrodynamic theory when reorientation times fall between the slip and stick boundary conditions.

Two classes of probe molecules are utilized for rotational diffusion studies depending on the system of study and information sought: polar (including charged) molecules and nonpolar molecules. Nonpolar probes are often used to test hydrodynamic theories based on the relationship between solute rotation and physical properties of the system. ^{27,29-36} Interactions between nonpolar solutes and nonpolar solvents are typically non-specific in nature, and solutes reorient without large contributions from frictional interactions typically associated with specific intermolecular interactions. Systems interrogated by polar probe molecules, where specific interactions are common, often fail to show good agreement with hydrodynamic theory. The rotational diffusion of polar probes has been assessed in various media, where ionic association, hydrogen bonding, as well as structural features of probe molecules were reported to play a role in dynamic solvation. ³⁷⁻⁴¹

Rotational diffusion dynamics are known to depend on the size of the solute (hydrodynamic volume) relative to the size of the solvent, the shape of the solute, and the viscosity of the solvent. Solute size effects become apparent as solute size approaches the size of the solvent at which point, macroscopic diffusion theories break down, and a molecular scale hydrodynamic theory is necessary to describe solute diffusion. Jiang et al., studied the effect of solvent length on the rotational diffusion of a nonpolar probe, perylene, in a series of normal alkanes. Semi-quantitative agreement with the modified DSE model was achieved and a solvent chain length dependence was observed for the rotational diffusion of perylene. Solvent length was shown to affect the boundary condition, where reorientation times in solvent significantly smaller than perylene (n-alkanes: $C_5 - C_8$) was near the stick limit conditions, and reorientation times in solvents significantly larger than perylene (n-alkanes: C_9 , C_{10} , C_{12} , C_{16}) approached the slip limit. In this study, an increase in the solvent chain length to the approximate length of the solute molecule resulted in a change in boundary condition, which was attributed to a fundamental change in the solute-solvent interactions for longer chain length

alkanes compared to shorter chain length alkanes. Size effects of solutes relative to solvent will be addressed in chapter 2 in regards to the solvent, NOP.

Rotational diffusion dynamics of polar solutes in polar solvents have been shown to exhibit changes in boundary conditions as well as changes in the friction experienced by the solute due to the nature of the solvent. Dutt et al., studied four structurally similar polar probe molecules, cresyl violet, nile blue, nile red, and oxazine 720, in various solvents including amides, aprotic solvents, alcohols, polyalcohols, and water.²⁸ In amides and the aprotic solvent dimethyl sulfoxide (DMSO), reorientation of the probe molecules exhibits good agreement with the stick model of hydrodynamic theory. In *n*-alcohols, additional friction, denoted dielectric friction, ^{25,26,43-45} alters the reorientation as a result of the dielectric properties of the solvent, whereas, in polyalcohols, reorientation times lie between slip and stick boundary conditions. Reorientation times of the polar chromophores, cresyl violet, nile blue, and oxazine 720 in water showed good agreement with hydrodynamic theory and were reported to be affected the least by dielectric friction. The greater friction between the polar probe molecules and alcohols demonstrated increased strength of the solute-solvent interactions.

In forming the solvation structure, solvent-solvent interactions can also play a role in mediating local organization. This phenomenon is apparent in systems forming secondary structures, such as micelles, vesicles, and lipid bilayers. Studying local environments via rotational diffusion dynamics necessitates the incorporation of fluorescent probes into more complex systems to interrogate a specified region. Biological mimics exhibiting secondary structures are composed of amphiphilic molecules allowing for the interrogation of the nonpolar and polar regions separately. With the use of nonpolar probe molecules, studies have shown the internal structures of micelles and vesicles differ based on size, composition, and fluidity of the

system. Additionally nonpolar probes have been used to interrogate changes to the microviscosity of the aliphatic region of lipid vesicles upon perturbation. Probing polar regions has allowed for the determination of intermolecular interactions as a function of headgroup charge and interrogation of headgroup organization with different polar headgroup structure. Setiawan et al. interrogated the polar headgroup region of lipid bilayers dosed with varying concentrations of alcohol in order to assess the rotational dynamics and morphology of the bilayer. This study on lipid bilayers was accomplished using a confocal fluorescence lifetime and anisotropy imaging instrument, which allowed for scanning of surface structure of the lipid bilayer. In chapter 4, this instrument is utilized for measuring depth profiles adjacent to liquid phase boundaries.

The concept of solvent organization also relates to phase boundaries, where the ordering of molecules in the liquid occurs in a way similar to the formation of a lipid bilayer. This interfacial molecular ordering only persists for a few Angstroms into the bulk liquid.⁵⁴

Molecular dynamic simulations have been used to show the interfacial structure at liquid-liquid interfaces composed of immiscible and partially miscible liquids is molecularly sharp, with the partially miscible system of water and 1-hexanol forming a bilayer structure extending a few molecular lengths into the bulk.⁵⁵ An interfacial width on the order of 1 nm^{56,57} requires specialized measurement techniques in order to elucidate the solvation properties at liquid-liquid and liquid-solid interfaces. In addition to the spatial restrictions, there are inherent difficulties in differentiating interfacial from bulk phenomena at liquid-liquid interfaces. Molecular properties at the interface differ from those measured in the bulk liquid due to an asymmetry of surface forces that affects the structure and dynamics at the interface, however, many spectroscopic techniques cannot separate the signal from adsorbed species at the interface and the species

present in the bulk liquid.⁵⁸ Second order non-linear optical spectroscopic methods have been used previously to probe liquid-liquid interfaces including second harmonic generation (SHG),^{7,59-61} sum frequency generation (SFG),⁶²⁻⁶⁴ and total internal reflectance fluorescence (TIRF) spectroscopy.⁶⁵⁻⁶⁹ These techniques are utilized due to their surface specificity to within a few nanometers on either side of the interface.⁵⁸

Although interfacial regions are reported to only extend on the order of nm, there are phenomena that can be studied in the bulk adjacent to the interface. The Marken group utilized electrochemistry and photoelectrochemistry to monitor ion transfer in a two-phase flow system and at the liquid-liquid-solid interface, or three phase boundary, of a microdroplet. Three phase boundaries are unique in that coupled processes such as electron transfer from the organic phase to solid electrode and the anion transfer from the aqueous phase to the organic phase can be assessed using electrochemical techniques. MacDonald et al., formed a biphasic liquid-liquid flow system using NOP and aqueous electrolyte and were able to monitor redox reaction currents in the reaction zone at the three phase, organic aqueous electrolyte electrode, boundary. This study took advantage of the phase separation of water and NOP at room temperature.

The solvent systems of water and NOP used for the research presented in subsequent chapters were selected based on the success of the photoelectrochemical studies at three phase boundaries. NOP exhibits unique solvation properties and has been incorporated into a number of industrial formulations. Some important properties of NOP and are summarized here. NOP is a nonionic surfactant and is one of a series of N-alkyl-2-pyrrolidones which exhibit high surface activity in aqueous solutions. The structure of NOP (Fig. 1.1) contains a hydrophilic lactam functionality that is capable of hydrogen bonding and an alkyl chain contributing to the

hydrophobic character. N-alkyl-2-pyrrolidones, including NOP, are used in a variety of industrial processes and household products as non-toxic solvents (N-methyl) and wetting agents (N-hexyl thru N-dodecyl).⁷⁷ Binary temperature-composition phase diagrams show the water and NOP form two phases at room temperature and NOP has a lower consolute temperature (LCT) below 0 °C.⁷⁸ The solubility of NOP in water is 0.12% (v/v) (20 °C),⁷⁷ while no mutual solubility is reported.

Figure 1.1 Structure of N-octyl-2-pyrrolidone (NOP).

Mixed micelles form when NOP is in the presence of ionic surfactants, such as sodium dodecyl sulfate (SDS), however, due to the LCT, two phases form between NOP and aqueous solution prior to reaching a critical micelle concentration (CMC).⁷⁷ It is reported, pure NOP micelles do not form because the length of the alkyl chains in NOP is insufficient to drive formation of micelles, which requires aggregation of the amphiphile with the hydrophobic tails pointing inward to form a hydrophobic core.⁷⁹ The interaction between pyrrolidone headgroups typically dominates and the formation of dimers and/or inverse micelles is more likely to occur than traditional micelle formation. These unique properties make NOP a very interesting medium to study in order to uncover the intermolecular interactions of this solvent through incorporation of probe molecules and measurement of rotational diffusion dynamics.

In order to elucidate information on the organization and dynamics of fluorescent solutes in unique environments, we collect fluorescence lifetime and fluorescence anisotropy decay data using a time-resolved spectroscopic technique called time-correlated single photon counting

(TCSPC). Time-resolved measurements are made by using short pulses of light from a laser source to excite the fluorescent probe and then recording the emission intensity as a function of time. After excitation, the fluorescent probe emits photons, where the fluorescence lifetime is the average amount of time required to transition from the first excited singlet state (S_1) to the ground singlet state (S_0). The fluorescence intensity recorded after each excitation has a probability to emit within a given period of time.²¹ After many excitation and emission events a histogram builds up, which typically takes the form of an exponential decay (Fig 1.2). The principles of single-photon counting are based on the assumption that the probability distribution from detection of single photon emission built up after many excitation events is a representative sampling of the actual emission intensity versus time distribution of all photons.⁸⁰ Fluorescence lifetime is determined from the total emission intensity, whereas fluorescence anisotropy decay is calculated from the difference in intensity of two polarizations (parallel and perpendicular, with respect to the vertically polarized excitation polarization) divided by the total emission intensity. The lifetime decay in Fig. 1.2 is fit to a single exponential function defined by Eq. 1.2,

$$I(t) = I_0 \exp(-t/\tau_{fl})$$
 (1.2)

where I(t) is the intensity as a function of time, I_0 is the intensity at time zero, and τ_{fl} is the time constant of the fluorescence intensity decay. Fluorescence lifetime is recorded using magic angle conditions, where the sample is excited with vertically polarized excitation light and the emission polarizer set to the magic angle, 54.7° with respect to excitation polarization. Alternatively, the signal from emission transients collected at parallel and perpendicular polarizations with respect to the excitation light are combined ($\parallel +2 \perp$) to obtain the total fluorescence intensity.²¹ These two methods achieve equivalent results.

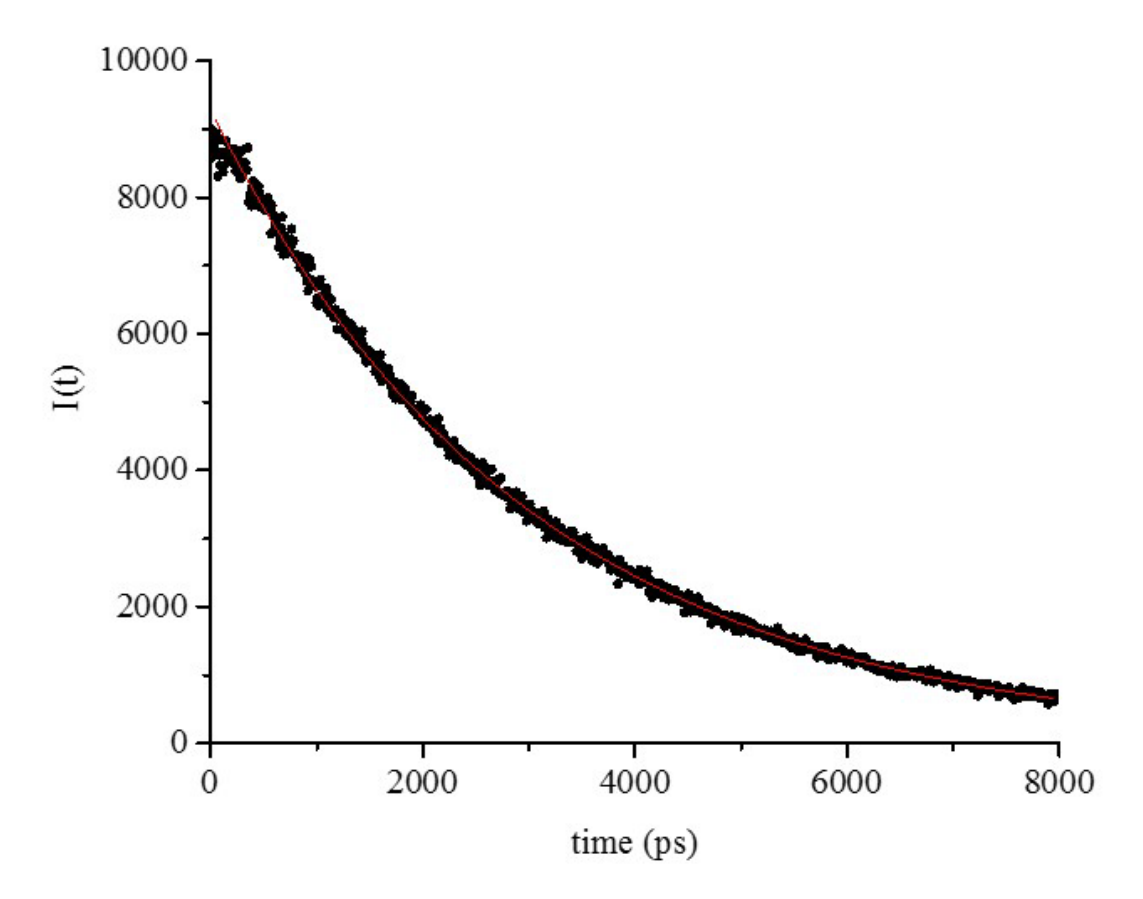


Figure 1.2 Time-resolved fluorescence lifetime decay for resorufin in aqueous solution. The best fit line (red) is a one-component exponential decay function.

An example of parallel and perpendicular emission transients is shown in Fig. 1.3a, where differences in the parallel and perpendicular counts are apparent at early times and the plots converge over time. This behavior is representative of the depolarization of the initial non-random population created by exciting with vertically polarized light into a random population with equal parallel and perpendicular counts at long times.⁸⁰ The orientational anisotropy function, R(t), is obtained from Eq. 1.3,

$$R(t) = \frac{I_{||}(t) - I_{\perp}(t)}{I_{||}(t) + 2I_{\perp}(t)}$$
(1.3)

where the intensity of fluorescence polarized parallel with respect to the vertically polarized excitation light is given by $I_{||}(t)$ and the fluorescence polarized perpendicular is given by $I_{\perp}(t)$.

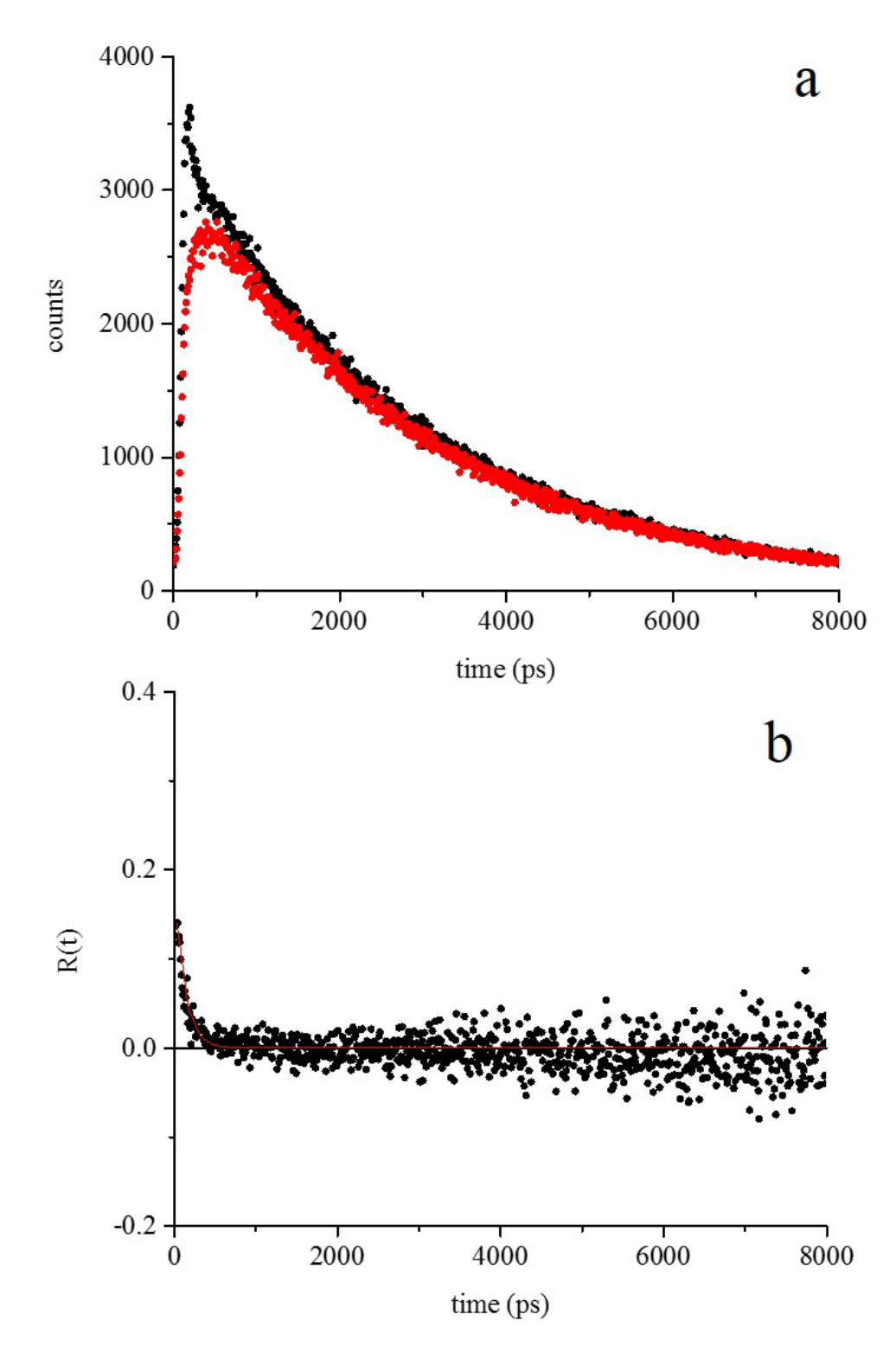


Figure 1.3 (a) Parallel (black) and perpendicular (red) emission transients and (b) orientational anisotropy function, R(t), for resorufin in aqueous solution. The best fit line (red) is a one-component exponential decay function.

The orientational anisotropy decay in Fig. 1.3b is fit to a single exponential function defined by Eq. 1.4,

$$R(t) = R_0 \exp(-t/\tau_{OR}) \tag{1.4}$$

where R(t) is the orientational anisotropy function, R_0 is the initial anisotropy, and τ_{OR} is the orientational relaxation time constant.

The work described in the subsequent chapters utilizes time-resolved fluorescence spectroscopy to collect fluorescence anisotropy decay and fluorescence lifetime data as a means of assessing the rotational diffusion dynamics of fluorescent probe molecules in various media. We use the molecular rotation of these probes as a tool to achieve the objective of understanding the structure and organization in solution phase media and in interfacial systems. In chapter 2, we elucidate solvent-solvent and solute-solvent interactions in aqueous and organic bulk media by measuring the rotational diffusion of structurally different probe molecules. In chapter 3, we study the effect of charged additives and the role of ion pairing on the rotational motion of probe molecules in aqueous electrolyte and NOP with added electrolyte. In chapter 4, we create a depth profile of fluorescence lifetime and reorientation time constants in a thin film as a function of distance from a liquid-solid interface and examine the composition of a colloidal suspension in the thin film. In chapter 5, we study the effect of a liquid-liquid (aqueous-NOP) interface formed normal to the liquid-solid interface on the droplet size and distribution in the colloidal suspension.

REFERENCES

REFERENCES

- 1. Liquid-Liquid Interfaces: Theory and Methods; Volkov, A. G.; Deamer, D. W., Eds.; CRC Press: Boca Raton, FL, 1996.
- 2. Nakaoka, S.; Surblys, D.; Yamaguchi, Y.; Kuroda, K.; Nakajima, T.; Fujimura, H. *Chemical Physics Letters* **2014**, *591*, 306.
- 3. Volkov, A. G.; Deamer, D. W.; Tanelian, D. L.; Markin, V. S. *Liquid Interfaces in Chemistry and Biology*; John Wiley & Sons, Inc.: New York, 1998.
- 4. Benjamin, I. Chemical Reviews **1996**, 96, 1449.
- 5. Benjamin, I. Chemical Physics Letters 2009, 469, 229.
- 6. Perera, J. M.; Stevens, G. W. Analytical and Bioanalytical Chemistry 2009, 395, 1019.
- 7. Fedoseeva, M.; Richert, S.; Vauthey, E. *Langmuir* **2012**, 28, 11291.
- 8. Interfacial Nanochemistry: Molecular Science and Engineering at Liquid-Liquid Interfaces; Watarai, H.; Teramae, N.; Sawada, T., Eds.; Kluwer Academic/Plenum Publishers: New York, 2005.
- 9. Dutt, G. B. ChemPhysChem 2005, 6, 413.
- 10. Reichardt, C.; Welton, T. Solute-Solvent Interactions. In *Solvents and Solvent Effects in Organic Chemistry*; Wiley-VCH Verlag GmbH & Co. KGaA, 2010; pp 7.
- 11. Reichardt, C.; Welton, T. Classification of Solvents. In *Solvents and Solvent Effects in Organic Chemistry*; Wiley-VCH Verlag GmbH & Co. KGaA, 2010; pp 65.
- 12. Intermolecular Forces: An Introduction to Modern Methods and Results; Huyskens, P. L.; Luck, W. A. P.; Zeegers-Huyskens, T., Eds.; Springer Berlin Heidelberg: Berlin, Heidelberg, 1991.
- 13. Ingle, J. D., Crouch, S.R. Spectrochemical Analysis; Prentice Hall: New Jersey, 1988.
- 14. Biwersi, J.; Tulk, B.; Verkman, A. S. Analytical Biochemistry 1994, 219, 139.
- 15. Morandeira, A.; Furstenberg, A.; Gumy, J. C.; Vauthey, E. *Journal of Physical Chemistry A* **2003**, *107*, 5375.
- 16. Morandeira, A.; Furstenberg, A.; Vauthey, E. *Journal of Physical Chemistry A* **2004**, *108*, 8190.
- 17. Montejano, H. A.; Gervaldo, M.; Bertolotti, S. G. Dyes and Pigments 2005, 64, 117.

- 18. Weber, G.; Lakowicz, J. R. Chemical Physics Letters 1973, 22, 419.
- 19. Vincent, M.; Gallay, J.; Demchenko, A. P. Journal of Physical Chemistry 1995, 99, 14931.
- 20. Toptygin, D.; Brand, L. Chemical Physics Letters 2000, 322, 496.
- 21. Lakowicz, J. R. *Principles of fluorescence spectroscopy*, 3rd ed.; Springer: New York, 2006.
- 22. Debye, P. *Polar Molecules* Chemical Catalog Co.: New York 1929.
- 23. Hu, C. M.; Zwanzig, R. Journal of Chemical Physics 1974, 60, 4354.
- 24. Perrin, F. Journal of Physics and Radium 1934, 5, 497.
- 25. Wiemers, K.; Kauffman, J. F. Journal of Physical Chemistry A 1999, 104, 451.
- 26. Dutt, G. B.; Srivatsavoy, V. J. P.; Sapre, A. V. Journal of Chemical Physics 1999, 110, 9623.
- 27. Dutt, G. B. *Journal of Chemical Physics* **2000**, *113*, 11154.
- 28. Dutt, G. B.; Doraiswamy, S.; Periasamy, N.; Venkataraman, B. *Journal of Chemical Physics* **1990**, *93*, 8498.
- 29. Ben-Amotz, D.; Scott, T. W. Journal of Chemical Physics 1987, 87, 3739.
- 30. Ben-Amotz, D.; Drake, J. M. Journal of Chemical Physics 1988, 89, 1019.
- 31. Jiang, Y.; Blanchard, G. J. Journal of Physical Chemistry 1994, 98, 6436.
- 32. Jas, G. S.; Wang, Y.; Pauls, S. W.; Johnson, C. K.; Kuczera, K. *Journal of Chemical Physics* **1997**, *107*, 8800.
- 33. Dutt, G. B.; Krishna, G. R. *Journal of Chemical Physics* **2000**, *112*, 4676.
- 34. Goldie, S. N.; Blanchard, G. J. Journal of Physical Chemistry A 2001, 105, 6785.
- 35. Inamdar, S. R.; Mannekutla, J. R.; Mulimani, B. G.; Savadatti, M. I. *Chemical Physics Letters* **2006**, *429*, 141.
- 36. Mize, H. E.; Blanchard, G. J. Journal of Physical Chemistry B 2013, 117, 16260.
- 37. Blanchard, G. J. Journal of Physical Chemistry 1991, 95, 5293.
- 38. Yu, J. W.; Berg, M. Chemical Physics Letters 1993, 208, 315.
- 39. Rasimas, J. P.; Blanchard, G. J. Journal of Physical Chemistry 1996, 100, 11526.
- 40. Dela Cruz, J. L.; Blanchard, G. J. Journal of Physical Chemistry A 2002, 106, 10718.

- 41. Esquivelzeta-Rabell, M.; Peon, J.; Cuevas, G. *Journal of Physical Chemistry B* **2009**, *113*, 8599.
- 42. Dutt, G. B.; Raman, S. Journal of Chemical Physics 2001, 114, 6702.
- 43. Madden, P.; Kivelson, D. Journal of Physical Chemistry 1982, 86, 4244.
- 44. Simon, J. D.; Thompson, P. A. Journal of Chemical Physics 1990, 92, 2891.
- 45. Balabai, N.; Sukharevsky, A.; Read, I.; Strazisar, B.; Kurnikova, M.; Hartman, R. S.; Coalson, R. D.; Waldeck, D. H. *Journal of Molecular Liquids* **1998**, *77*, 37.
- 46. Stevenson, S. A.; Blanchard, G. J. Journal of Physical Chemistry B 2006, 110, 13005.
- 47. Lapinski, M. M.; Blanchard, G. J. Chemistry and Physics of Lipids 2008, 153, 130.
- 48. Pillman, H. A.; Blanchard, G. J. Journal of Physical Chemistry B 2010, 114, 3840.
- 49. Pillman, H. A.; Blanchard, G. J. Journal of Physical Chemistry B 2011, 115, 3819.
- 50. Dela Cruz, J. L.; Blanchard, G. J. Journal of Physical Chemistry B 2003, 107, 7102.
- 51. Greenough, K. P.; Blanchard, G. J. Spectrochimica Acta Part A-Molecular and Biomolecular Spectroscopy **2009**, 71, 2050.
- 52. Setiawan, I.; Blanchard, G. J. Journal of Physical Chemistry B 2014, 118, 537.
- 53. Setiawan, I.; Blanchard, G. J. Journal of Physical Chemistry B 2014, 118, 3085.
- 54. Ding, F.; Hu, Z.; Zhong, Q.; Manfred, K.; Gattass, R. R.; Brindza, M. R.; Fourkas, J. T.; Walker, R. A.; Weeks, J. D. *Journal of Physical Chemistry C* **2010**, *114*, 17651.
- 55. Wang, H. B.; Carlson, E.; Henderson, D.; Rowley, R. L. *Molecular Simulation* **2003**, 29, 777.
- 56. Carpenter, I. L.; Hehre, W. J. Journal of Physical Chemistry 1990, 94, 531.
- 57. Steel, W. H.; Walker, R. A. Nature 2003, 424, 296.
- 58. Brevet, P. F.; Girault, H. H. Second Harmonic Generation at Liquid/Liquid Interfaces. In *Liquid-Liquid Interfaces: Theory and Methods*; Volkov, A. G., Deamer, D. W., Eds.; CRC Press: Boca Raton, FL, 1996.
- 59. Grubb, S. G.; Kim, M. W.; Rasing, T.; Shen, Y. R. *Langmuir* **1988**, 4, 452.
- 60. Uchida, T.; Yamaguchi, A.; Ina, T.; Teramae, N. *Journal of Physical Chemistry B* **2000**, 104, 12091.

- 61. Yamaguchi, A.; Uchidai, T.; Inai, T.; Nochi, K.; Teramae, N. Bunseki Kagaku 2006, 55, 457.
- 62. Messmer, M. C.; Conboy, J. C.; Richmond, G. L. *Journal of the American Chemical Society* **1995**, *117*, 8039.
- 63. Brown, M. G.; Walker, D. S.; Raymond, E. A.; Richmond, G. L. *Journal of Physical Chemistry B* **2003**, *107*, 237.
- 64. Walker, D. S.; Richmond, G. L. Journal of Physical Chemistry C 2008, 112, 201.
- 65. Wirth, M. J.; Burbage, J. D. Journal of Physical Chemistry 1992, 96, 9022.
- 66. Sassaman, J. L.; Wirth, M. J. Colloids and Surfaces A-Physicochemical and Engineering Aspects **1994**, 93, 49.
- 67. Ishizaka, S.; Habuchi, S.; Kim, H. B.; Kitamura, N. Analytical Chemistry 1999, 71, 3382.
- 68. Ishizaka, S.; Nakatani, K.; Habuchi, S.; Kitamura, N. Analytical Chemistry 1999, 71, 419.
- 69. Ishizaka, S.; Kim, H. B.; Kitamura, N. Analytical Chemistry 2001, 73, 2421.
- 70. Collins, A. M.; Zhang, X. H.; Scragg, J. J.; Blanchard, G. J.; Marken, F. *ChemPhysChem* **2010**, *11*, 2862.
- 71. Collins, A. M.; Blanchard, G. J.; Hawkett, J.; Collison, D.; Marken, F. *Langmuir* **2011**, *27*, 6471.
- 72. Collins, A. M.; Blanchard, G. J.; Marken, F. Electroanalysis 2012, 24, 246.
- 73. MacDonald, S. M.; Watkins, J. D.; Gu, Y.; Yunus, K.; Fisher, A. C.; Shul, G.; Opallo, M.; Marken, F. *Electrochemistry Communications* **2007**, *9*, 2105.
- 74. MacDonald, S. M.; Watkins, J. D.; Bull, S. D.; Davies, I. R.; Gu, Y.; Yunus, K.; Fisher, A. C.; Page, P. C. B.; Chan, Y.; Elliott, C.; Marken, F. *Journal of Physical Organic Chemistry* **2009**, 22, 52.
- 75. Marken, F.; Watkins, J. D.; Collins, A. M. *Physical Chemistry Chemical Physics* **2011**, *13*, 10036.
- 76. Rosen, M. J.; Zhen, H. Z.; Gu, B.; Murphy, D. S. *Langmuir* **1988**, *4*, 1273.
- 77. Login, R. B. Journal of the American Oil Chemists Society 1995, 72, 759.
- 78. Lou, A. J.; Pethica, B. A.; Somasundaran, P.; Yu, X. *Journal of Colloid and Interface Science* **2002**, *256*, 190.
- 79. Login, R. B.; Chaudhuri, R. K.; Haldar, R. K.; Hashem, M. M.; Helioff, M. W.; Tracy, D. J. Surface active lactams US Patent No. 5093031, 1992.

80. O'Connor, D. V.; Phillips, D. *Time-Correlated Single Photon Counting*; Academic Press, Inc.: Orlando, FL, 1984.

Chapter 2

Solvent-Dependent Changes in Molecular Reorientation Dynamics: The Role of Solvent-Solvent Interactions

2.1 Introduction

The interaction between dissimilar molecules is central to a wide range of chemical phenomena. In the solution phase, such interactions are termed 'solvation' phenomena, which mediate processes, such as chemical separations, heterogeneous and homogeneous catalytic reactions, and organic syntheses. Despite the centrally important role of solvation to a variety of chemical phenomena, there remains to be developed a comprehensive and predictive model of solute-solvent interactions that takes into account the molecular structure and functionality of both the solute and the solvent. To this point, there have been many studies of solvation, with a host of inertial and dielectric phenomena being shown to contribute to solvent accommodation of solute(s).¹⁻¹² Longer timescale interactions, typically evaluated using solute rotational diffusion measurements have shown that van der Waals, dipole-dipole, and hydrogen-bonding interactions can all contribute to the observed dynamics. In most cases, specific interactions between solute and solvent are found to play important roles in mediating solute dynamics, but garnering solute-independent information on the way solvents interact with like molecules has proven to be elusive.

The interactions between solute and solvent are thought to depend on solvent molecular structure and organization, and the rotational diffusion dynamics of the solute have been used as a sensitive means of evaluating such interactions.^{5,13-33} For many systems, reorientation dynamics can be treated in the context of the modified Debye-Stokes-Einstein (DSE) equation,³⁴⁻³⁶ where solute motion, characterized by a reorientation time, is related to its hydrodynamic volume, the bulk viscosity of the solvent, and the temperature of the system. The initial form of

this model is predicated on the assumption of a spherical solute rotating in a continuum solvent, and the predicted form of the anisotropy decay for such a system is a single exponential decay.³⁴ This model has been modified to include solvent shape and the frictional contribution to solutesolvent interactions in an effort to include ellipsoidal solutes and to provide better agreement between experiment and theory. 35,36 This model, with modifications, first discussed in chapter 1 (Eq. 1.1) has worked well to provide a qualitative picture of solute-solvent interactions for a variety of systems, but there are notable instances where the anisotropy decay is characterized by more than one exponential decay, ^{17,20,21} and under such circumstances a more comprehensive model of molecular reorientation is required. The theoretical treatment derived by Chuang and Eisenthal allows for the characterization of the anisotropy decay function by up to five exponentials, and these decays are related to the Cartesian components of the rotational diffusion constant, D.³⁷ Relating variations in D and, in particular, the relative values of D_x , D_y , and D_z , provides insight into the shape of the volume swept out by the reorienting solute. The shape of this volume is related to both the shape of the solute molecule and any constraints imposed by the surrounding solvent system.

In this work, we report on the orientational relaxation behavior of two molecules, resorufin and 6-[N-(7-nitrobenz-2-oxa-1,3-diazol-4-yl)amino] hexanoic acid (NBDHA) (Fig. 2.1), in two solvents, water and N-octyl-2-pyrrolidone (NOP). NOP has an amphiphilic structure (Fig. 1.1) with a polar lactam functionality capable of hydrogen-bonding and a hydrocarbon chain. Both solvents have potential for specific solute-solvent interactions, however, water and NOP differ significantly in size and organization. We selected water and NOP for their ability to form a liquid-liquid interface at room temperature, which is the focus of the study in chapter 5.

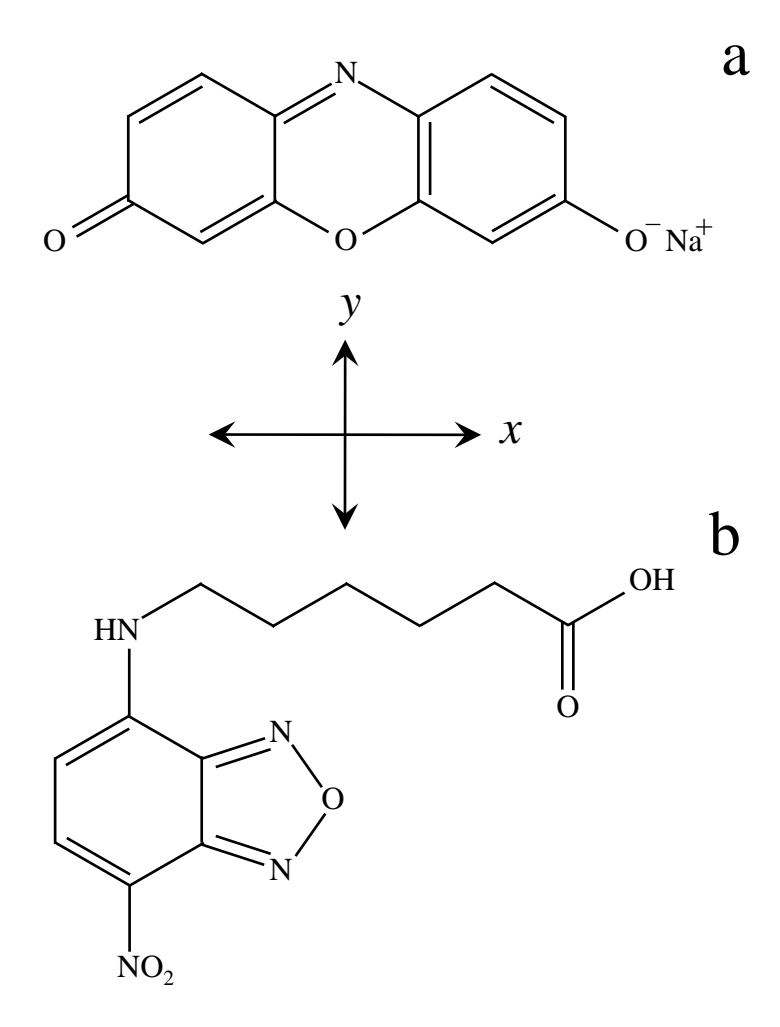


Figure 2.1 Structures of (a) resorufin sodium salt and (b) NBD hexanoic acid (NBDHA) shown with Cartesian *x* and *y* axes for clarity.

The two chromophores selected are similar in the sense that they are both polar, with several heteroatom sites present in their conjugated ring structures. The overall shape and aspect ratio of the two molecules differ significantly, and this difference has, in most previous works, led to anisotropy decay dynamics that either cannot be compared directly or modeled using the same solute-solvent boundary condition. The two chromophores we have examined here produce decay dynamics that can be understood in the context of the Chuang and Eisenthal model,³⁷ and despite their dissimilar shapes, these molecules exhibit commensurate reorientation dynamics in each solvent system. Specifically, we observe a single exponential anisotropy decay for both

chromophores in water, and a two-component exponential decay for both chromophores in NOP. The observed changes in rotor shape for resorufin and NBDHA in the solvents, water and NOP, demonstrate that solvent-solvent interactions and local organization can play a deterministic role in mediating solute-solvent interactions. These findings are consistent with the steady-state excitation and emission data for the solutes, and suggest that it is possible, with further investigation, to achieve an understanding of solute-solvent interactions that relies to a significant extent on the organization and properties of the solvent system.

2.2 Experimental Methods

The chromophore, NBDHA, was obtained from Invitrogen and used as received. Resorufin sodium salt was purchased from Sigma Aldrich and used as received. NOP was purchased from Aldrich at 98% purity and used without further purification. The water used in these experiments was purified in-house with a Milli-Q filtration system (Millipore). For steady-state absorption measurements in both aqueous and NOP solvents, chromophore concentrations between 10⁻⁴ and 10⁻⁵ M were used. These concentrations of NBDHA and resorufin in both solvents were also used for time-resolved fluorescence measurements.

Steady-state absorbance measurements were made with a Cary 300 Bio, double-beam UV-visible absorbance spectrophotometer over the range of 400 nm to 700 nm, at a spectral resolution of 1 nm for all measurements. Steady-state spontaneous emission spectra were recorded using a Jobin-Yvon Fluorolog III spectrometer over the range of 450 nm to 700 nm. The excitation wavelength was set to 400 nm for both resorufin and NBDHA emission spectral acquisition. The spectral resolution for emission experiments was 3 nm in all cases.

Time-resolved measurements, fluorescence lifetime and fluorescence anisotropy decay, were collected using the spectrometer described below. A schematic of the time-correlated

single photon counting (TCSPC) set-up is shown in Figure 2.2. The light source for the system is a CW mode-locked Neodymium: Yttrium Vanadate (Nd: YVO₄) laser with 13 ps 1064 nm pulses and 80 MHz repetition rate (Spectra Physics Vanguard). The Nd:YVO₄ laser pumps a cavity-dumped dye laser (Coherent 702-2) characterized by 5 ps pulses at wavelengths between 430 nm and 850 nm. The repetition rate of the laser is adjustable between 80 kHz and 80 MHz and is determined by the cavity dumping electronics (Gooch & Housego). A typical repetition rate is 4 MHz. The dye used to excite the NBDHA solutions was stilbene 420 (Exciton), providing excitation wavelengths between 445 nm and 465 nm, while pyrromethene 567 (Exciton) with an excitation range of 550 nm to 595 nm was used to excite resorufin solutions. The fundamental excitation pulse from the dye laser is split, with one portion directed to a reference photodiode the other portion directed to the sample. The sample excitation pulse is polarized vertically. Emission from the sample is collected using a 40X reflecting microscope objective. The collected emission is separated into polarization components parallel and perpendicular to that of the excitation pulse using a polarizing cube beamsplitter. The parallel and perpendicular polarized signal components are detected simultaneously using Spectral Products CM-112 subtractive double monochromators equipped with Hamamatsu R3809U-50 microchannel plate-photomultiplier tube (MCP-PMT) detectors. The detection electronics (Becker & Hickl SPC-132) resolve the parallel and perpendicular transients separately, yielding ca. 30 ps response functions for each detection channel. The detection electronics include a time-to-amplitude converter (TAC) and constant fraction discriminator (CFD) that temporally resolve the fluorescence signal for each polarization component. In Figure 2.2, a delay is used in the reference channel to ensure proper timing of the reference and emission signals. Data are collected using multichannel analyzers (MCA) that are integral components of the SPC-132

electronics. Data acquisition, detector bias, and collection wavelength are controlled using a program written in-house using National Instruments LabVIEW® software on a PC.

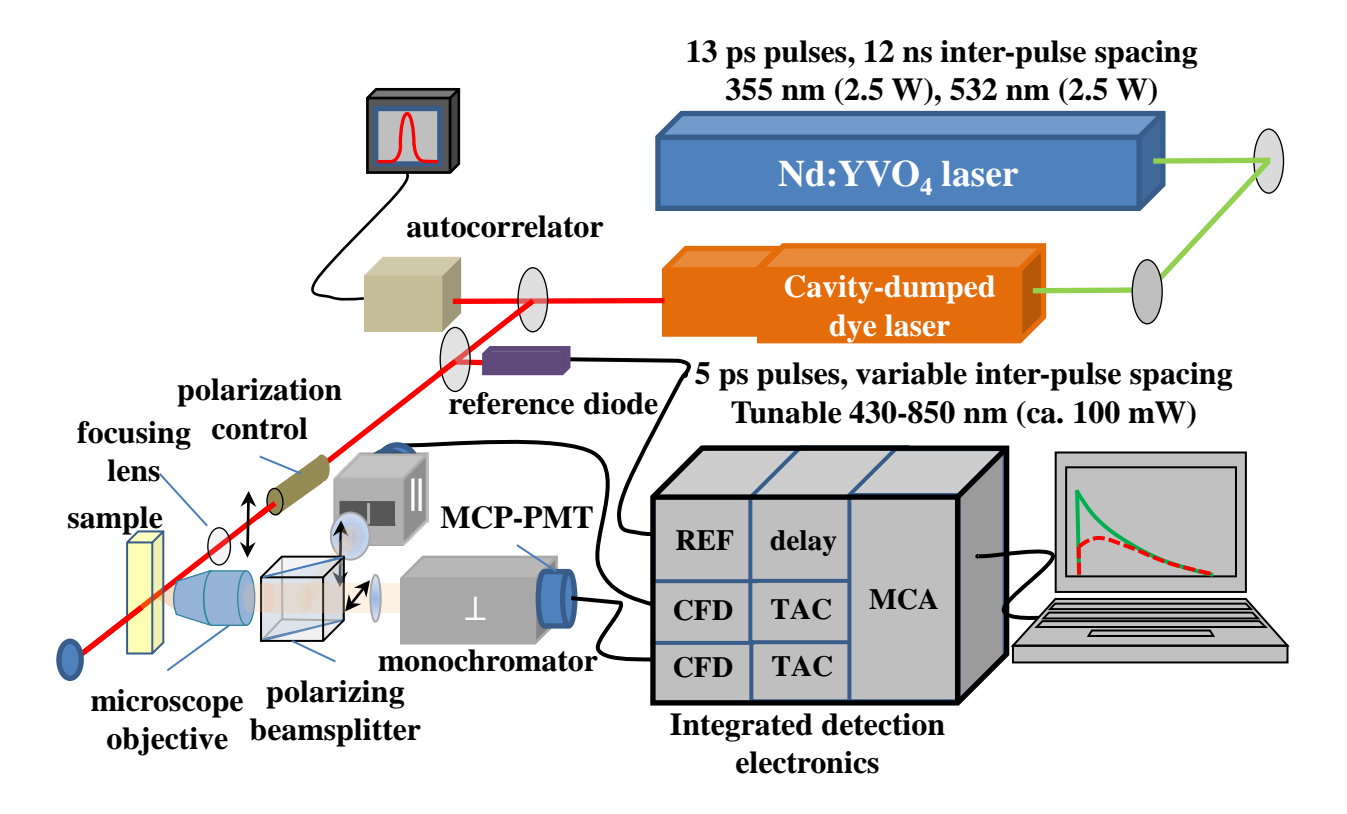


Figure 2.2 Time-correlated single photon counting (TCSPC) instrument.

2.3 Results and Discussion

In this work, we report on the steady-state spectroscopy and dynamics of the chromophores resorufin and NBDHA in the solvents water and NOP. Both of these spectroscopic measurements provide insight into the local environments of these probe molecules, and we consider the steady-state optical response first. The absorption and emission spectra of these two chromophores reveal a measurable dependence on solvent, and the information obtained from the spectral characteristics can be used to infer information about the chromophore local environment. For NBDHA in water $(\epsilon_0 \sim 80, n = 1.33)^{38}$ (Figs. 2.3a), we observe that both the absorption and emission spectra are red-shifted relative to the same data taken in NOP solvent (Fig2.3b). NBDHA absorption maxima in water and NOP were 484 nm and 469 nm, respectively, and the emission maxima were 555 nm and 529 nm in water and NOP, respectively. While there is scant data in the literature on the dielectric response of NOP, we infer from the dielectric constant for N-methyl pyrrolidone ($\varepsilon_0 \sim 32$, n = 1.49) ³⁸ that NOP has a dielectric constant well below that of water. The red-shifted absorption and emission spectra suggest that either the ground state of NBDHA is stabilized in NOP to a greater extent than it is in water, or the excited state of NBDHA is stabilized more in water than in NOP. Given the Stokes shift observed for NBDHA in both solvent systems, it appears that the excited state of NBDHA is more polar than its ground state and is therefore stabilized by the more polar solvent, which is predicted by spectroscopic theory.³⁹ In comparison, the absorption and emission spectra of resorufin in water (Fig. 2.4a) are slightly blue-shifted compared to the same data taken in NOP (Fig. 2.4b), and the spectral shape and Stokes shift appears to be solvent-dependent for resorufin to a greater extent than for NBDHA.

Absorption maxima for resorufin were 571 nm and 594 nm in water and NOP, respectively, while the emission maxima were 585 nm and 616 nm in water and NOP, respectively. For resorufin, either the excited state is stabilized to a greater extent in NOP than in water or the ground state is stabilized more efficiently than the excited state in water. While either of these is a possibility, it is instructive to consider that resorufin can exist either as a contact ion pair with its sodium (Na⁺) counter ion, or as a dissociated ionic species, depending on the ability of the solvent system to accommodate charged molecules.⁴⁰

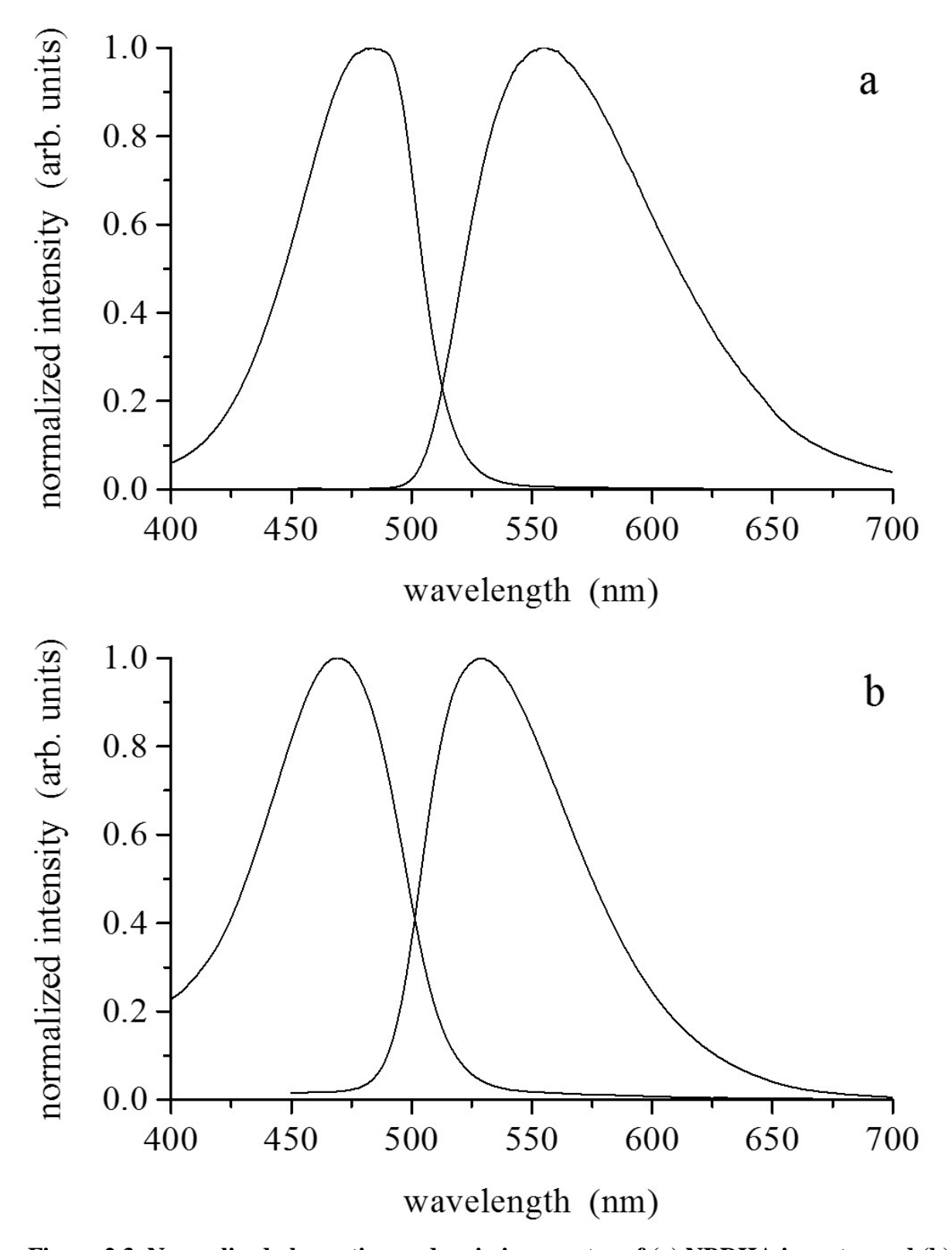


Figure 2.3 Normalized absorption and emission spectra of (a) NBDHA in water and (b) NBDHA in NOP.

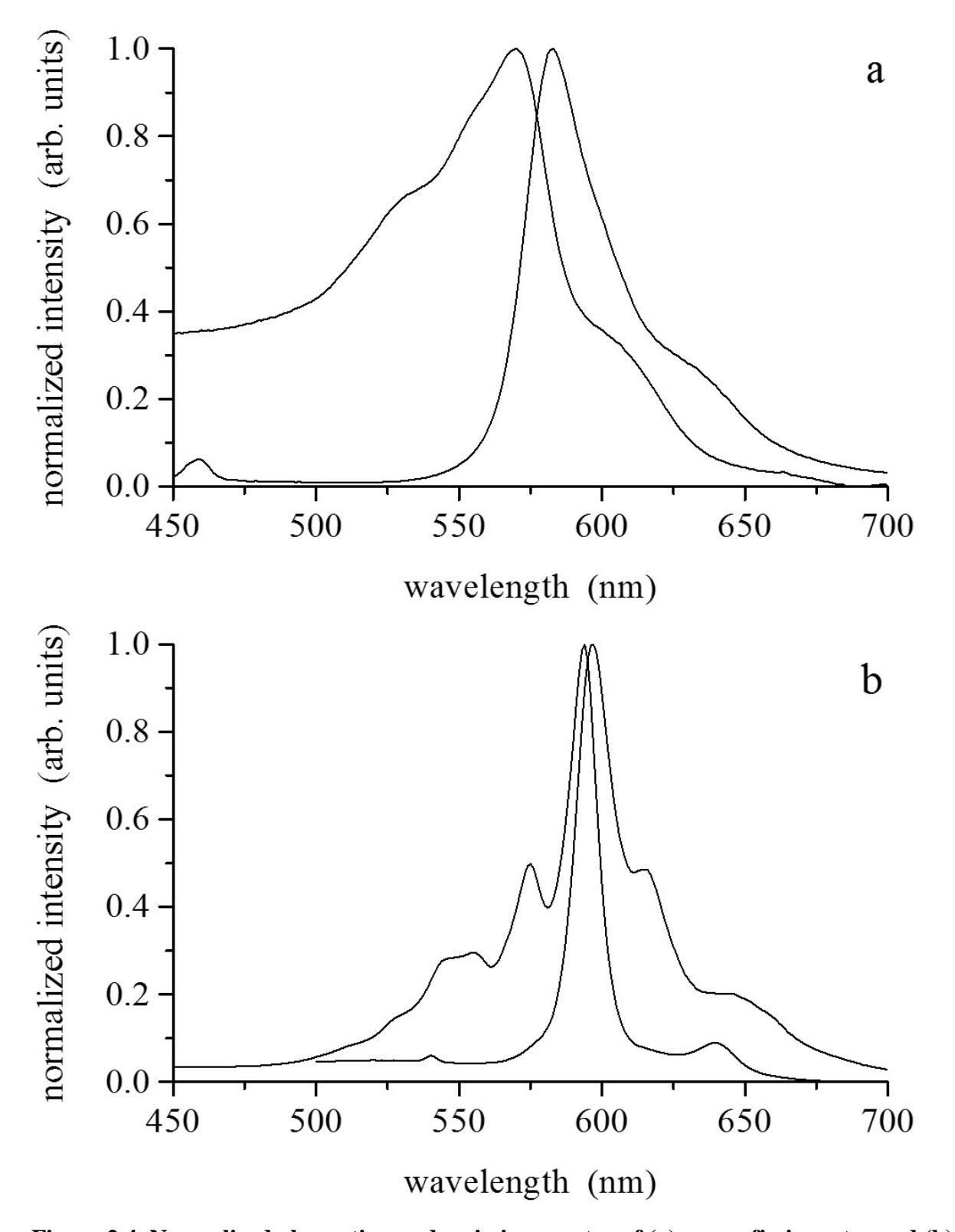


Figure 2.4 Normalized absorption and emission spectra of (a) resorufin in water and (b) resorufin in NOP.

We consider the information available from the Stokes shifts for these chromophores in the different solvents. There are several models in the literature that attempt to relate fluorescence Stokes shift to molecular properties of the solute, such as its size and change in dipole moment upon excitation, and the dielectric response of the solvent system. The difference between these models lies in the manner in which the dielectric response of the solvent is treated. We use the Bakhshiev formulation in this work,

$$\Delta \overline{v} = \overline{v}_a - \overline{v}_f = \frac{2\Delta\mu^2}{a_0^3 hc} \left(\frac{\varepsilon_0 - 1}{\varepsilon_0 + 2} - \frac{n^2 - 1}{n^2 + 2} \right) \frac{\left(2n^2 + 1\right)}{\left(n^2 + 2\right)}$$
(2.1)

where $\Delta \overline{\nu}$ is the fluorescence Stokes shift, $\Delta \mu$ is the change in solute permanent dipole moment upon excitation, a_0 is the solute cavity radius, h is Planck's constant, c is the speed of light, ϵ_0 is the zero-frequency dielectric constant of the solvent, and n is the solvent refractive index. The quantity $\Delta \overline{\nu}$ is measured experimentally and we use this value to determine the quantity of interest, which is the change in dipole moment on excitation, $\Delta \mu$. Using Eq. 2.1 we calculate $\Delta \mu$ for the two chromophores in water and NOP (Table 2.1).

Table 2.1 Calculated changes in permanent dipole moment, $\Delta\mu$, upon excitation for the chromophores resorufin and NBDHA in solvents water and NOP.

Solvent	Resorufin Δμ (D)	NBDHA Δμ (D)	
Water	1.02	1.63	
NOP	0.58	1.67	

 $D = Debye \; (3.335641 \times 10^{-30} \; Coulomb \times meter)^{44}$

These calculations, based on the experimental Stokes shift data (Figs. 2.3 and 2.4), show that resorufin experiences a substantial change in its permanent dipole moment on excitation, with the change being almost a factor of two greater for water ($\Delta\mu=1.02$ D) than for NOP ($\Delta\mu=0.58$ D). This is not a surprising result based on the fact that resorufin is a sodium salt and the extent of dissociation is mediated by the solvent. Thus, in NOP we expect little or no dissociation and we observe a spectral red shift and line narrowing (Fig. 2.3b) relative to that observed for resorufin in water (Fig. 2.3a), where dissociation is expected. The chromophore of NBDHA does not possess a dissociable proton, so we expect a different result. We find that for NBDHA in both water and NOP, we recover a change in dipole moment of $\Delta\mu\sim1.65$, with no difference between the different solvents. The spectral shifts and changes in band shape for both chromophores in the two solvents suggest that the solvation environment formed by these two solvents differs significantly. While these data are interesting and provide some insight into solute-solvent interactions, we require a means of probing such local environments in more detail. For this purpose we turn to time-resolved fluorescence spectroscopy.

As noted above, the two chromophores exhibit similar reorientation dynamics in the two solvent systems, producing single exponential anisotropy decays in water and two-component anisotropy decays in NOP (Figs. 2.5 and 2.6). The similarity between the reorientation behavior of these two outwardly different chromophores bears closer examination because of its implications on the role of solvent-solvent interactions in mediating solute-solvent interactions. To compare these data, we need to understand in detail the information content of the reorientation data. The starting point in the interpretation of our data is to generate the induced orientational anisotropy function, R(t), from the combination of the polarized fluorescence transients according to Eq. 2.2,

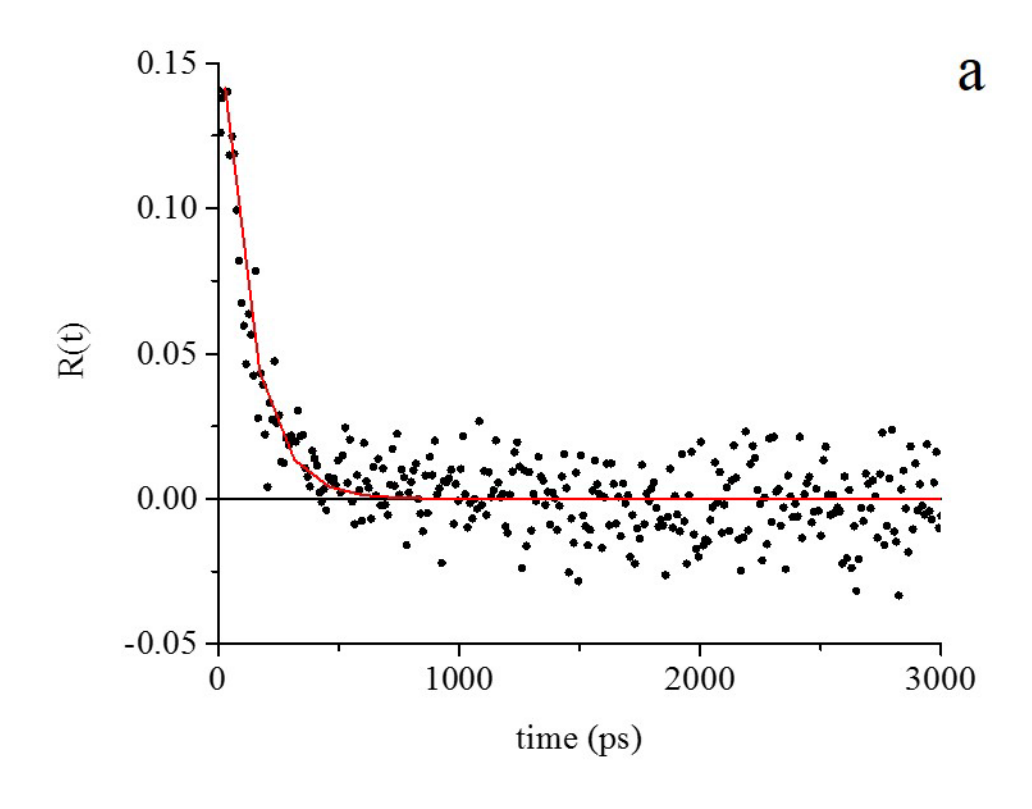
$$R(t) = \frac{I_{||}(t) - I_{\perp}(t)}{I_{||}(t) + 2I_{\perp}(t)}$$
(2.2)

where $I_{||}$ (t) is the fluorescence transient polarized parallel to the vertically polarized excitation pulse and I_{\perp} (t) is the fluorescence transient polarized perpendicular to the excitation pulse. It is the functional form and the time constant(s) associated with the decay of R(t) that are related to the local environment of the reorienting molecule. Chuang and Eisenthal developed a model for fluorescence anisotropy decay that provides a means of interpreting anisotropy decay functions containing up to five exponential components.^{5,29,45,47} Despite this potential for complexity, one or two decays are the functional forms observed most commonly. For the excitation and emission transition moments oriented parallel to one another, along the long axis in the chromophore π -system plane, reorientation of the chromophore as a prolate rotor ($D_x > D_y = D_z$) gives rise to a single exponential decay of R(t) (Eq. 2.3) and reorientation as an oblate rotor ($D_z > D_x = D_y$) produces a two-component R(t) function, as described by Eq. 2.4.

$$R(t) = \frac{4}{10} \exp(-6D_z t) \tag{2.3}$$

$$R(t) = \frac{1}{10} \exp(-(2D_x + 4D_z)t) + \frac{3}{10} \exp(6D_x t)$$
 (2.4)

With these relationships in mind, we consider the experimental data for resorufin and NBDHA in water and NOP, with an eye toward understanding how the solvent local environment influences the average diffusion constant, D.



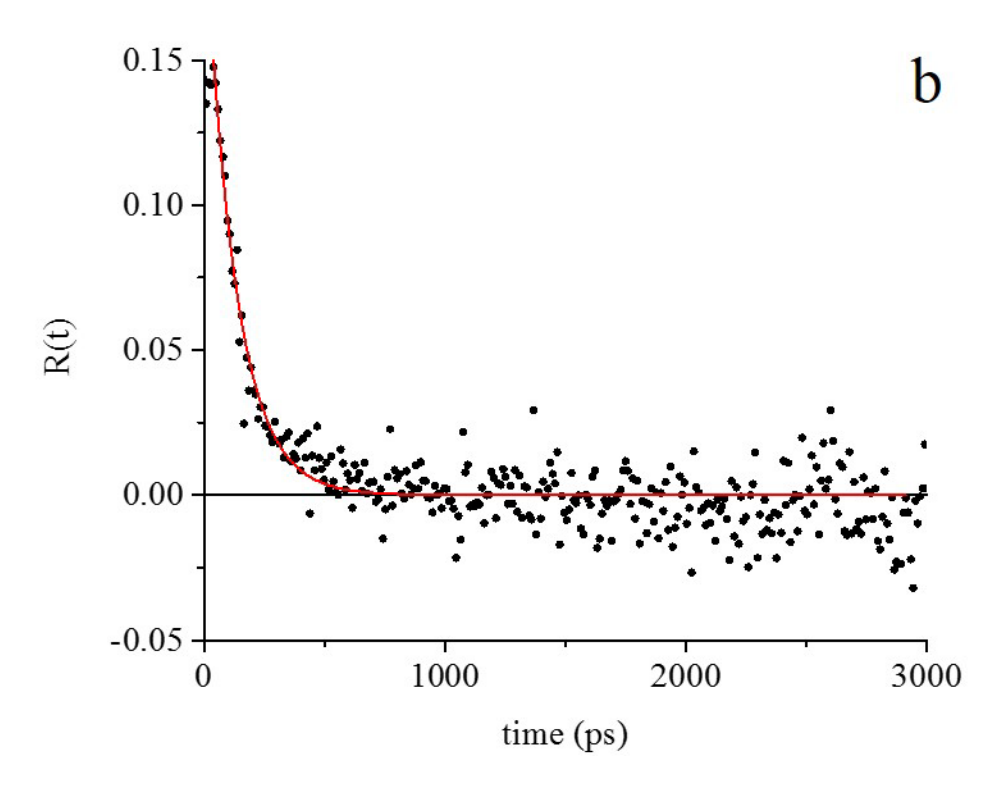
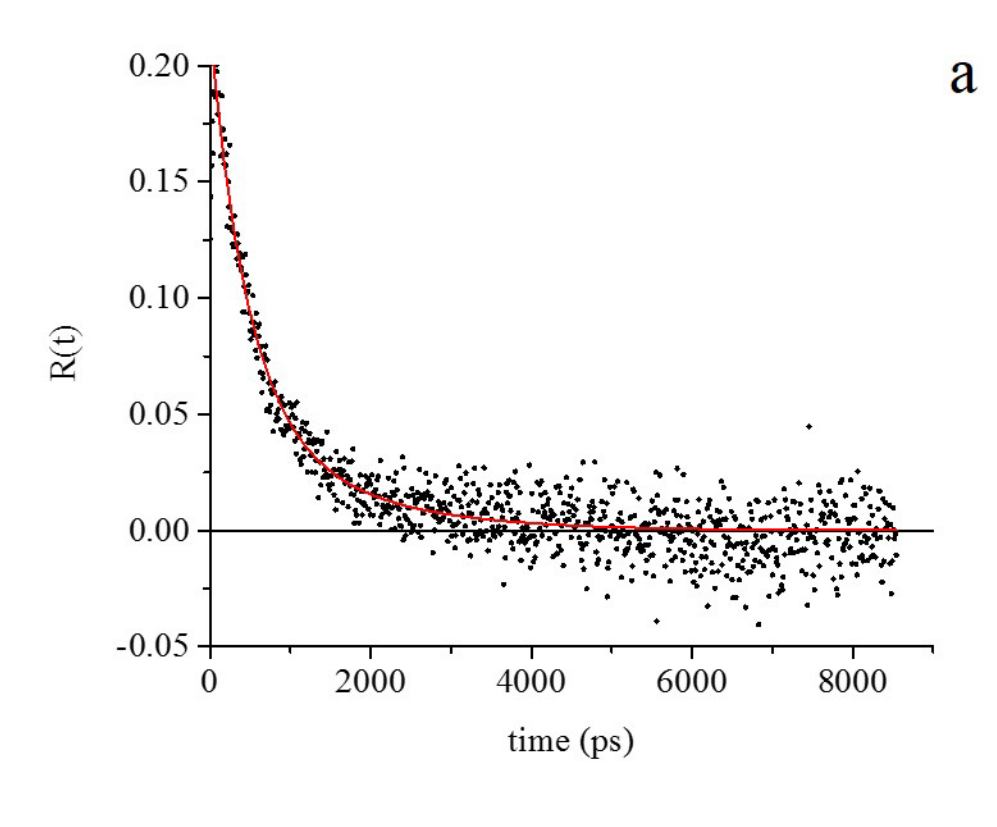


Figure 2.5 (a) Orientational anisotropy function, R(t), plotted as a function of time for resorufin in water. (b) R(t) as a function of time for NBDHA in water. The data are fitted to single exponential decays.



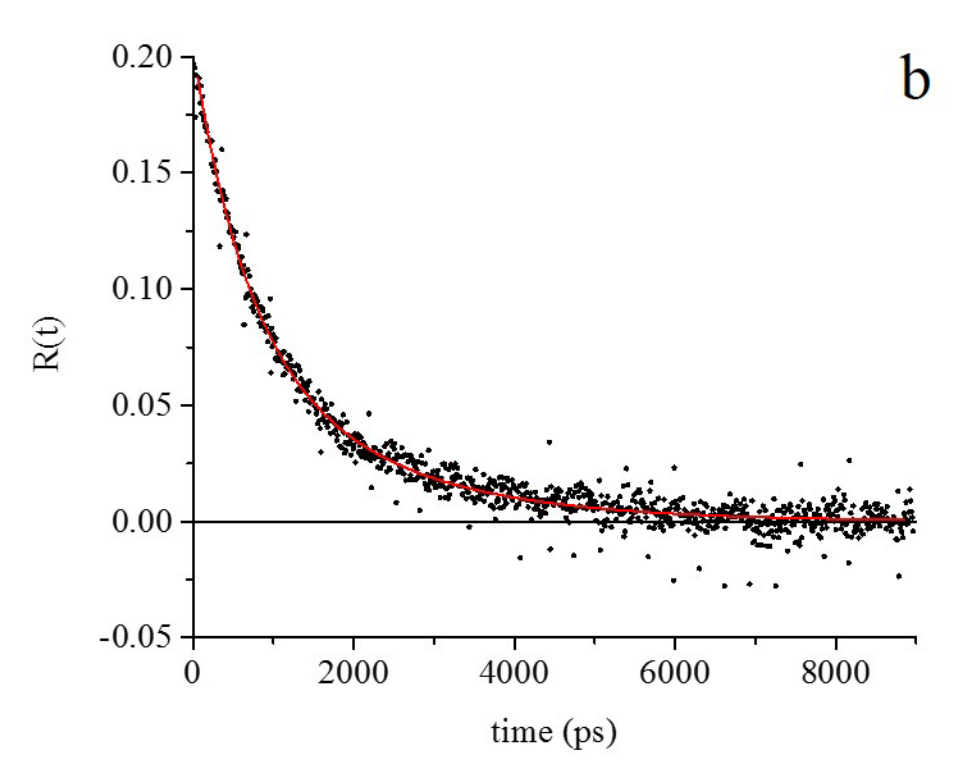


Figure 2.6 (a) Orientational anisotropy function, R(t), plotted as a function of time for resorufin in NOP. (b) R(t) as a function of time for NBDHA in NOP. The data are fitted to two-component exponential decays.

The rotational diffusion behavior of resorufin and NBDHA in several solvents has been studied previously, ^{18,22,24,45,48} and there is a frame of reference for the interpretation of the data we present here. Resorufin, a molecule capable of dissociation to produce an anionic chromophore and Na⁺, is characterized by a transition dipole moment that lies along its long (x), π -plane axis as shown in Figure 2.1a.⁴⁸ Resorufin reorients as a prolate rotor in small polar solvents such as methanol and acetonitrile, and has been shown to exhibit varying degrees of Na⁺ dissociation in the butanols.^{22,40} The NBD chromophore is used widely as a probe in biological studies and has been attached to phospholipids or cholesterol for the interrogation of lipid bilayer structure and dynamics. 45-47 NBDHA (Fig. 2.1b) has a hexanoic acid pendant functionality and reorients as a prolate rotor in solvents such as n-alcohols, acetonitrile, DMF and DMSO.⁴⁵ Figure 2.7 depicts the different volumes swept out by prolate and oblate rotors that are polarized along the long (x) axis. There is a limited range of solvents in which both chromophores have been studied, and those data are compiled in Table 2.2. These data suggest that the reorientation dynamics of resorufin and NBDHA bear a very limited resemblance to one another, and this result is typical for head-to-head comparisons of the reorientation dynamics of most chromophores. This chromophore-specific behavior may be expected due to the charge state of the resorufin and NBDHA chromophores, and their significantly different shapes.

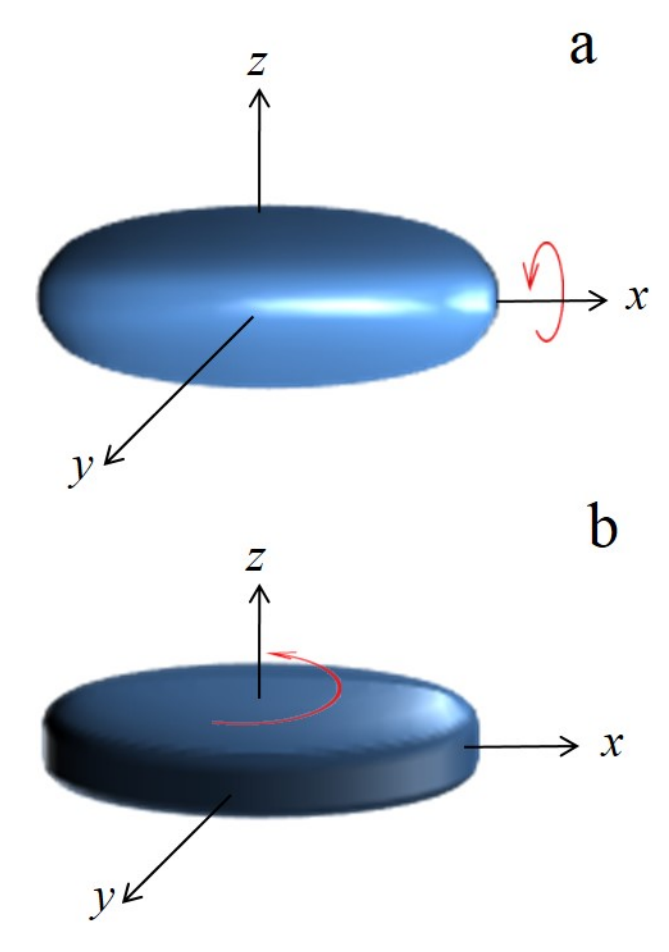


Figure 2.7 Three-dimensional shape representing the volume swept out when a long-axis polarized chromophore (a) rotates about the x-axis as a prolate rotor and (b) rotates about the z-axis as an oblate rotor.

Table 2.2 Comparison of reorientation dynamics of resorufin 48 and NBDHA 45 in selected solvents.

Solvent	η (cP) ^a	Resorufin ⁴⁸ $ au_{OR}$ (ps)	NBDHA ⁴⁵ tor (ps)
Methanol	0.544	78 ± 14	131 ± 24
Ethanol	1.074	216 ± 45	174 ± 6
1-propanol	1.945	361 ± 47	302 ± 16
1-butanol	2.544	434 ± 69	570 ± 26
Acetonitrile	0.369	34 ± 8	50 ± 3
DMF	0.794	54 ± 14	162 ± 11
DMSO	1.987	56 ± 10	273 ± 10

^a Viscosity (25 °C) taken from CRC Handbook⁴⁴

For the data we report here on NBDHA and resorufin reorientation in water and in NOP, we find that the results are qualitatively consistent with the hydrodynamic volume of each chromophore (165 Å³ for resorufin, 242 Å³ for NBDHA)⁴⁹ in the sense that the anisotropy decays for NBDHA are somewhat slower than for resorufin (Table 2.3). For the reorientation of both chromophores in water, a single exponential anisotropy decay is observed.

Table 2.3 Anisotropy decay time constants, τ_{OR} , and Cartesian components of the average rotational diffusion constants, D, for resorufin and NBDHA in water and in NOP.

	Res	sorufin	NBDHA		
Solvent	τ _{OR} (ps)		τor (ps)		
	fast	slow	fast	slow	
Water	133 ± 11		213 ± 63		
NOP	347 ± 19	1432 ± 172	657 ± 97	1718 ± 395	
Solvent	$D_z/10^8~(Hz)$	$D_x(=D_y)/10^8 (Hz)$	$D_z/10^8(Hz)$	$D_x(=D_y) / 10^8 (Hz)$	
Water	12.6 ± 1.1		8.4 ± 2.5		
NOP	6.6 ± 0.4	1.2 ± 0.2	3.4 ± 0.4	1.0 ± 0.2	

Resorufin and NBDHA likely reorient as non-spherical rotors in water, but based on the limited information content available from a single exponential decay (Eq. 2.3) compared to a two-component decay (Eq. 2.4), we are left to interpret our data in the context of the simplest model that relates molecular reorientation to the properties of the solvent, the DSE model.³⁴ In the most basic form of this model, the recovered reorientation time constant, τ_{OR} , is related to the solvent bulk viscosity, η , the solute hydrodynamic volume, V, and the thermal energy in the system, k_BT by the relation in Equation 2.5.

$$\tau_{OR} = \frac{\eta V}{k_B T} \tag{2.5}$$

This formulation assumes a spherical rotor in a "continuum" solvent, and it is known that the DSE model is a qualitative predictor of experimental data. For many systems, either polar/charged solutes in polar solvents or nonpolar solvents, there exists a discrepancy between model and experiment. This difference is frequently explained in the context of the solute-solvent boundary condition, *i.e.* the strength of frictional interactions between the solvent and solute. Due to the structural difference between resorufin and NBDHA and the possible difference in the charge state of the molecules, it would be reasonable to expect that there is a difference in the solute-solvent boundary conditions for the two systems, where the boundary condition denoted "stick" or "slip" is a measure of the frictional interaction between the solute and the solvent.

We can evaluate whether or not this is the case by comparing the quantity τ_{OR}/V for the two solutes. This comparison is valid because the solvent and the temperature are the same for both reorientation measurements. For resorufin, $\tau_{OR}/V = 0.80 \pm 0.07$ ps/Å³ and for NBDHA, $\tau_{OR}/V = 0.82 \pm 0.27$ ps/Å³. The similarity in these ratios indicates that the frictional

contribution(s) to solute-solvent interactions for these two solutes is fundamentally the same, despite the structural differences between these two solutes.

The reorientation dynamics for the two chromophores in water may not be as revealing as they could be because of the comparatively low viscosity and fast reorientation time constants measured, however, these reorientation time constants we report for resorufin and NBDHA in water are substantially longer than the instrumental response function for our TCSPC system (ca. 30 ps). As a result, time resolution is not a factor for our measurements and the similarity in chromophore behavior in NOP is significant. Resorufin and NBDHA both produce a twocomponent exponential anisotropy decay in NOP. This finding indicates that in NOP, both chromophores reorient as oblate rotors, and in water both chromophores reorient as prolate rotors. From Eqs. 2.3 and 2.4 it is possible to extract the Cartesian components of the rotational diffusion constant, D. The ratio of D, calculated from the average of the Cartesian components for resorufin and NBDHA (Table 2.3), was found to be 1.67. This ratio is in reasonably close agreement with the ratio of chromophore hydrodynamic volumes when taking into account the DSE model where D is inversely proportional the hydrodynamic volume. There are two important issues we consider based on these results. The first is the comparability of the results for the two chromophores, which stands in contrast to many other cross-chromophore comparisons, and the second point is that the change in rotor shape observed for both chromophores in the two solvents implies that it is solvent local organization in at least one of these solvents that is responsible for our findings.

It is instructive to examine the dynamics of these chromophores in the solvent NOP because these data provide additional insight into the solvation behavior of both solutes. For both chromophores, we observe a two-component anisotropy decay in NOP, consistent with the

functional form presented in Eq. 2.4. The two-component anisotropy decay for both chromophores implies that they are reorienting as oblate rotors, which is a substantial change from the behavior of the chromophores in water. The recovery of a two-component anisotropy decay allows for the evaluation of the Cartesian components of D (Table 2.3). The ratio of D_z/D_x for these chromophores is related to the ellipticity of the volume swept out during reorientation. For resorufin, $D_z/D_x = 5.5 \pm 1.3$ and for NBDHA, $D_z/D_x = 3.4 \pm 1.1$. These values may appear to be slightly different, but when uncertainties in the data are taken into account, they are not distinguishable from one another. Given the different structures of these two chromophores, the similarity in their reorientation dynamics in NOP suggests that the local environments in which they reside bear some similarity.

As a result of the similar behavior of the two chromophores in both water and NOP, it is useful to consider why both chromophores exhibit different effective rotor shapes in the two solvents and also why such a difference in the observed dynamics may occur. To address the first issue, we look to the relative sizes of the solute and solvent molecules. As noted above, resorufin has a hydrodynamic volume of 165 ų and for NBDHA V = 242 ų calculated using the method of atomic increments. ⁴⁹ The DSE model, which cannot be applied directly to our NOP data for reasons of its functional form, has as a core assumption that the solvent behaves as a dielectric continuum. This is approximated by the condition that individual solvent molecules are much smaller than the solute. This condition is met for water but not for NOP. The hydrodynamic volume of water is 21 ų and that of NOP is 219 ų. ⁴⁹ Aside from a key assumption of the DSE model being violated, the more significant point is that the volumes of the chromophores are close to the same as that of NOP, and under that condition, solvent-solvent interactions could become competitive with solute-solvent interactions in determining the local

organization of the solution. The fact that both chromophores reorient as oblate rotors (Fig. 2.7b) in NOP suggests that the local environment formed by the solvent has a propensity to preferentially restrict out-of-plane rotation relative to in-plane rotation. The amphiphilic properties of NOP point to a tendency to form organized clusters, but it is not appropriate, necessarily, to view these data as indicating the formation of lamellar structure(s) in neat NOP. Although it is apparent that the confinement imposed on the chromophores by NOP provides more restriction for motions involving significant out-of-plane components.

The observation of a solvent-dependent change of rotor shape has been observed previously. Cresyl violet, a cationic oxazine dye, was shown to reorient as a prolate rotor in ethylene glycol and as an oblate rotor in n-dodecanol. ^{17,50} In that work, it was shown that the existence of a mesophase in *n*-dodecanol between 24 °C and 30 °C gave rise to solvent organization that mediated the rotational diffusion dynamics of the chromophore. This effect was observed due to the hydrodynamic volumes of *n*-dodecanol and the chromophore, cresyl violet. Analogous behavior has been reported for nonpolar systems as well. The reorientation dynamics of perylene and 1-methyl perylene were shown to change as the size of the *n*-alkane solvent increased relative to the size of the chromophores.^{20,21} Thus, the existence of changes in local solvation environment is known to occur in both polar and nonpolar systems. The unique aspect of the work we present here is that the change in dynamics for two substantially different chromophores as they are examined in two solvent systems can be understood in the context of a single explanation; the solvent-solvent interactions for NOP mediate the local environment(s) in which solutes can reside. In previous work, the results were only known to be chromophore specific, and the relative importance of solute-solvent and solvent-solvent interactions could only be speculated upon. In the present work, it is clear that solvent-solvent interactions determine

the local solvation environments that are possible in a given solvent. We were able to resolve this issue in the present case because of the specific solvent system we used, but the result could be more general with the caveat that the dominant role of solvent-solvent interactions will be manifested when the solute is similar in size to the solvent.

2.4 Conclusions

We have examined the steady-state and time-resolved spectroscopic behavior of two chromophores, resorufin and NBDHA, in the solvents water and NOP. The steady-state spectroscopic data point to significantly different solute-solvent interactions for the two chromophores in the different solvents, with resorufin exhibiting a different change in dipole moment upon excitation for the two solvents and NBDHA not exhibiting the analogous change. The time-resolved fluorescence anisotropy decay data show that both chromophores reorient as prolate rotors in water, with the same frictional interactions. For reorientation in NOP, a different rotor shape is observed, but both chromophores behave in the same manner, exhibiting an oblate rotor shape. The change in rotor shape is correlated with the increase in the hydrodynamic volume of the solvent relative to the solutes. Because of the similarity of the dynamics for the two chromophores, solvent-solvent interactions are implicated as the mediating factor in determining the local solvation environments that are allowed to form in this solvent. In the next chapter, the reorientation dynamics of resorufin are evaluated in the presence of ionic species.

REFERENCES

REFERENCES

- 1. Dote, J. L.; Kivelson, D.; Schwartz, R. N. Journal of Physical Chemistry 1981, 85, 2169.
- 2. Dote, J. L.; Kivelson, D. Journal of Physical Chemistry 1983, 87, 3889.
- 3. Madden, P.; Kivelson, D. Journal of Physical Chemistry 1982, 86, 4244.
- 4. Kivelson, D.; Spears, K. G. Journal of Physical Chemistry 1985, 89, 1999.
- 5. Dutt, G. B.; Doraiswamy, S.; Periasamy, N.; Venkataraman, B. *Journal of Chemical Physics* **1990**, *93*, 8498.
- 6. Alavi, D. S.; Hartman, R. S.; Waldeck, D. H. Journal of Chemical Physics 1991, 94, 4509.
- 7. Hartman, R. S.; Alavi, D. S.; Waldeck, D. H. Journal of Physical Chemistry 1991, 95, 7872.
- 8. Dutt, G. B.; Raman, S. Journal of Chemical Physics 2001, 114, 6702.
- 9. Kawski, A.; Bojarski, P. Asian Journal of Spectroscopy 2003, 7, 97.
- 10. Gayathri, B. R.; Mannekutla, J. R.; Inamdar, S. R. Journal of Fluorescence 2008, 18, 943.
- 11. Mannekutla, J. R.; Inamdar, S. R.; Mulimani, B. G.; Savadatti, M. I. *Journal of Fluorescence* **2010**, *20*, 797.
- 12. Kawski, A.; Bojarski, P. Chemical Physics 2010, 375, 52.
- 13. Maroncelli, M.; Fleming, G. R. Journal of Chemical Physics 1987, 86, 6221.
- 14. Castner, E. W.; Maroncelli, M.; Fleming, G. R. Journal of Chemical Physics 1987, 86, 1090.
- 15. Nagarajan, V.; Brearley, A. M.; Kang, T. J.; Barbara, P. F. *Journal of Chemical Physics* **1987**, *86*, 3183.
- 16. Ben-Amotz, D.; Scott, T. W. Journal of Chemical Physics 1987, 87, 3739.
- 17. Blanchard, G. J. Journal of Chemical Physics 1987, 87, 6802.
- 18. Blanchard, G. J.; Cihal, C. A. Journal of Physical Chemistry 1988, 92, 5950.
- 19. Blanchard, G. J. Journal of Physical Chemistry 1989, 93, 4315.
- 20. Jiang, Y.; Blanchard, G. J. Journal of Physical Chemistry 1994, 98, 6436.
- 21. Goldie, S. N.; Blanchard, G. J. Journal of Physical Chemistry A 1999, 103, 999.

- 22. Spears, K. G.; Steinmetz, K. M. Journal of Physical Chemistry 1985, 89, 3623.
- 23. Alavi, D. S.; Waldeck, D. H. Journal of Physical Chemistry 1991, 95, 4848.
- 24. Kurnikova, M. G.; Balabai, N.; Waldeck, D. H.; Coalson, R. D. *Journal of the American Chemical Society* **1998**, *120*, 6121.
- 25. Dutt, G. B.; Srivatsavoy, V. J. P.; Sapre, A. V. Journal of Chemical Physics 1999, 110, 9623.
- 26. Dutt, G. B.; Ghanty, T. K. Journal of Physical Chemistry A 2004, 108, 6090.
- 27. Dela Cruz, J. L.; Blanchard, G. J. Journal of Physical Chemistry A 2002, 106, 10718.
- 28. Kubinyi, M.; Grofcsik, A.; Papai, I.; Jones, W. J. Chemical Physics 2003, 286, 81.
- 29. Indirapriyadharshini, V. K.; Ramamurthy, P. Journal of Chemical Sciences 2007, 119, 161.
- 30. Zhou, P. W.; Song, P.; Liu, J. Y.; Shi, Y.; Han, K. L.; Het, G. Z. *Journal of Physical Chemistry A* **2008**, *112*, 3646.
- 31. Mali, K. S.; Dutt, G. B.; Mukherjee, T. Journal of Chemical Physics 2008, 128.
- 32. Esquivelzeta-Rabell, M.; Peon, J.; Cuevas, G. *Journal of Physical Chemistry B* **2009**, *113*, 8599.
- 33. Zhou, P.; Song, P.; Liu, J.; Han, K.; He, G. *Physical Chemistry Chemical Physics* **2009**, *11*, 9440.
- 34. Debye, P. *Polar Molecules* Chemical Catalog Co.: New York 1929.
- 35. Hu, C. M.; Zwanzig, R. *Journal of Chemical Physics* **1974**, *60*, 4354.
- 36. Perrin, F. Journal of Physics and Radium 1934, 5, 497.
- 37. Chuang, T. J.; Eisenthal, K. B. Journal of Chemical Physics 1972, 57, 5094.
- 38. CRC Handbook of Chemistry and Physics, 71st Edition; Lide, D. R., Ed.; CRC Press: Boca Raton, FL, 1990-1991.
- 39. Lakowicz, J. R. *Principles of fluorescence spectroscopy*, 3rd ed.; Springer: New York, 2006.
- 40. Rasimas, J. P.; Blanchard, G. J. Journal of Physical Chemistry 1996, 100, 11526.
- 41. Lippert, E. Zeitschrift für Elektrochemie **1957**, 61, 962.
- 42. Bakhshiev, N. G. Optika I Spektroskopiya 1964, 16, 821.

- 43. Chamma, A.; Vaillet, P. Comptes Rendus de l'Académie des Sciences Series IIC Chemistry **1970**, 270, 1901.
- 44. *CRC Handbook of Chemistry and Physics, 94th Edition*; Haynes, W. M., Ed.; CRC Press/Taylor and Francis: Boca Raton, FL, 2013-2014.
- 45. Greenough, K. P.; Blanchard, G. J. Journal of Physical Chemistry B 2006, 110, 6351.
- 46. Greenough, K. P.; Blanchard, G. J. Journal of Physical Chemistry A 2007, 111, 558.
- 47. Greenough, K. P.; Blanchard, G. J. *Spectrochimica Acta Part A-Molecular and Biomolecular Spectroscopy* **2009**, *71*, 2050.
- 48. Gudgin Templeton, E. F.; Quitevis, E. L.; Kenney-Wallace, G. A. *Journal of Physical Chemistry* **1985**, *89*, 3238.
- 49. Edward, J. T. Journal of Chemical Education 1970, 47, 261.
- 50. Blanchard, G. J.; Wirth, M. J. Journal of Physical Chemistry 1986, 90, 2521.

Chapter 3

The Effects of Electrolyte Concentration on the Rotational Dynamics of Resorufin

3.1 Introduction

The study of fluorescent probe rotational diffusion dynamics in solution is an important tool in an ongoing effort to understand solvation phenomena. Rotational diffusion of a probe molecule is sensitive to both solute-solvent and solvent-solvent interactions, and it is primarily the interactions between solute and solvent that mediate processes such as chemical separations and catalytic reaction efficiency. The interactions between a solute and its local environment include van der Waals interactions, dipole-dipole, and hydrogen-bonding interactions, among others, and the molecular structures of the solute and solvent determine which of these forces play significant roles in the observed solute behavior.¹⁻⁷ The introduction of ionic species into a solution increases the number of interactions that can potentially occur, especially when the solute is also a charged species. A phenomenon known as dielectric friction is often cited as contributing to the rotational diffusion dynamics of cationic and anionic solutes.^{3-5,8-19} The frictional forces experienced by a polar or charged solute in solution are reported to be a combination of both hydrodynamic friction due to in part to the size of the solute and dielectric friction caused by electrostatic interactions, although the contribution of the latter phenomenon is typically modest. Rotational diffusion studies of solutions with added electrolyte have reported changes in chromophore dynamics citing alteration of the solvent local organization in the vicinity of the chromophore and in some cases the formation of contact ion pairs. ²⁰⁻²⁶

The most widely used model to treat rotational diffusion is the modified Debye-Stokes-Einstein (DSE) model first introduced in chapter 1 and shown in Eq. 3.1,²⁷⁻²⁹

$$\tau_{OR} = \frac{1}{6D} = \frac{\eta V f}{k_B T S} \tag{3.1}$$

which relates the rotational diffusion time constant, τ_{OR} , to the solute hydrodynamic volume, V, the solvent bulk viscosity, η , Boltzmann constant, k_B , and the system temperature, T. Additionally, the modified DSE model, which forms the basis of hydrodynamic theory of rotational diffusion, takes into account, a frictional term, f, reflecting the solute-solvent boundary condition, 28 and a shape factor, S, to account for the non-spherical shape of the reorienting moiety.²⁹ The reorientation time, τ_{OR} , which is an experimentally measured quantity, is also inversely proportional to the average rotational diffusion constant, D. The original form of the DSE equation (Eq. 2.5) assumes spherical rotors, whereas the modified DSE equation (Eq. 3.1) accounts for an ellipsoidal rotor executing rotational motion in a continuum solvent. Despite the obvious oversimplification of the solute-solvent system, the modified DSE model has been shown to provide remarkably close agreement with experimental data. Among the issues that are most limiting to the DSE model is the assumption of a solute-solvent boundary condition, and the approximation that the chromophore sweeps out a spherical volume as it reorients in solution. The terms f and S that are included in the modified form of the DSE equation account for the solute-solvent frictional boundary condition²⁸ and the shape of the volume swept out by the solute.²⁹ The coefficient f ranges from 0 and 1, where 0 is the "slip" boundary with minimal solute-solvent interactions and 1 the "stick" limit, characterized by significant frictional solutesolvent interactions.²⁸ The shape factor, S, derived from Perrin's equations, accounts for the non-spherical shape of both the solute and solvent.²⁹ Incorporation of frictional and shape factors into the DSE model provides reasonable agreement between experiment and theory, but cannot account quantitatively for rotational diffusion data because the solvent is treated as a continuum fluid. The DSE model also is not capable of accounting directly for two-component

anisotropy decays, and the incidence of this functional form requires consideration of factors that are not included in the assumptions of the model. For example, in cases where the hydrodynamic volume of the solvent equals or exceeds that of the solute, the approximation of a continuum solvent is violated, and solvent organization can exert a measurable influence on the shape of the volume swept out by the rotating solute. The solute-solvent system of resorufin (Fig. 2.1a) in N-octyl-2-pyrrolidone (NOP) (Fig. 1.1) exhibited a two-component exponential decay, which was interpreted in the context of the solute sweeping out an oblate ellipsoidal volume because the solvent-solvent interactions of NOP hindering out-of-plane chromophore rotation.³⁰ The rotational diffusion of resorufin in NOP contrasts with a single exponential anisotropy decay observed for resorufin in water, where the approximation of a continuum solvent is violated less seriously. Since solvent organization plays a significant role in mediating resorufin rotational motion, it is important to understand the potential role of solution phase ionic species in mediating chromophore rotational motion.

The work presented here addresses the role of electrolyte (ionic species) in mediating the rotational diffusion behavior of resorufin in two different solvent systems, water and NOP. As was shown in chapter 2, the local environment of resorufin in NOP is characterized by organization determined substantially by solvent-solvent interactions, while the second system, resorufin in water, manifests a chromophore local environment where solute-solvent interactions play an important role. In the presence of ionic species, resorufin reorients as a prolate rotor, exhibiting a single exponential anisotropy decay in both water and NOP. This behavior represents a change in the effective rotor shape of resorufin in NOP upon the addition of electrolyte. Three electrolytes were selected to study the effect of complexation between electrolyte cations and the sodium salt of resorufin. The role of ion pairing between resorufin

anion, which is present in aqueous solution is probed by addition of lithium perchlorate (LiClO₄), an electrolyte utilized in aqueous electrochemical studies. Two quaternary ammonium bromide non-aqueous electrolytes, tetrabutylammonium bromide (TBAB) and tetraoctylammonium bromide (TOAB) (Fig. 3.1), which contain bulky cations are added to NOP solutions in an attempt to disrupt the solvation shell created by NOP. In water, the lithium cation (Li⁺) from LiClO₄ can replace the sodium counter-ion of resorufin without significant perturbation, however, the size and shape of the quaternary ammonium cations used in NOP solutions gives rise to a pronounced change in resorufin reorientation dynamics. Since the hydrodynamic volumes of TBAB and TOAB exceed that of NOP, the solvent-solvent interactions reported to mediate the reorientation of resorufin are disrupted when the cationic ammonium species are associated with the anionic chromophore. We use the Chuang and Eisenthal model³¹ to interpret the decay dynamics of resorufin in water and NOP in the presence of electrolyte, and the modified DSE equation to estimate the equilibrium constant for complexation. Our data point to measurable complexation between the anionic chromophore and the cationic ammonium species.

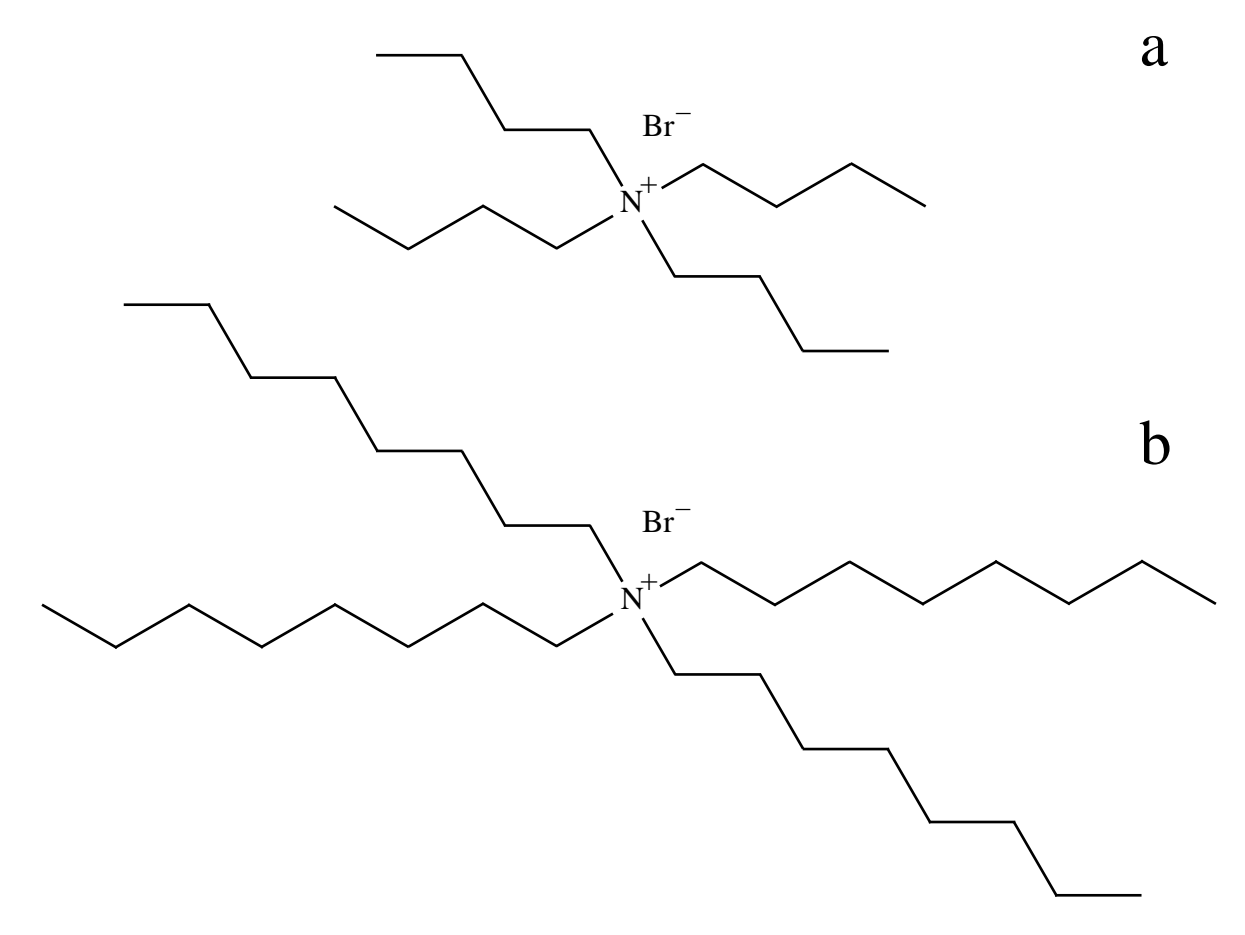


Figure 3.1 Non-aqueous electrolytes, (a) tetrabutylammonium bromide (TBAB) and (b) tetraoctylammonium bromide (TOAB), with hydrodynamic volumes of 299 $\rm \mathring{A}^3$ and 571 $\rm \mathring{A}^3$, respectively.

3.2 Experimental Methods

The sodium salt of resorufin was purchased from Sigma Aldrich and used as received. N-octyl-2-pyrrolidone (NOP) was purchased from Aldrich at 98% purity and used without further purification. The water used in these experiments was purified in-house with a Milli-Q filtration system (Millipore). Lithium perchlorate (LiClO₄) was purchased from Aldrich at 99.99% purity and used as received. The two non-aqueous electrolytes, tetrabutylammonium bromide (TBAB) and tetraoctylammonium bromide (TOAB) (Aldrich), were used without further purification. Aqueous solutions of LiClO₄ were prepared with electrolyte concentrations between 5×10^{-3} M and 10^{-1} M. TBAB and TOAB were dissolved in NOP with electrolyte concentrations between 5×10^{-4} M and 10^{-1} M. For steady-state absorption measurements in both aqueous and NOP solvents, chromophore concentrations of 10^{-5} M were used. The resorufin solution (10^{-5} M) was mixed with the electrolyte solution at 50% (v/v) for both steady-state and time-resolved fluorescence measurements.

Steady-state absorbance measurements were performed using a Hitachi U-4001, double-beam UV-visible absorbance spectrophotometer over the range of 400 nm to 700 nm, at a spectral resolution of 1 nm for all measurements. Steady-state spontaneous emission spectra were recorded using a Hitachi F-4500 fluorescence spectrophotometer over the range of 500 nm to 700 nm for sample in water and 530 nm to 700 nm for samples in NOP. The excitation wavelengths were set to 490 nm and 520 nm for the emission spectral acquisition of resorufin in water and resorufin in NOP, respectively.

Time-resolved measurements, fluorescence lifetime and fluorescence anisotropy decays, were collected using the time-correlated single photon counting (TCSPC) system described in detail in section 2.2. The dye used to excite resorufin solutions was pyrromethene 567 (Exciton)

dissolved in 1-phenoxy-2-propanol (Exciton), providing excitation wavelengths in the range of 550 nm to 595 nm.

3.3 Results and Discussion

We report here on the effects of electrolyte concentration on the reorientation dynamics of resorufin in water and in NOP. Due to the differences in these bodies of data, we consider the NOP and aqueous solutions separately. Both systems are characterized by measurable interactions between the anionic chromophore and the cationic species present in solution. It is the difference in the sizes of the cations that are primarily responsible for the different reorientation dynamics observed in these two systems.

NOP Solutions. Resorufin is known to exhibit single exponential anisotropy decay dynamics in water and a two-component anisotropy decay in NOP with reorientation time constants in neat solvent.³⁰ In the work presented in chapter 2, we found that solvent-solvent interactions between NOP molecules dominated the environment formed around the resorufin chromophore, mediating its reorientation dynamics by restricting rotation to primarily about the axis perpendicular to the chromophore π -system plane (z-axis, Fig. 2.1). The addition of electrolytes, TBAB and TOAB, with hydrodynamic volumes larger than that of the solvent affects solvent organization and also gives rise to ionic interactions between the electrolyte and the chromophore, resulting in a change in the effective rotor shape of resorufin. The rotational decay times of resorufin in NOP exhibit an electrolyte concentration dependence in solutions containing TBAB and TOAB.

The induced orientational anisotropy function, R(t) is generated from the fluorescence transients polarized parallel, $I_{\parallel}(t)$, and perpendicular, $I_{\perp}(t)$, to the vertically polarized excitation pulse according to Eq. 2.2. It is the functional form of R(t) that contains information that can be

related to the local environment of the reorienting species. Chuang and Eisenthal have shown that R(t) can contain up to five exponential decay components.³¹ The most commonly observed functional forms are one- and two-component decays. The relationship between the number of decays and the time constant(s) recovered from R(t) depends on the orientation of the excited and emitting transition dipole moments relative to the molecular structure. For the transition moments oriented along the long (x) molecular axis, the functional form of R(t) is related to the Cartesian components of the solute rotational diffusion constant according to Eqs. 2.3 and 2.4, where D_x, D_y, and D_z are the Cartesian components of the rotational diffusion constant, D. We assign the x-axis to be the long axis in the chromophore π -system plane of resorufin, where y is taken to be short in-plane axis and z is the out-of-plane axis (Fig. 2.1). For a prolate rotor, the dominant motion is rotation about the x-axis $(D_x > D_y = D_z)$ and for the oblate rotor the dominant rotation is about the z-axis ($D_z > D_x = D_y$). The two-component decay for resorufin in NOP changes to a single exponential decay when a quaternary ammonium salt is added to the solution. This change in decay functionality corresponds to a change in the rotor shape of the reorienting moiety. We assert that this change is caused by interactions between the chromophore and the quaternary ammonium ions, and rationalize our findings as follows. The notion that the anionic chromophore can interact with the cationic ammonium species is based on simple ionic considerations. The change in rotor shape associated with this putative interaction is based on the relative sizes of the species present in solution. The chromophore is the smallest of the molecules in solution with a hydrodynamic volume of 165 Å³. The NOP solvent molecules have hydrodynamic volumes of 219 Å³,³² and the organization of the comparatively large solvent molecules around the chromophore mediates its reorientation dynamics, leading to the observed two-component anisotropy decay. With the addition of electrolyte, any association between the

resorufin anion and the ammonium cation will perturb the chromophore local environment. The hydrodynamic volumes of the non-aqueous electrolytes are 299 Å³ for TBAB and 571 Å³ for TOAB,³² therefore association of the chromophore and electrolyte will give rise to a substantial change in the volume and shape of the reorienting species. A visual representation of our assertion (Fig. 3.2) shows the rotational dynamics of resorufin change from the motion of an oblate rotor to a prolate rotor after forming a complex with a cation with a large hydrodynamic volume.

The hydrodynamic volume of the electrolyte relative to that of the chromophore can have a major influence on the local environment experienced by the reorienting moiety and we have shown that this effect is dependent on the concentration of the electrolyte. As the electrolyte concentration increases, the single exponential anisotropy decay exhibits an increasing reorientation time constant for both TBAB/NOP and TOAB/NOP solutions (Fig. 3.3). There are several possible explanations for this observation.

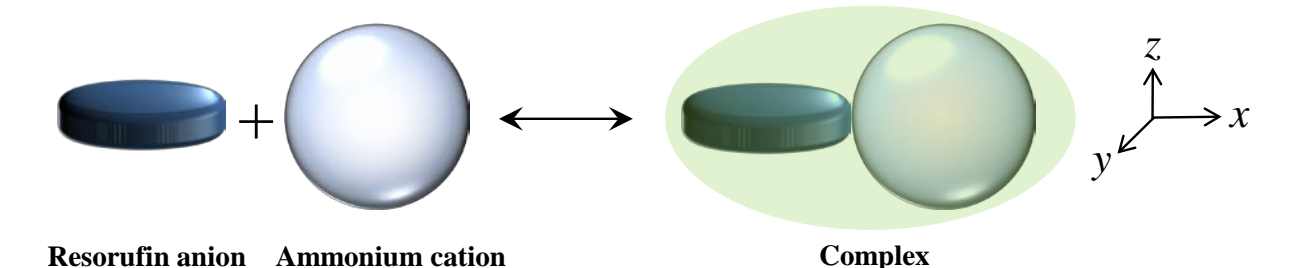


Figure 3.2 Illustration of the resorufin anion reorienting as an oblate rotor with diffusion primarily about the z-axis in neat NOP and sweeping out a volume representative of a prolate rotor after formation of a complex with a tetrabutyl- or tetraoctylammonium cation.

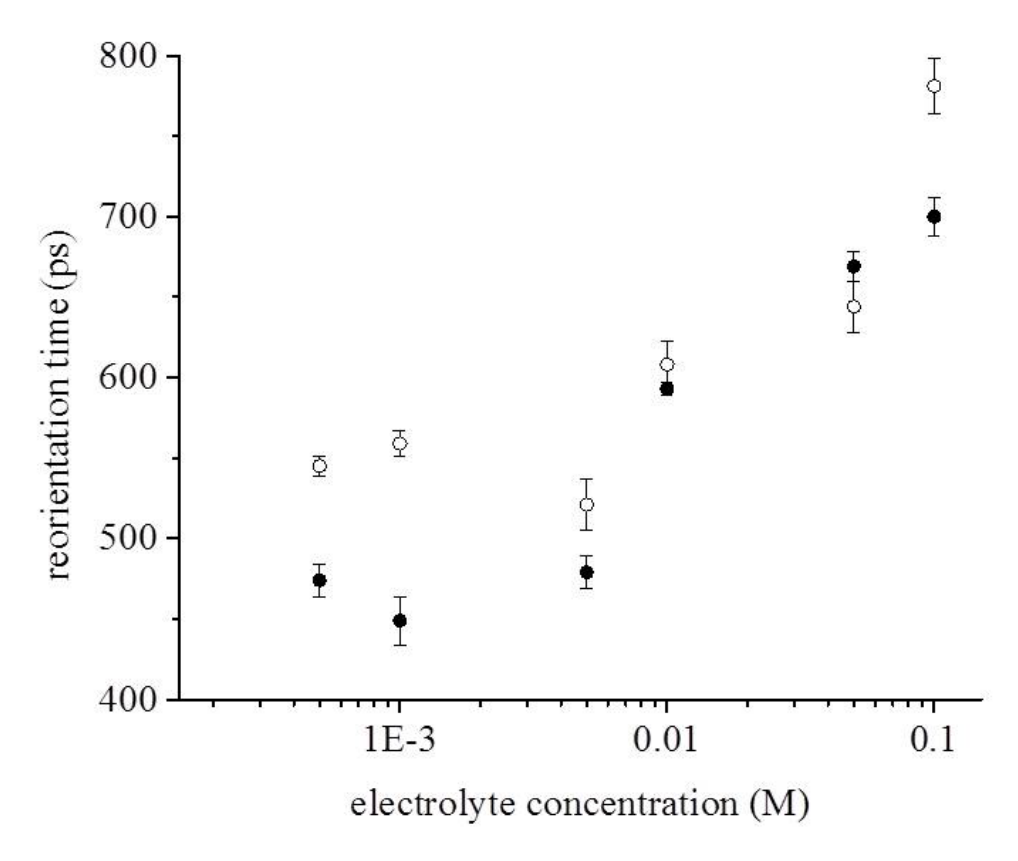


Figure 3.3 Reorientation time of the reorienting moiety as a function of electrolyte concentration (log_{10} scale) for resorufin in TBAB/NOP (filled circles) and TOAB/NOP (open circles). Error bars represent ± 1 standard deviation.

It is instructive to examine these data using the modified DSE model for rotational diffusion.²⁷⁻²⁹ The modified DSE equation relates the reorientation time to the properties of the solute and solvent (Eq. 3.1). In the context of this equation, the electrolyte concentrationdependent increase in the reorientation time constant, τ_{OR} , could be the result of an increase in local viscosity, an increase in the hydrodynamic volume of the reorienting moiety, or a decrease in temperature. The third possible explanation is ruled out because the experiments are performed at constant temperature. The friction factor, f, and shape factor, S, terms may also change with a change in electrolyte concentration but they would do so in concert with either n or V, respectively. The terms η and V can be evaluated within the framework of experimental data and existing, well established models. Balabai et al. showed that the reorientation times of resorufin exhibit a concentration dependence in electrolyte/methanol and electrolyte/DMSO solutions when normalized to the solvent viscosity.²² Their results point to a change in the hydrodynamic volume of the reorienting entity in the presence of electrolyte (or, more accurately, a change in V/S), and this finding can be accounted for in the context of complex formation between the anionic resorufin chromophore and the cationic electrolyte. For the experiments we report on here, the cations are quaternary amines with relatively large hydrodynamic volumes compared to the chromophore volume. If there is a direct contact ion pair complex formed, such a species would experience significantly slower rotational diffusion owing to its larger hydrodynamic volume. Based on our observation of the dependence of reorientation time on electrolyte concentration, we can use these data to estimate the equilibrium constant for the complex.

The hydrodynamic volume of the putative complex is given by the sum of the hydrodynamic volumes of resorufin and the cationic electrolyte. By using the DSE equation to

determine the effective hydrodynamic volume of the reorienting moiety as a function of electrolyte concentration, we can estimate the relative contributions of the free and complexed chromophore to each observed reorientation time. This interpretation assumes that the complex formation is a dynamic equilibrium with a characteristic exchange time on the order of the reorientation time or faster. For the determination of the complex equilibrium constant, we assume that the resorufin-electrolyte complex is characterized by 1:1 stoichiometry (Eq. 3.2),

$$k_{eq} = \frac{[R - E]}{[R][E]} \tag{3.2}$$

where [R–E] is the concentration of resorufin-electrolyte complex, and [R] and [E] are the concentrations of resorufin and the electrolyte, respectively. In order to solve for the equilibrium constant, k_{eq} , we use the concentrations of electrolyte in Table 3.1 and designate the ratio of resorufin-electrolyte complex to free resorufin to be (1-x)/x, where (1-x) and x are used as weighting factors for the complexed and free forms of resorufin, respectively. In this model, we determine the quantities x and 1-x at each electrolyte concentration using Eq. 3.3,

$$\tau_{OR} = (x)\tau_R + (1-x)\tau_{R-F} \tag{3.3}$$

where τ_R represents the reorientation time for uncomplexed resorufin and τ_{R-E} is the reorientation time for the resorufin–electrolyte complex. The key to the accuracy of this model is the ability to evaluate τ_R and τ_{R-E} .

There are two approaches to the evaluation of τ_R and τ_{R-E} . The first is to use modified DSE model parameters to achieve agreement, or alternatively to use an empirical factor to achieve agreement between model and experiment. Regardless of the methodology used, the functional dependence of the model used on the hydrodynamic volume of the reorienting moiety does not change.

Table 3.1 Reorientation times, τ_{OR} , of resorufin in neat NOP and NOP with various concentrations of TBAB or TOAB electrolytes.

Electrolyte Concentration (M)		NOP ³⁰ R (ps) slow	NOP w/ TBAB τοr (ps)	NOP w/ TOAB τοr (ps)
0	347 ± 19	1432 ± 172		
5×10^{-4}			474 ± 10	545 ± 6
1×10^{-3}			449 ± 15	559 ± 8
5×10^{-3}			479 ± 10	521 ± 16
1×10^{-2}			593 ± 4	608 ± 15
5×10^{-2}			669 ± 9	644 ± 16
1×10^{-1}			700 ± 12	781 ± 17

In the first case, if we assume a stick limit solute-solvent boundary condition (f = 1), the agreement between model predictions and experimental data is poor, which is not surprising. For the vast majority of polar and ionic species in water or other polar solvents, the measured reorientation time constants exceed those predicted by the modified DSE model in the stick limit. The reasons for this behavior have not been resolved fully, but it is typically held that strong, associative solute-solvent interactions are responsible. In this case, reaching agreement between experiment and model is best achieved through the use of an empirical correction factor. For the experiments reported here, we find that the empirical factor required to achieve agreement between model and experiment for τ_R is (f/S = 2.49). The molecular dimensions of resorufin lead to a shape factor, S, of 0.768, implying a value of f = 1.91, which exceeds the limits of the model. Using this same correction factor and the sum of the hydrodynamic volumes of resorufin and TOAB allow for the calculation of τ_{R-E} . The theoretical reorientation time calculated for free resorufin using f/S = 2.49 is 555 ps, and the calculated value of τ_{R-E} for complexation with TOAB is 2476 ps. Using these values for τ_R and τ_{R-E} , and the τ_{CR} data given in Table 3.1, we

apply Eqs. 3.2 and 3.3 to extract the equilibrium constant, $k_{eq} = 2 \pm 1$ for the resorufin-TOAB complex. Applying the same data analysis to resorufin in TBAB/NOP solution yields a value of $k_{eq} = 11 \pm 8$. For both systems, there is significant uncertainty associated with the experimentally determined values of k_{eq} , but the key point is that these values are modest. Resorufin forms a stronger complex with the tetrabutylammonium cation than with the tetraoctylammonium cation, consistent with screening effects associated with the length of the cation alkyl chains of the tetraoctylammonium cation. We have examined the steady-state spectra of resorufin in NOP as a function of electrolyte concentration and have also used semi-empirical calculations (Hyperchem®) to evaluate the likely intermolecular interactions that are responsible for the formation of the complexes we have observed.

The existence of the complex has little effect on the steady-state absorption and emission spectra of resorufin in TBAB/NOP and TOAB/NOP solution. The normalized absorption spectra (Fig. 3.4a) and emission spectra (Fig. 3.4b) exhibit only minor spectral shifts with the addition of TOAB. There are subtle changes in the vibronic band intensities for both the absorption and emission spectra, which are suggestive of the interaction of the chromophore with the cation, but the subtle intensity variations of these bands do not allow for a detailed understanding of the nature of the interaction(s). In conjunction with semi-empirical calculations (not shown), where the most stable complex is between the resorufin terminal carbonyl groups and the tetraalkylammonium cation, we can infer that the spectral changes shown in Fig. 3.4 are related primarily to the chromophore C=O groups.

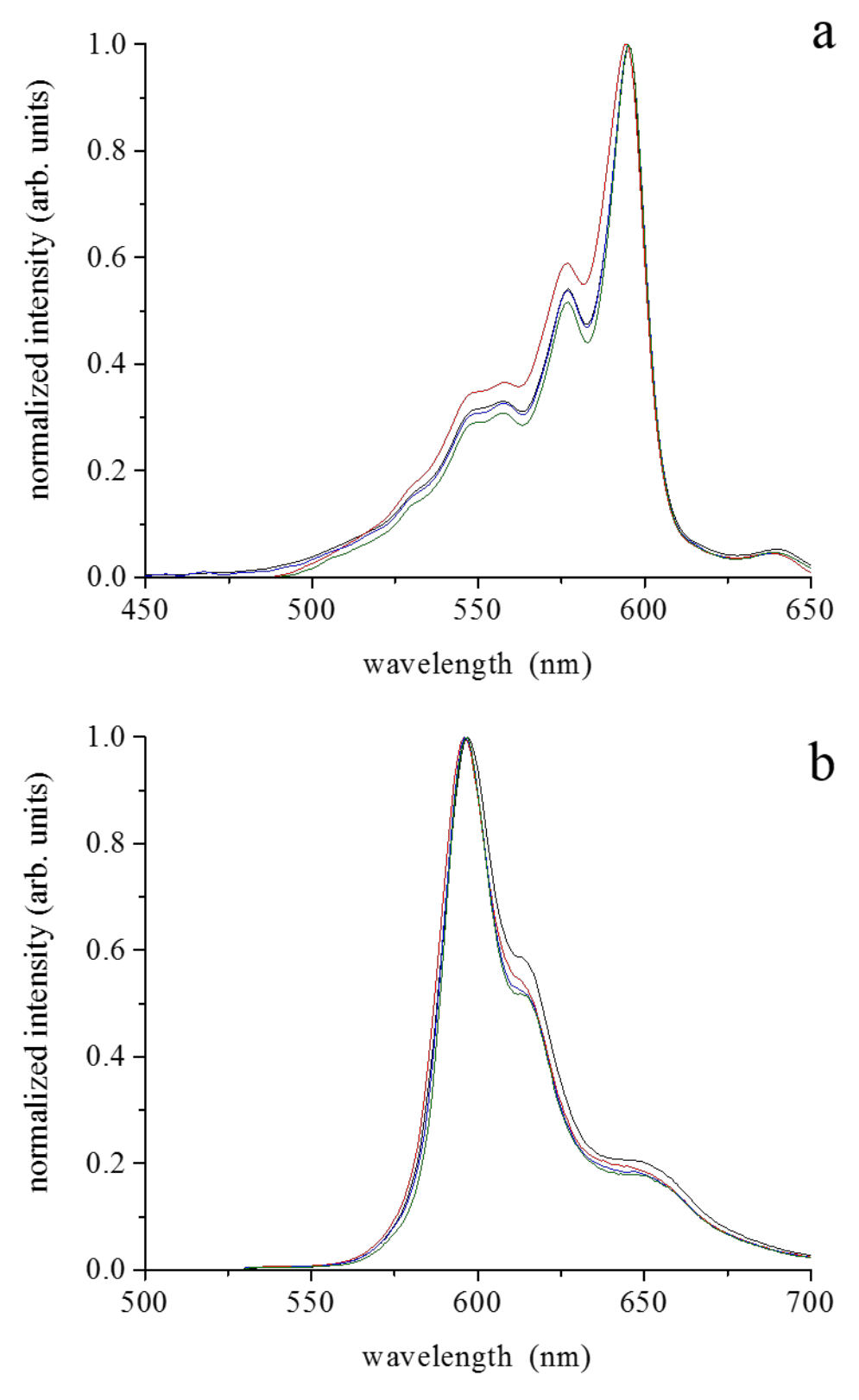


Figure 3.4 Normalized (a) absorption and (b) emission spectra of resorufin in neat NOP (black), 10^{-3} M TOAB (red), 10^{-2} M TOAB (blue), and 10^{-1} M TOAB (green).

The semi-empirical calculations indicate that for interactions between the cation and the chromophore, the closest approach of the cation is ca. 4.5 Å if the approach is along the chromophore z-axis (perpendicular to the π -plane). For the cation approaching along the chromophore x-axis (long in-plane axis), the optimum interaction distance is calculated to be ca. 3.2 Å. We hasten to point out that these results should not be taken as proof of any complex geometry, but rather that chromophore-cation interactions in the π -plane of the chromophore are favored over interactions perpendicular to the chromophore π -plane. This result is consistent with the reorientation data, where the chromophore reorients as a prolate rotor in the presence of the electrolyte. Complexation with the chromophore end group(s) would serve to diminish rotation about the z-axis relative to rotation about the x-axis, making rotation about the x-axis the dominant rotational motion (Fig. 3.2).

Aqueous solutions. In contrast to the results obtained for resorufin in electrolyte/NOP solution, the reorientation dynamics of resorufin in aqueous electrolyte solutions exhibit a decrease in the reorientation time constant with increasing electrolyte concentration (Fig. 3.5). The reorientation time constant ranges from 130 ps at 5 × 10⁻³ M LiClO₄ to 100 ps for 10⁻¹ M LiClO₄ (Table 3.2). A comparison of these data to the reorientation time constant for resorufin in water (133 ps, Table 3.2), shows that the low concentrations of electrolyte have a negligible effect on the reorientation of resorufin.³⁰ Previous studies on the reorientation of resorufin in Li⁺ containing electrolyte solution show the reorientation times in water increasing, but the effect of concentration is much less significant in water compared to other solvents, such as methanol and DMSO.^{20,22} The reorientation time of resorufin increased by almost 400% for neat DMSO vs.

change for resorufin in water that we report here suggests that the concentration dependence is not linearly dependent on electrolyte concentration (Fig. 3.5).

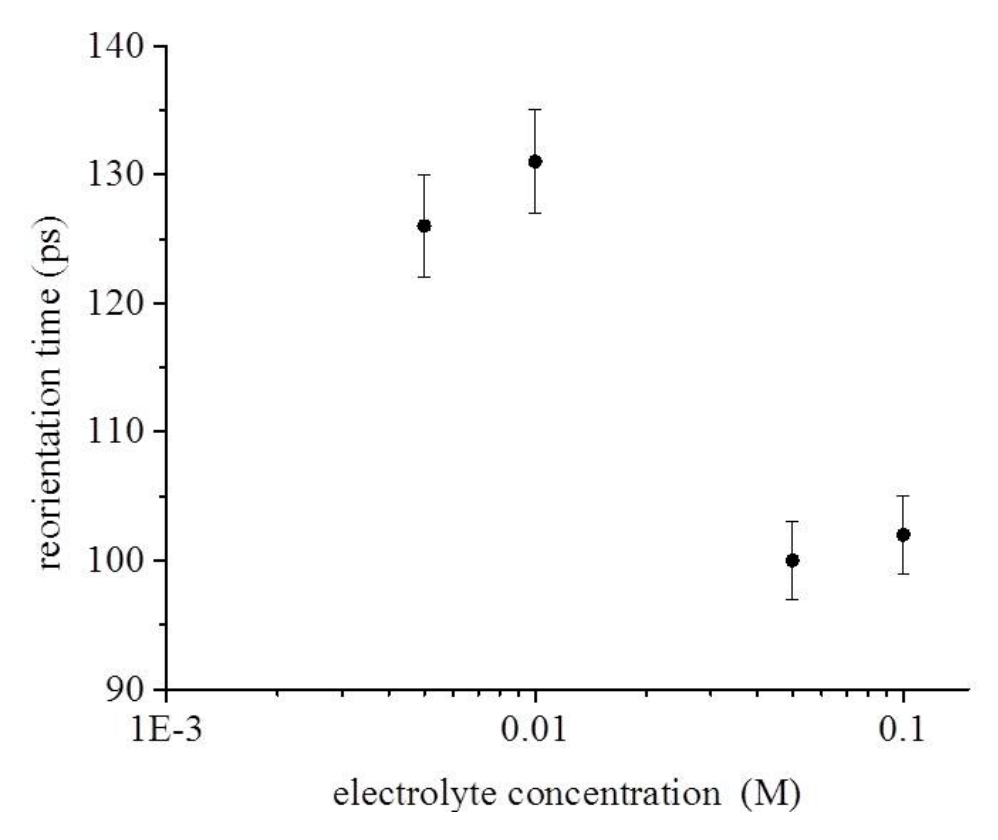


Figure 3.5 Reorientation time as a function of electrolyte concentration (log_{10} scale) for resorufin in aqueous LiClO₄. Errors bars represent \pm 1 standard deviation.

Table 3.2 Reorientation times, τ_{OR} , of resorufin in water and various concentrations of LiClO₄(aq).

Electrolyte Concentration (M)	Water ³⁰ τοr (ps)	LiClO ₄ (aq) τ _{OR} (ps)
0	133 ± 11	
5×10^{-3}		126 ± 4
1×10^{-2}		131 ± 4
5×10^{-2}		100 ± 3
1 × 10 ⁻¹		102 ± 3

Our data are consistent with complexation between the resorufin chromophore and Li⁺, where for low concentrations the free anionic chromophore is observed and for higher Li⁺ concentrations, a Li⁺-resorufin complex is present. We attribute the faster reorientation time of the Li⁺-resorufin complex to be a consequence of the complex being a neutral moiety, where solute-solvent interactions are different than those with the anionic chromophore. It is important to consider that the Li⁺ ion will exist in a hydrated form in aqueous solution and the fate of the waters of hydration is not clear when complexation with resorufin occurs. Regardless of the fate of the waters of hydration, the formation of a Li⁺-resorufin complex gives rise to a neutral reorienting species in solution. The absorption and emission spectra of resorufin, with and without Li⁺ present indicate that the primary interaction occurs between Li⁺ and the ground state chromophore (Fig. 3.6).

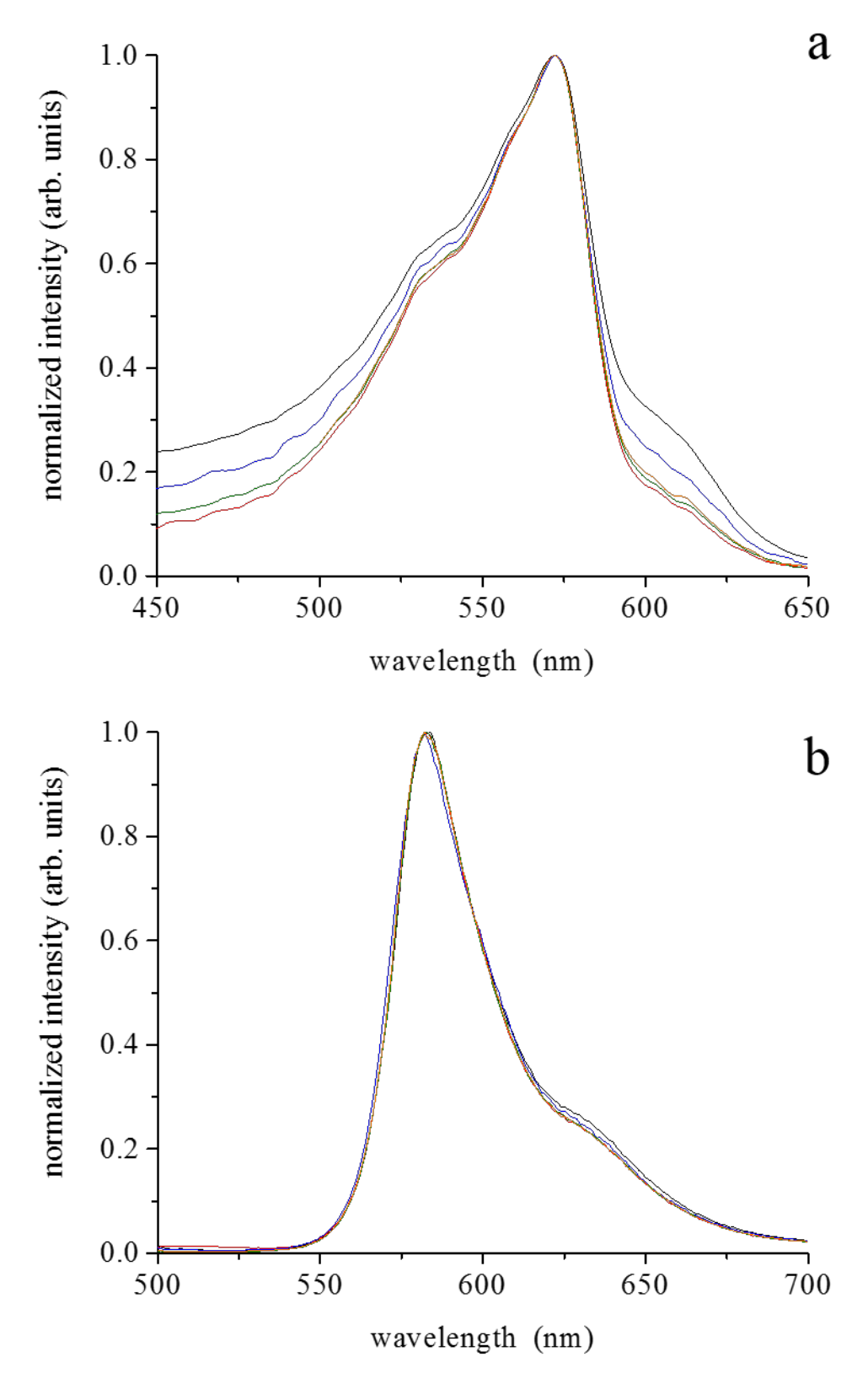


Figure 3.6 Normalized (a) absorption and (b) emission spectra of resorufin in water (black), 5×10^{-3} M LiClO₄ (red), 10^{-2} M LiClO₄ (blue), 5×10^{-2} M LiClO₄ (green), and 10^{-1} M LiClO₄ (orange).

It is clear that the details of the interactions between the comparatively small Li cation and resorufin in water are fundamentally different than those observed for the same chromophore with quaternary ammonium salts in NOP, but our findings do provide consistent evidence for the propensity of the resorufin anion to form ionic complexes with a number of cations in different solvents. This finding is consistent with earlier reports of Na⁺-resorufin interactions in the series of butanols.³³ Resorufin is a useful probe for the interrogation of ionic interactions in a variety of different systems.

3.4 Conclusions

We have examined the effect of electrolyte concentration on the rotational diffusion dynamics of the anionic chromophore resorufin in aqueous and NOP solutions. There is a change in the chromophore rotor shape from oblate to prolate for reorientation in NOP upon the addition of quaternary ammonium salts to the solution. These findings are consistent with interactions between the anionic chromophore and the cationic quaternary ammonium species, and from the dependence of the reorientation time constants on electrolyte concentration we can estimate the equilibrium constant for the complex to be 2 ± 1 for TOAB and 11 ± 8 for TBAB. The absorption and emission spectra in conjunction with semi-empirical calculations indicate that the ionic complexation occurs along the chromophore long in-plane axis with the carbonyl (=O) functionalities, and this finding is consistent with the change of effective rotor shape reported for the reorientation experiments.

Qualitatively different behavior is observed for resorufin in water. The addition of LiClO₄ to aqueous resorufin solutions causes a decrease in the measured reorientation time constant. These data are also consistent with the formation of an ionic complex, but in this system where the cation is comparatively small, the dominant change in reorientation dynamics

is the result of the complex being a nominally neutral species. For both aqueous and NOP systems, we find that resorufin complexes relatively efficiently with cationic species present in solution, with the detailed manner in which this complexation phenomenon is manifested depending on the specific cationic species used and its size relative to that of the chromophore. The next two chapters describe the rotational diffusion dynamics in interfacial systems containing water and NOP.

REFERENCES

REFERENCES

- 1. Ben-Amotz, D.; Scott, T. W. Journal of Chemical Physics 1987, 87, 3739.
- 2. Ben-Amotz, D.; Drake, J. M. Journal of Chemical Physics 1988, 89, 1019.
- 3. Blanchard, G. J.; Cihal, C. A. Journal of Physical Chemistry 1988, 92, 5950.
- 4. Blanchard, G. J. Journal of Physical Chemistry 1988, 92, 6303.
- 5. Wiemers, K.; Kauffman, J. F. Journal of Physical Chemistry A 1999, 104, 451.
- 6. Dela Cruz, J. L.; Blanchard, G. J. Journal of Physical Chemistry A 2001, 105, 9328.
- 7. Gayathri, B. R.; Mannekutla, J. R.; Inamdar, S. R. Journal of Fluorescence 2008, 18, 943.
- 8. Madden, P.; Kivelson, D. Journal of Physical Chemistry 1982, 86, 4244.
- 9. Kivelson, D.; Spears, K. G. Journal of Physical Chemistry 1985, 89, 1999.
- 10. Dutt, G. B.; Doraiswamy, S.; Periasamy, N.; Venkataraman, B. *Journal of Chemical Physics* **1990**, *93*, 8498.
- 11. Hartman, R. S.; Alavi, D. S.; Waldeck, D. H. Journal of Physical Chemistry 1991, 95, 7872.
- 12. Spears, K. G.; Steinmetz, K. M. Journal of Physical Chemistry 1985, 89, 3623.
- 13. Gudgin Templeton, E. F.; Quitevis, E. L.; Kenney-Wallace, G. A. *Journal of Physical Chemistry* **1985**, *89*, 3238.
- 14. Blanchard, G. J. Journal of Chemical Physics 1987, 87, 6802.
- 15. Kenney-Wallace, G.; Paone, S.; Kalpouzos, C. Faraday Discussions 1988, 85, 185.
- 16. Blanchard, G. J. Journal of Physical Chemistry 1989, 93, 4315.
- 17. Blanchard, G. J. Journal of Physical Chemistry 1991, 95, 5293.
- 18. Alavi, D. S.; Waldeck, D. H. Journal of Physical Chemistry 1991, 95, 4848.
- 19. Zhou, P. W.; Song, P.; Liu, J. Y.; Shi, Y.; Han, K. L.; Het, G. Z. *Journal of Physical Chemistry A* **2008**, *112*, 3646.
- 20. Hartman, R. S.; Konitsky, W. M.; Waldeck, D. H. *Journal of the American Chemical Society* **1993**, *115*, 9692.

- 21. Balabai, N.; Waldeck, D. H. Journal of Physical Chemistry B 1997, 101, 2339.
- 22. Balabai, N.; Kurnikova, M. G.; Coalson, R. D.; Waldeck, D. H. *Journal of the American Chemical Society* **1998**, *120*, 7944.
- 23. Argaman, R.; Huppert, D. Journal of Physical Chemistry B 2000, 104, 1338.
- 24. Argaman, R.; Molotsky, T.; Huppert, D. Journal of Physical Chemistry A 2000, 104, 7934.
- 25. Dutt, G. B.; Ghanty, T. K. Journal of Physical Chemistry B 2003, 107, 3257.
- 26. Esquivelzeta-Rabell, M.; Peon, J.; Cuevas, G. *Journal of Physical Chemistry B* **2009**, *113*, 8599.
- 27. Debye, P. *Polar Molecules* Chemical Catalog Co.: New York 1929.
- 28. Hu, C. M.; Zwanzig, R. Journal of Chemical Physics 1974, 60, 4354.
- 29. Perrin, F. Journal of Physics and Radium 1934, 5, 497.
- 30. Hay, C. E.; Marken, F.; Blanchard, G. J. Journal of Physical Chemistry A 2010, 114, 4957.
- 31. Chuang, T. J.; Eisenthal, K. B. Journal of Chemical Physics 1972, 57, 5094.
- 32. Edward, J. T. Journal of Chemical Education 1970, 47, 261.
- 33. Rasimas, J. P.; Blanchard, G. J. Journal of Physical Chemistry 1996, 100, 11526.

Chapter 4

Detection and Characterization of a Liquid|Solid Interfacial Compositional Gradient of Water Nano-Droplets in Wet N-Octyl-2-Pyrrolidone

4.1 Introduction

The study of liquid-solid interfaces has attracted significant interest because of the central role such interfaces play in areas ranging from tribology through chemical sensing and separations to electrode processes and reactions. The examination of the liquid phase at and near such interfaces typically relies on the use of techniques that were designed for the study of bulk liquids and, as such, there is limited information available on the organization of the interfacial region. Electrochemical studies have, of course, provided exquisitely detailed information on the organization of solutions in contact with electrode surfaces, and there is a well-established body of theoretical understanding of the electric double layer and short range organization at the electrode surface itself.¹⁻³ It is well established that the spatial extent of surface charge effects is on the order of tens to hundreds of nanometers, at most. Beyond this distance it is held that the liquid phase behaves in the same manner as the corresponding bulk liquid.

Many processes of central importance to chemical and physical events that occur at the liquid-solid interface can extend over µm length scales. Diffusion, precipitate formation, and the existence of temperature gradients are three examples. It is thus of fundamental interest to understand the limit(s) to the validity of the assumption that liquids located at the liquid-solid interface behave as bulk liquids over distances on the order of microns. It is the purpose of this work to investigate two chemical systems; one that is expected to behave as a bulk liquid and one that has the potential to exhibit anomalous behavior. The two systems studied are ethylene glycol (EG) and N-octyl-2-pyrrolidone (NOP), each at a borosilicate glass interface. EG is miscible with water in all proportions and is expected to exhibit properties of a bulk liquid in the

presence or absence of water, whereas amphiphilic NOP is not completely miscible with water. NOP readily phase separates from water at room temperature and has a lower consolute temperature below 0 °C.^{4,5} The solubility of water in NOP is not reported explicitly, although phase diagrams indicate a single phase may exist at water concentrations less than 40% (w/w).^{5,6} The low miscibility of water in NOP, as well as the possibility of the formation of secondary structures in the presence of water provides an opportunity for anomalous behavior.

While there are a variety of ways to study the liquid-solid interface, examining such an interface with a depth resolution of less than one µm and an operating depth range on the order of 100 µm, and providing spatially localized information on viscoelastic properties can be a significant challenge. We use a confocal scanning microscope equipped with time-resolved detection gear to resolve the fluorescence lifetime and reorientation dynamics of a chromophore in the liquid phase with ca. 50 ps time resolution. Using this instrument we have demonstrated previously the ability to obtain fluorescence lifetime and anisotropy decay images for planar supported lipid bilayer structures.^{7,8} This is the first report utilizing this instrument primarily for its ability to achieve depth resolution, as opposed to lateral resolution. We have found that the lifetime and anisotropy decay dynamics of a rhodamine chromophore behave in the expected manner, more or less as a bulk liquid, when measured as a function of distance from the solvent|glass interface for the solvent EG. For the interface between NOP containing water (wet NOP) and glass, we resolve a depth dependent gradient in fluorescence anisotropy decay dynamics that persists for tens of microns into the liquid phase. Using the information from these two interfacial systems, we are able to identify the presence of a compositional inhomogeneity in the wet NOP system in the form of a nano-emulsion. We consider the possible origins of this interfacial gradient.

The contribution of NOP as a minor component in industrial products is well-established, however, there is limited information on NOP as a major component contributing to the uptake and solvation of polar molecules. Longer chain N-alkyl-2-pyrrolidones including NOP exhibit surface activity in aqueous solutions and are effective as co-surfactants forming micelles with anionic surfactants.^{4,9} The work presented in chapter 2 on the decay dynamics of chromophores solvated in neat NOP illustrated the role of solvent-solvent interactions in mediating solute-solvent interactions and the impact on rotational diffusion.¹⁰ The solvation of chromophores by NOP was markedly different than that seen for water. In the binary mixture of NOP and water studied here, we are interested in the composition of wet NOP and the interactions that influence the solvation and local environment experienced by the fluorescent probe molecule.

4.2 Experimental Methods

The chromophore lissamine rhodamine B sulfonyl chloride (LRSC) (Fig. 4.1a, ≥ 99% Acros Organic) was used as received. N-octyl-2-pyrrolidone (NOP) (Fig. 4.1b, 98% Aldrich) and ethylene glycol (EG) (≥ 99%, Macron Fine Chemicals) were used as received. Water used in these studies was purified in-house with a Milli-Q filtration system (Millipore). For steady-state absorbance and emission measurements, the chromophore concentration was 10⁻⁴ M in water and dry NOP. The concentration of LRSC in EG was 10⁻⁵ M. Upon exposure to water, the chromophore is likely hydrolyzed to the sulfonic acid. We refer to the chromophore as LRSC throughout because we have not verified the hydrolysis reaction for each system. The sample holder for optical measurements on the microscope was an Attofluor® cell chamber (Invitrogen) fitted with a round borosilicate glass coverslip (25 mm diameter, No. 1.5 Thomas Scientific). In order to contain the liquid samples in a smaller area, a glass microscope slide (1 mm thick, 1.7 cm diameter, Globe Scientific) with a bored hole (inner diameter of 5.1 mm) was placed in the

sample holder. Solutions of 10⁻⁴ M LRSC in dry NOP were exposed to water for 3 hours and then approximately 150 μL was deposited in the center of the bored microscope slide onto a clean glass surface. Excess liquid filled the space between the glass surface and the microscope slide. The microscope slide and coverslips were cleaned prior to use by immersing in piranha solution (a 3:1 ratio of concentrated sulfuric acid and 30% hydrogen peroxide – caution *strong oxidizer*!) for 30 minutes. An alternative method of cleaning the borosilicate glass slides was rinsing with ethanol prior to exposure to UV-generated ozone for 15 minutes.

Figure 4.1 Structures of (a) lissamine rhodamine B sulfonyl chloride (LRSC) and (b) Noctyl-2-pyrrolidone (NOP).

Steady-state absorbance measurements were made with an ATI Unicam double-beam UV-visible absorbance spectrophotometer over the range of 400 nm to 700 nm, at a spectral resolution of 1 nm for all measurements. Steady-state spontaneous emission spectra were recorded using a Jobin-Yvon Fluorolog III spectrometer over the range of 550 nm to 700 nm. The excitation wavelength was set to 540 nm for LRSC in water and NOP emission spectral acquisition.

The fluorescence lifetime and anisotropy decays were collected with the time-resolved fluorescence imaging instrument (Fig. 4.2) described previously. A brief description of the instrumental set-up is provided here. The light source for the system is a CW mode-locked Nd:YVO4 laser that produces 13 ps pulses at 1064 nm with an 80 MHz repetition rate (Spectra Physics Vanguard). The Nd:YVO4 laser second or third harmonic output excites a cavity-dumped dye laser (Coherent 702-2), with output characterized by 5 ps pulses at wavelengths between 430 nm and 850 nm. The repetition rate of the laser is adjustable between 80 kHz and 80 MHz using the cavity dumping electronics. The dye used to excite the samples was pyrromethene 567 (Exciton), providing excitation wavelengths between 550 nm and 595 nm. The average power at the sample is 1 mW or less.

A vertically polarized pulse of light is input to an inverted optical microscope (Nikon Eclipse Ti-U) through a confocal scanner (Becker & Hickl DCS-120). The excitation pulses pass through the microscope objective and the focused beam can be localized at one position or rastered across the surface of the sample using the galvo-drive unit (Becker & Hickl GDA-120) in the confocal scanner. The emission collected by the microscope objective is split into parallel and perpendicular polarized signal components in the confocal scanner, passed through long-pass and bandpass wavelength selection filters, and detected using two avalanche photodiode

detectors (ID-Quantique ID100). Time-correlated single photon counting (TCSPC) detection electronics (Becker & Hickl SPC-152) are used for signal processing and collection. SPCM software (Becker & Hickl) for a Windows-based PC is used to control the data acquisition parameters.

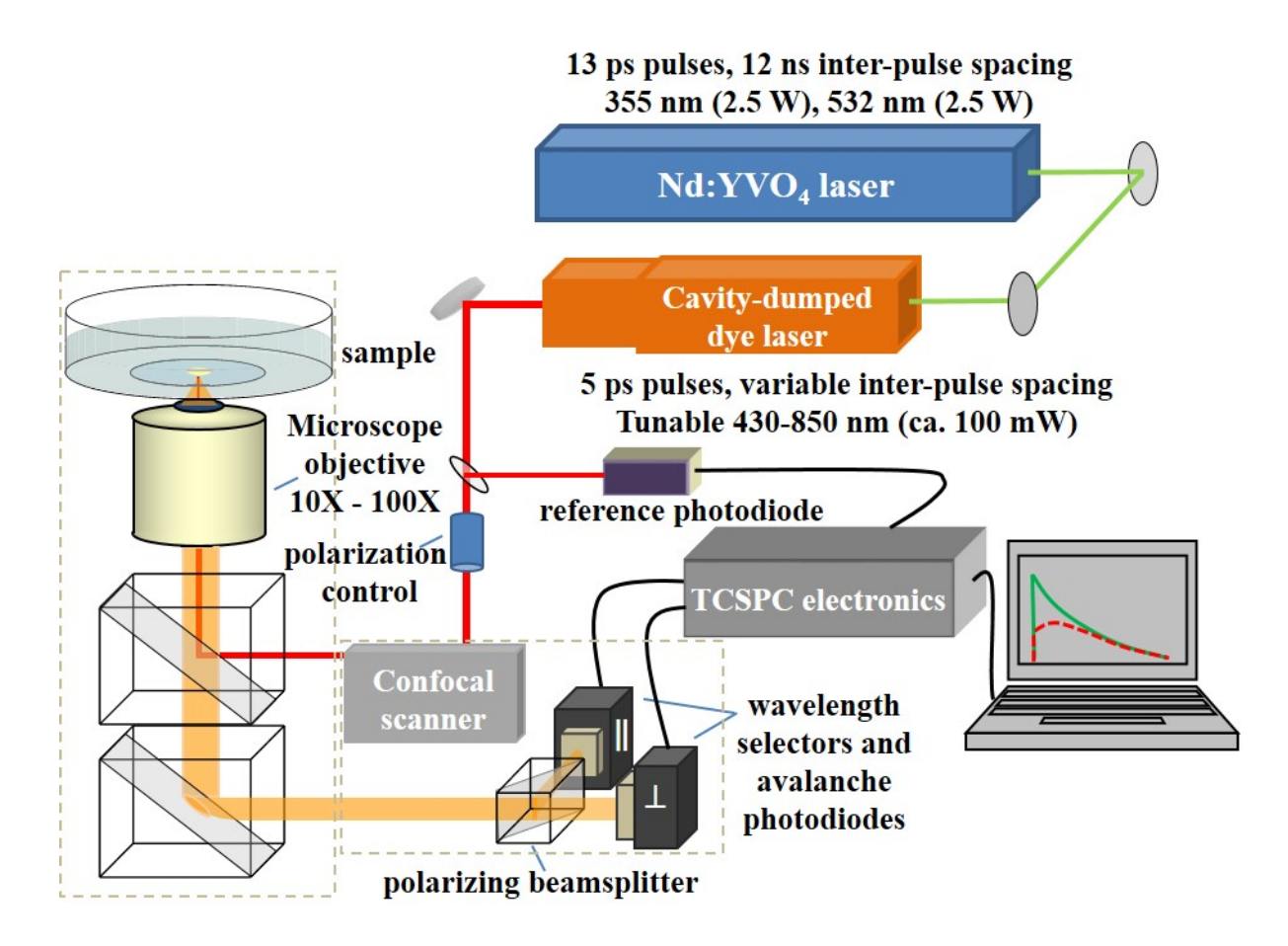


Figure 4.2 Time-resolved fluorescence lifetime and anisotropy imaging instrument with time-correlated single photon counting (TCSPC) detection.

An oil immersion microscope objective (Nikon, 100X magnification, NA 1.45, working distance 0.13 mm, depth of field *ca.* 0.45 µm) was used for all data acquisition, and the experimental setup is schematized in Fig. 4.3. Depth profiles were generated by collecting individual data sets in triplicate with the beam parked at a fixed position. The positions along the *x*-axis were fixed using the SPCM galvanometer control window and the depth along the *z*-axis was controlled mechanically. The time-resolved fluorescence data were analyzed using MicroCal Origin Pro v. 9.0 to obtain fluorescence lifetime and anisotropy decay time constants.

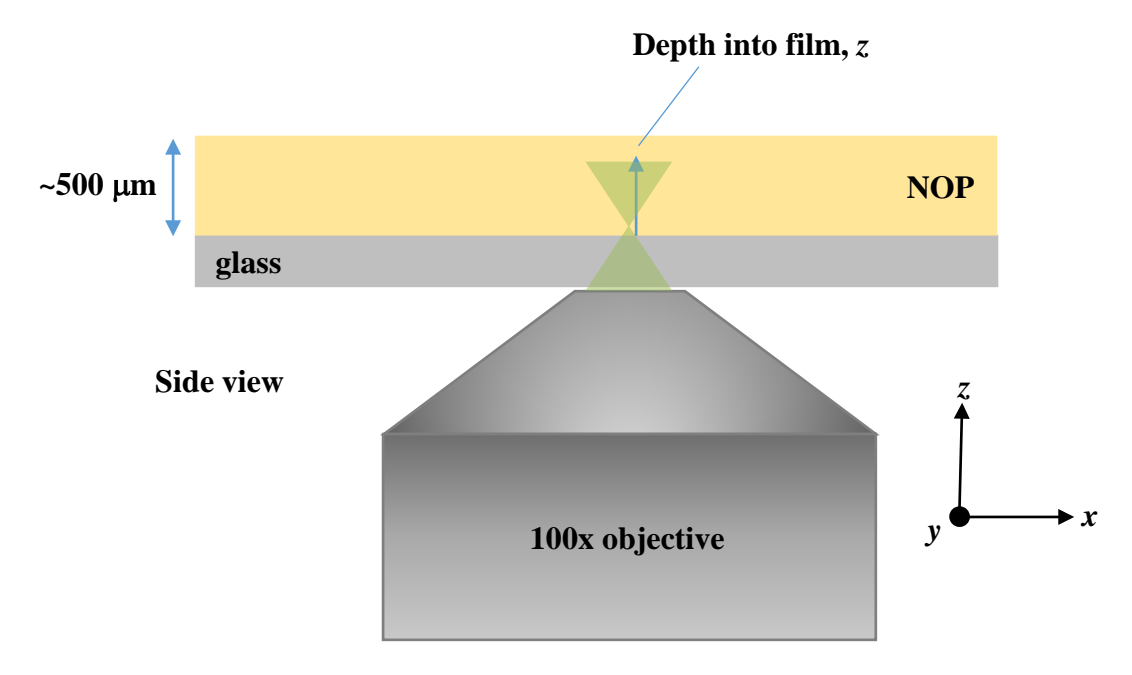


Figure 4.3 Schematic of sample and optical excitation/collection configuration for NOP|glass and EG|glass interfaces. (NOP|glass interface shown.)

Particle size determinations were performed by dynamic light scattering (DLS) using a Malvern Zetasizer Nano ZS with a 632.8 nm light source for dry NOP and NOP exposed to water. All measurements were made at 20 ± 1 °C. The wet NOP was prepared by adding dry NOP to a layer of water in a glass vial, where NOP was 6.67% (v/v). The NOP layer was removed and analyzed by DLS.

4.3 Results and Discussion

An important area of understanding in interfacial science is the role that the solid (interface) may play in mediating organization of the liquid phase(s) in contact with it. This is a well explored and understood area in the context of solution|electrode interfaces, for example, where control over the potential of the electrode surface allows for the evaluation of short range electrostatic or Coulombic forces on solution phase local organization. It is understood that the spatial extent of the electric double layer is less than one micron, typically much less. ^{1,2,11} We report in this paper on the existence of a gradient in the fluorescence anisotropy decay dynamics of LRSC in wet NOP present at a glass surface, as a function of distance from the surface. This gradient is anomalous because of its spatial extent and we are concerned with understanding the fundamental reason(s) for its existence. Achieving this understanding will allow for such gradients to be predicted and, possibly, the extent and nature of the gradient to be controlled for pre-determined purposes.

The instrumentation we have used to acquire information on interfacial organization and dynamics is designed to acquire images in the plane of the sample (x,y) (see Fig. 4.3).^{7,8} For the work we report here, the sample is uniform in the x,y plane and we have examined the depth (z) dependence of chromophore lifetime and dynamics. Because this imaging instrument is confocal, the z-resolution (depth of focus) is sub- μ m, and the data have been acquired at 10 μ m z-intervals. Each data point presented is the average of at least five individual measurements, with the uncertainties being reported as the standard deviation $(\pm 1\sigma)$ of the average of the individual acquisitions.

The fluorescence lifetimes and anisotropy decays plotted as a function of distance from the NOP|glass interface are shown in Fig. 4.4. There are several important features contained in

these data. The first is that at the interface, the chromophore is adsorbed on or interacting with the glass support and its fluorescence lifetime and anisotropy decay time constants are different than for the liquid NOP layer. This is not surprising given the polar nature of the chromophore and the interface and the comparatively less polar NOP solvent. The second feature of note is that, to within the experimental uncertainty, the fluorescence lifetime is constant as a function of depth into the NOP layer. We believe that this is likewise not a surprising result. The third feature contained in these data is the depth dependence of the anisotropy decay time constant. The existence of a depth dependence is reproducible and unexpected. The aim of this work is to describe the physical and chemical basis for this finding.

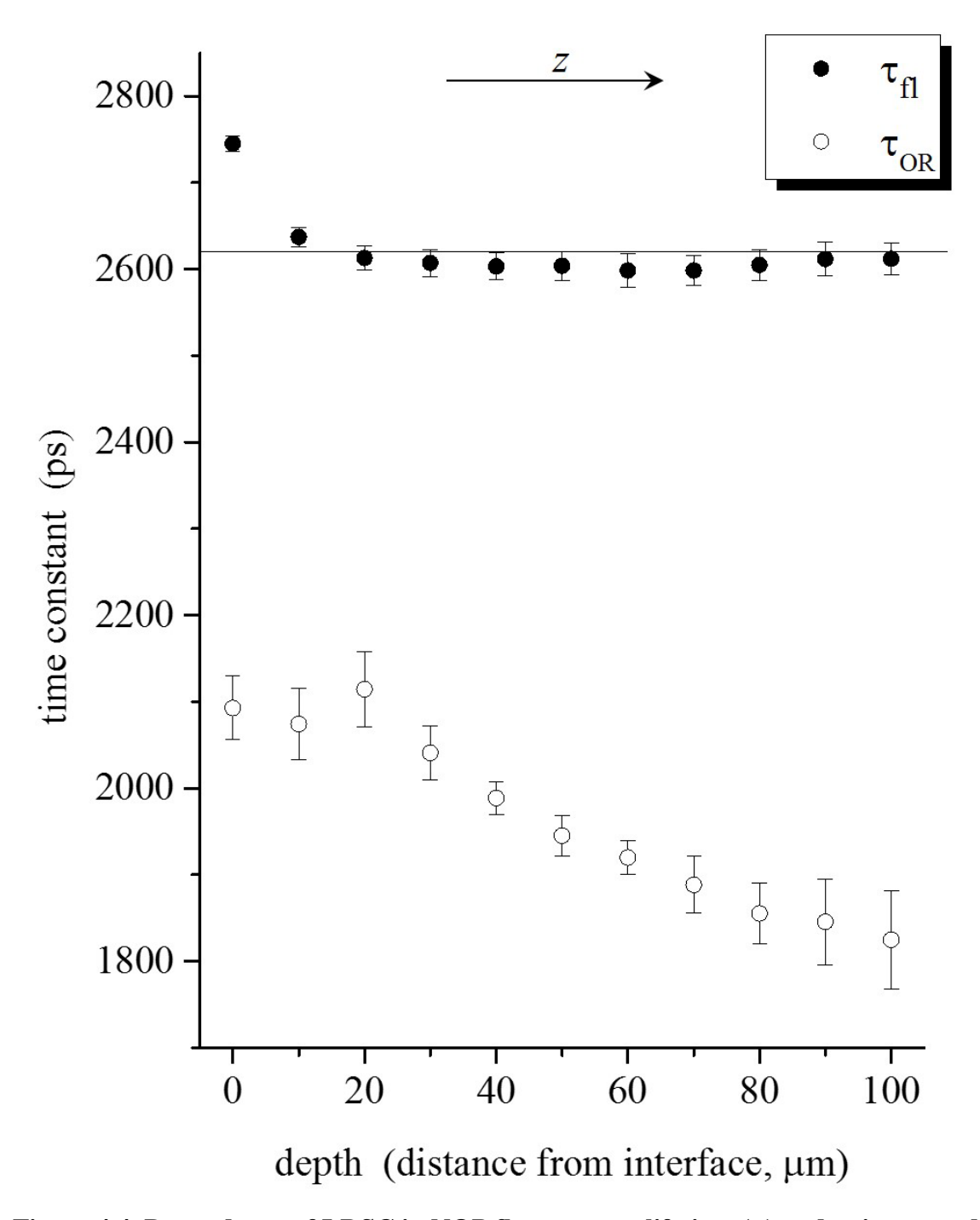


Figure 4.4 Dependence of LRSC in NOP fluorescence lifetime (\bullet) and anisotropy decay time constant (\circ) on distance from the glass interface. The line drawn through the fluorescence lifetime data is intended as a guide to the eye. The glass support was cleaned with piranha solution and rinsed with water prior to use. Refer to Fig. 4.3 for the experimental configuration and the x, y, z coordinate designation.

Before turning to a detailed interpretation of these findings, it is instructive to consider several potential causes. We presume that the depth dependence of the anisotropy decay time constant seen in Fig. 4.4 is the result of either an electric field gradient or a compositional gradient. One of the first issues that must be addressed is whether or not this effect is a result of contamination. The cleaning of the glass surface could, in principle, leave residue that could diffuse slowly into the NOP solvent system. We cleaned the glass support used for the data reported in Fig. 4.4 using piranha solution, followed by rinsing with deionized water (vide infra). If there were any residue remaining from the washing process it could potentially diffuse from the surface and create a compositional gradient, the form of which would change over time. For this reason, we performed the same study using a glass support that had been rinsed with ethanol and then cleaned using a UV/ozone cleaner. Any residual contaminant profile for this interface would be different than for the interface cleaned with piranha solution and rinsed with water. We show the results obtained for the ethanol/ozone prepared surface in Fig. 4.5. These results show an identical trend to those shown in Fig. 4.4, and from this comparison we conclude that contamination resulting from preparation of the support surface does not contribute to the depth dependence of the LRSC anisotropy decay we observe.

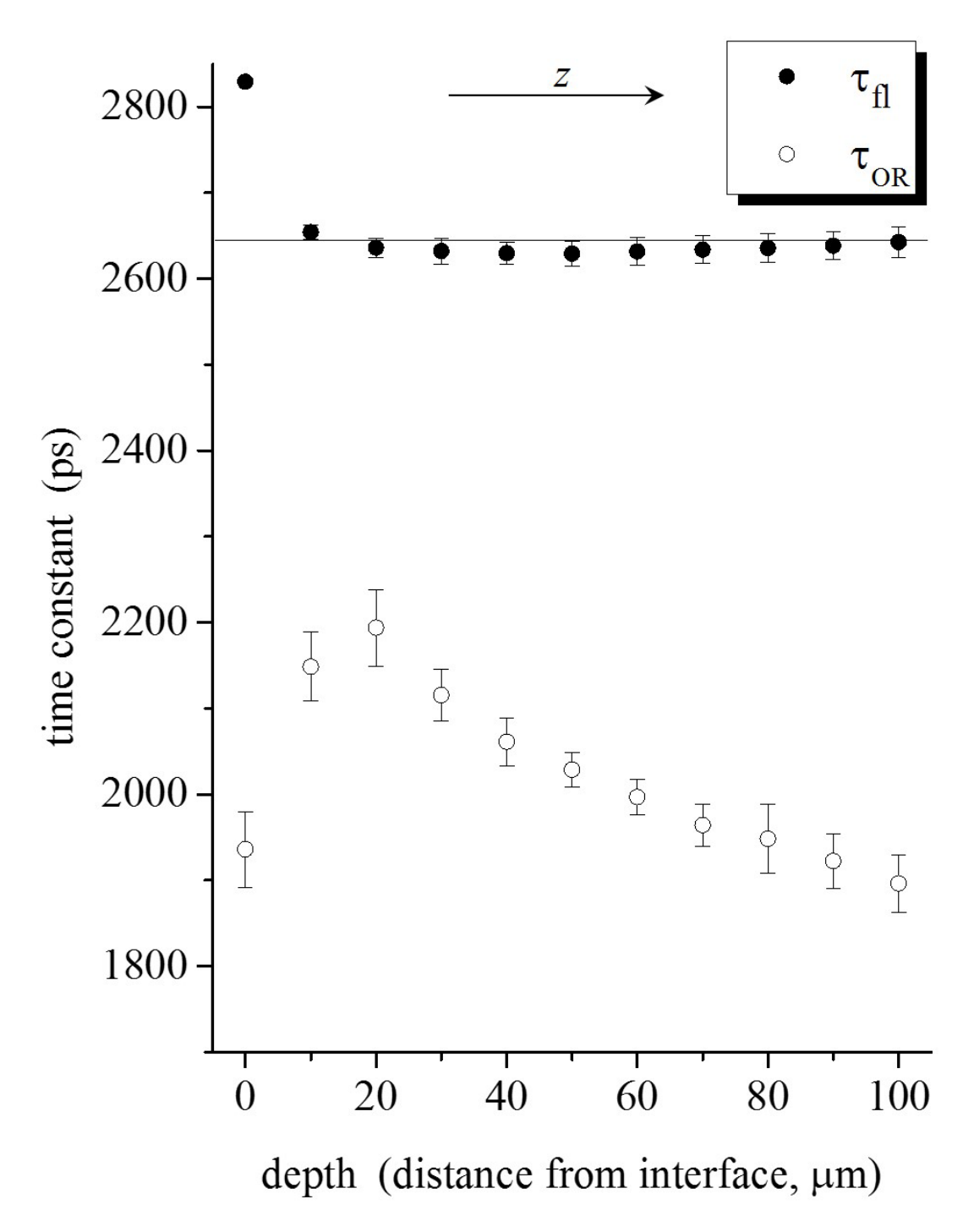


Figure 4.5 Dependence of LRSC in NOP fluorescence lifetime (\bullet) and anisotropy decay time constant (\circ) on distance from the glass interface. The line drawn through the fluorescence lifetime data is intended as a guide to the eye. The glass support was cleaned using UV-generated ozone and rinsed with ethanol prior to use. Refer to Fig. 4.3 for the experimental configuration and the x, y, z coordinate designation.

Given the inherently charged nature of the glass interface, it is important to consider any potential role of Coulombic/electrostatic forces in producing the results shown in Figs. 4.4 and 4.5. The spatial extent of Coulombic effects is related to the propensity of the medium to screen charge, and for polar systems containing electrolytes the spatial extent of the Coulombic effects that give rise to the electric double layer and the diffuse double layer regions are typically under 100 nm. For nonpolar systems that contain very few charged species, the spatial extent of surface charge effects can be longer, but in any event such effects operate on the sub-micron length scale, and the effect we observe persists for tens of microns.

For these reasons, and the extent of the gradient in the anisotropy decay time we observe experimentally (Figs. 4.4 and 4.5), we assert that neither contaminant-related nor Coulombic effects play a significant role in the phenomenon we observe. By process of elimination, the explanation for the anisotropy decay gradient we observe must be related to a compositional gradient in the liquid (NOP) phase. We have exposed NOP to deionized water with the expectation that the solution will reach an equilibrium water concentration in NOP after a few hours. Because the solvent system we use is a binary system, there is the opportunity for a compositional gradient to exist. There is potential for the composition of the liquid near the NOP|glass interface to be affected by adsorption of NOP as has been observed for other nonionic 12-14 and ionic 15-17 surfactants. As a result of adsorption, micelles, hemi-micelles, monolayer or bilayer structures may form at the solid surface depending on the concentration and interaction with surface charge. However, the spatial extent of the secondary structures would only be on the order of nanometers and would not account for micron scale gradient we observe. Additionally, NOP and longer chain N-alkyl-2-pyrrolidones are known to form micelles only in

presence of co-surfactants.^{4,9,19} We return to discussion of the observed compositional gradient after evaluating the generality of the phenomenon.

If the anisotropy decay gradient we observe is indeed related to a compositional gradient in the wet NOP phase, then the replacement of NOP with a different solvent system, particularly one which is miscible with water in all proportions, should alter the gradient. We show in Fig. 4.6 the fluorescence lifetime and anisotropy decay data for LRSC in EG as a function of distance from the EG|glass interface. The fluorescence lifetime data for LRSC in EG resemble those for LRSC in wet NOP, exhibiting depth-independent lifetimes for the chromophore away from the surface, and a different lifetime for the chromophore interacting with the glass interface (depth = 0). The anisotropy decay data for LRSC in EG exhibit a depth *independence* to within the experimental uncertainty, in sharp contrast to the data for NOP. The behavior of LRSC at the EG|glass interface is expected and this finding points to the NOP system exhibiting a compositional gradient. We turn next to the possible reasons for the observed compositional gradient.

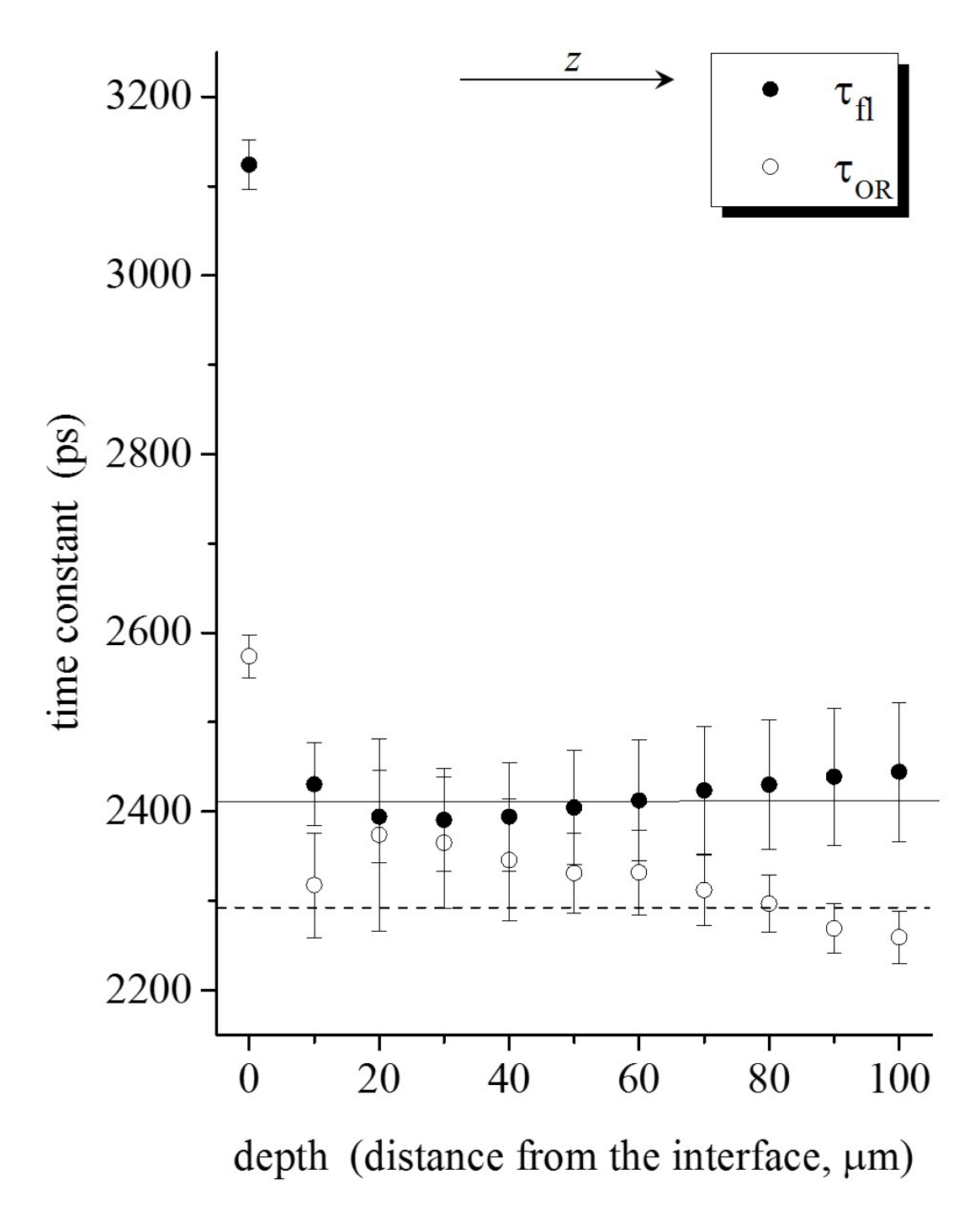


Figure 4.6 Dependence of LRSC in EG fluorescence lifetime (\bullet) and anisotropy decay time constant (\circ) on distance from the glass interface. The line drawn through the fluorescence lifetime data (solid) and the anisotropy decay data (dashed) are intended as guides to the eye. The glass support was cleaned using piranha solution and rinsed with water prior to use. Refer to Fig. 4.3 for the experimental configuration and the x, y, z coordinate designation.

We consider the following discussion of these anisotropy decay data, and the physical/chemical basis for them in the context of known models of rotational diffusion. The fluorescence lifetime and anisotropy decay data are derived from polarized fluorescence transients. The sample is excited with a polarized picosecond pulse of light and the emission from the sample is collected for polarizations parallel ($I_{\parallel}(t)$) and perpendicular ($I_{\perp}(t)$) to that of the excitation pulse. The fluorescence lifetime ($I_{\text{fl}}(t)$) and anisotropy decay functions (R(t)) are formulated according to Eqs. 4.1 and 4.2.

$$I_{fl}(t) = I_{||}(t) + 2I_{\perp}(t)$$
 (4.1)

$$R(t) = \frac{I_{||}(t) - I_{\perp}(t)}{I_{fl}(t)}$$
(4.2)

For all cases, we observe a single exponential decay of $I_{fl}(t)$, indicating the absence of anomalous excited state relaxation phenomena. The chemical information of interest is contained in the functional form and time constant(s) of the decay of R(t). In this work the chromophore is not tethered to either a solvent molecule or to the glass interface and its motion can be considered in the context of a free rotor. Chuang and Eisenthal²⁰ have developed the theoretical framework for relating the Cartesian components of the rotational diffusion constant, D, and the angle between the excited and emitting transition dipole moments, to the pre-factors and time constants of the exponential decay(s) contained in the experimental R(t) data. The chromophore, LRSC, is characterized by a nominally planar π system and the $S_1 \leftarrow S_0$ transition is polarized along the chromophore ring system long axis (x).^{21,22} For these conditions, a single exponential decay of R(t) is consistent with reorientation as a prolate rotor, and a two-component exponential decay is consistent with reorientation as an oblate rotor. For all of the measurements we report here R(t) decays as a single exponential, and the anisotropy decay time constant is given by $\tau_{RR} = (6D_z)^{-1}$.

Even with the limited information provided by a single exponential decay component, where only one Cartesian component of the rotational diffusion constant is sensed, we can speak to the possible reasons for the gradient we observe.

The anisotropy decay time constant is related to the size of the reorienting moiety, the viscosity of the surrounding medium and the temperature of the system through the modified Debye-Stokes-Einstein (DSE) model.²³

$$\tau_{OR} = \frac{1}{6D} = \frac{\eta V f}{k_B T S} \tag{4.3}$$

where η is the viscosity of the bulk solvent, V is the hydrodynamic volume of the reorienting entity, f is a term describing the frictional interaction between the reorienting moiety and the surrounding medium ($0 < f \le 1$), $k_B T$ is the thermal energy term and S is a shape factor to account for the non-spherical shape of the chromophore. We calculate the hydrodynamic volume of LRSC to be 560 Å³ using the method of van der Waals increments, and the shape factor S has been determined for rhodamine chromophores to be S = 0.9.21 Using this information and the bulk solvent viscosity of $\eta = 5.6$ cP for NOP, we obtain an estimate of $\tau_{OR} = 862$ ps from Eq. 4.3. This estimate is significantly lower than the anisotropy decay time constants we have observed experimentally for the NOP|glass interface. The data in Fig. 4.4 show τ_{OR} varying from ca. 2100 ps near the glass surface to ca. 1800 ps at 100 μ m from the interface.

It is fair, of course, to question the accuracy or validity of the DSE model for this application. We can gauge the accuracy of the DSE model by comparing its predictions to experimental data for a system that is not seen to behave in an anomalous manner. For LRSC in EG we observe τ_{OR} for distances of $10-100~\mu m$ from the interface of 2320 ± 38 ps. Taking the viscosity of EG to be 16.1 cP at 25 °C, 28 with f=1 (stick limit) and S=0.9, 21,22 we calculate τ_{OR}

= 2435 ps. The slight difference between experiment and theory is compelling evidence for the accuracy and applicability of the modified DSE model for these data. While the LRSC/EG interactions and the LRSC/NOP interactions may differ, it is the *z*-dependent trend in the data that is of primary importance here, and we consider how that trend can be explained in the context of Eq. 4.3.

In considering the discrepancy between the simple estimate from the DSE model (Eq. 4.3) and the experimental results, there are a limited number of ways to account for the data. Specifically, the temperature remains constant, we presume the chromophore does not change shape as a function of proximity to the glass surface, and the viscosity of the NOP solvent does not vary with proximity to the surface. We are thus left, within the framework of the DSE model, to conclude the anisotropy decay gradient is reflective of a gradient in the hydrodynamic volume of the reorienting entity. We recognize that the gradient in τ_{OR} corresponds to changes in ηVf and that these terms cannot be separated cleanly. Despite this limitation, we assert on physical grounds that the most plausible change is occurring with the effective hydrodynamic volume of the reorienting species. Deviations from hydrodynamic theory as described by the modified DSE equation have been reported previously in binary systems, where specific solutesolvent interactions and changes the hydrodynamic volume have been cited as reasons for nonconformity to model behavior. 29-32 Stevenson et al. reported a compositional dependence in the reorientation times of 4-benzylamino-7-nitrobenzylfurazan (BBD) in 1-propanol/water binary systems, where the hydrodynamic volume of the reorienting entity was found to change based on the inclusion of interacting solvent molecule(s).³² Specific solute-solvent interactions, such as hydrogen bonding, can account for reorientation times greater than model predictions by strong association of solute and solvent molecule(s). Hydrogen bonding interactions provide for this

adjustment in hydrodynamic volume because the duration of hydrogen bonds can be on the same order as the rotational diffusion time.

In the case of the wet NOP system, the change in hydrodynamic volume of the reorienting entity can be accounted for in the context of the chromophore residing in a primarily aqueous environment that is surrounded by NOP molecules, and the reorienting entity is (LRSC $\cdot nH_2O$), with n being the depth-dependent quantity. In this model, the reorienting entity would be a nominally spherical chromophore-water complex (S = 1). To account for the reorientation times observed experimentally, we add n H₂O molecules (21 Å³ each), as shown in Table 4.1. The results of this model show that there is a monotonic trend in the number of water molecules surrounding the chromophore, decreasing with increasing distance from the interface. The number of water molecules in this model ranges from ca. 36 to ca. 48, a number that we believe to be consistent with absorbance and dynamic light scattering (DLS) data (vide infra). We show in Fig. 4.7a the calculated number of water molecules surrounding the LRSC chromophore, n, as a function of distance from the interface, and in Fig. 4.7b, we show the calculated diameter of the chromophore-water entity as a function of distance from the interface. We note that while there may appear to be a slight offset in the data for the interface cleaned using piranha solution and water compared to the interface cleaned using UV-generated ozone and ethanol, any difference between the two sets of results can be accounted for in the context of differences of ± 1 water molecule in the system. We take this to be acceptable agreement between the two data sets.

Table 4.1 Estimated number of water molecules surrounding LRSC (model prediction for number of waters, n).^a

τοκ calc (ps)	V _{total} (Å ³)	Vwater (Å ³)	n	d (nm)
1824	1316	756	36	1.36
1853	1337	777	37	1.37
1882	1358	798	38	1.37
1911	1379	819	39	1.38
1941	1400	840	40	1.39
1970	1421	861	41	1.39
1999	1442	882	42	1.40
2028	1463	903	43	1.41
2057	1484	924	44	1.42
2086	1505	945	45	1.42
2115	1526	966	46	1.43
2144	1547	987	47	1.43
2173	1568	1008	48	1.44

^a Number of water molecules, n, between 36 and 48 is used to determine the hydrodynamic volumes of water (V_{water}) and a total volume ($V_{LRSC} + nV_{water}$), which is used to calculate model reorientation times, (τ_{OR} calc). Diameters, d, are calculated assuming a spherical hydrodynamic volume.

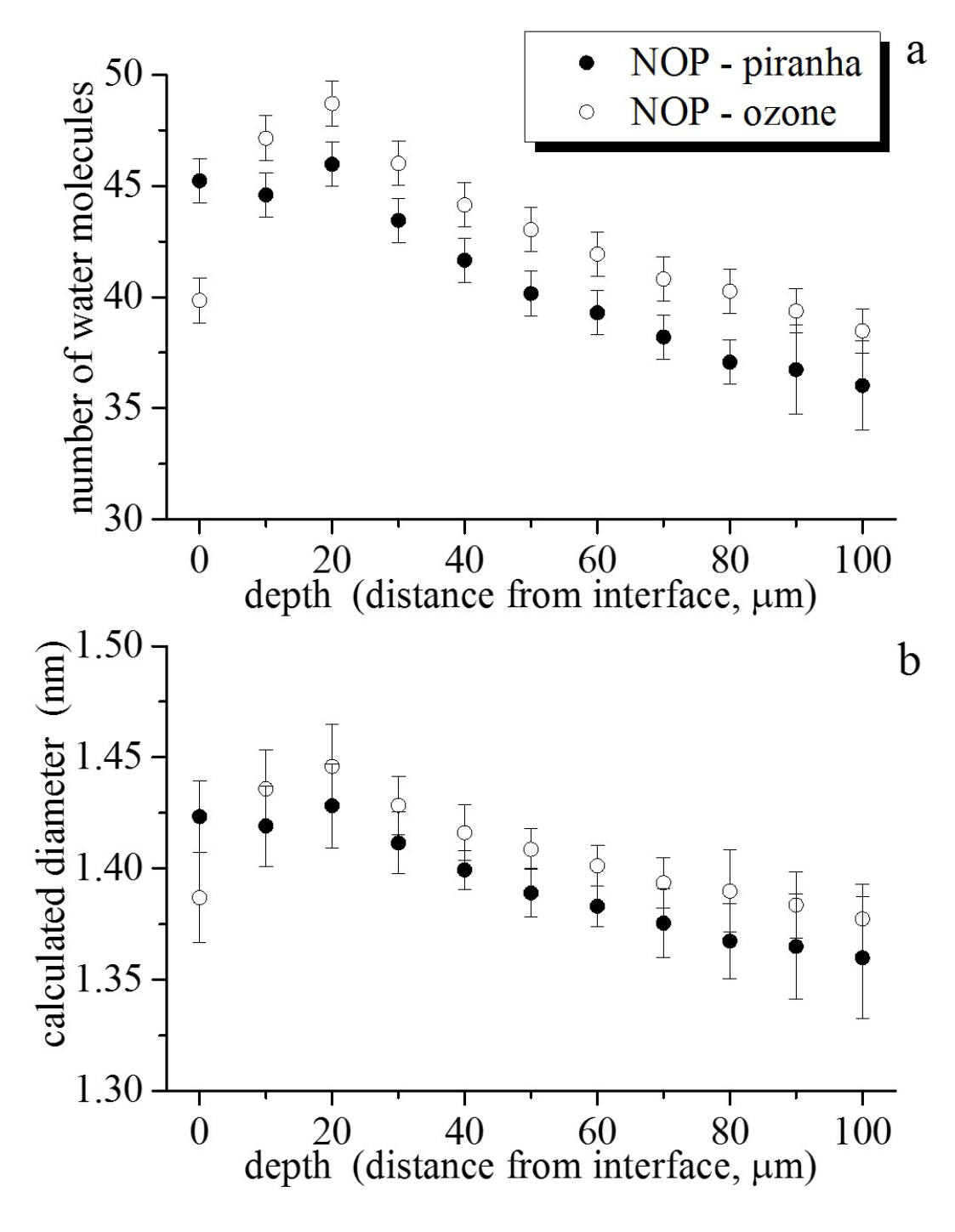


Figure 4.7 (a) Calculated number of water molecules in the immediate proximity of LRSC as a function of distance from the NOP|glass interface, for the interface cleaned with piranha solution and water (•) and cleaned with ethanol and UV-generated ozone (o). (b) Calculated diameters of the reorienting entities containing the chromophore and the number of water molecules indicated in (a), as a function of distance from the NOP|glass interface.

It is useful to note that the number of water molecules predicted by this model is dependent on the assumptions made, such as the local viscosity of the NOP. Local viscosity, as sensed by a rotating chromophore, is not necessarily the same as the bulk solvent viscosity, which is mediated by solvent-solvent intermolecular interactions. Also, the details of the solvent-solute coupling for the chromophore-water microenvironment are not addressed directly in this model. Despite these limitations, all data reported are interpreted using the same set of assumptions. Thus, the exact number of water molecules predicted by the model is subject to some uncertainty, the trend seen in these data is fully valid and is consistent with the chromophore sampling a nano-emulsion environment characterized by a compositional gradient normal to the plane of the glass support.

An important consideration is why the chromophore within the water droplet does not simply reorient as though it resided in bulk water with the NOP|water interface being decoupled from the LRSC/water interactions. To evaluate this issue is it instructive to consider the relative sizes of the water nano-droplets and the bare chromophore. As noted above, the calculated hydrodynamic volume for LRSC is 560 Å^3 , and if this volume is taken to be spherical it corresponds to a diameter of 1.02 nm. The water nano-droplets are measured by DLS to have a diameter of $1.26 \pm 0.25 \text{ nm}$ (*vide infra*), indicating a difference in diameter of $\sim 0.24 \text{ nm}$. The implication of this comparison is that the sizes of the bare chromophore and the water nano-droplets are sufficiently close that the decoupling of the chromophore/water and water/NOP interactions is not possible. In other words, the relative sizes of the chromophore and water nano-droplets are similar enough that the chromophore/water moiety needs to be treated as a single reorienting species.

There are two testable predictions of this model. The first is that the chromophore finds itself in a local environment influenced strongly by the presence of water. The absorption spectrum of LRSC is sensitive to the presence of water. We show in Fig. 4.8 the absorption spectra of LRSC in water, dry NOP, NOP saturated in water, and LRSC in NOP after extraction from water. The latter two spectra are overlapped. As can be seen from these data, the LRSC chromophore finds itself in a primarily aqueous environment in the water-saturated NOP solution. These data are consistent with the explanation put forth for the anisotropy decay gradient, which asserts water molecules surround LRSC forming reorienting entities with hydrodynamic volumes greater than the chromophore alone.

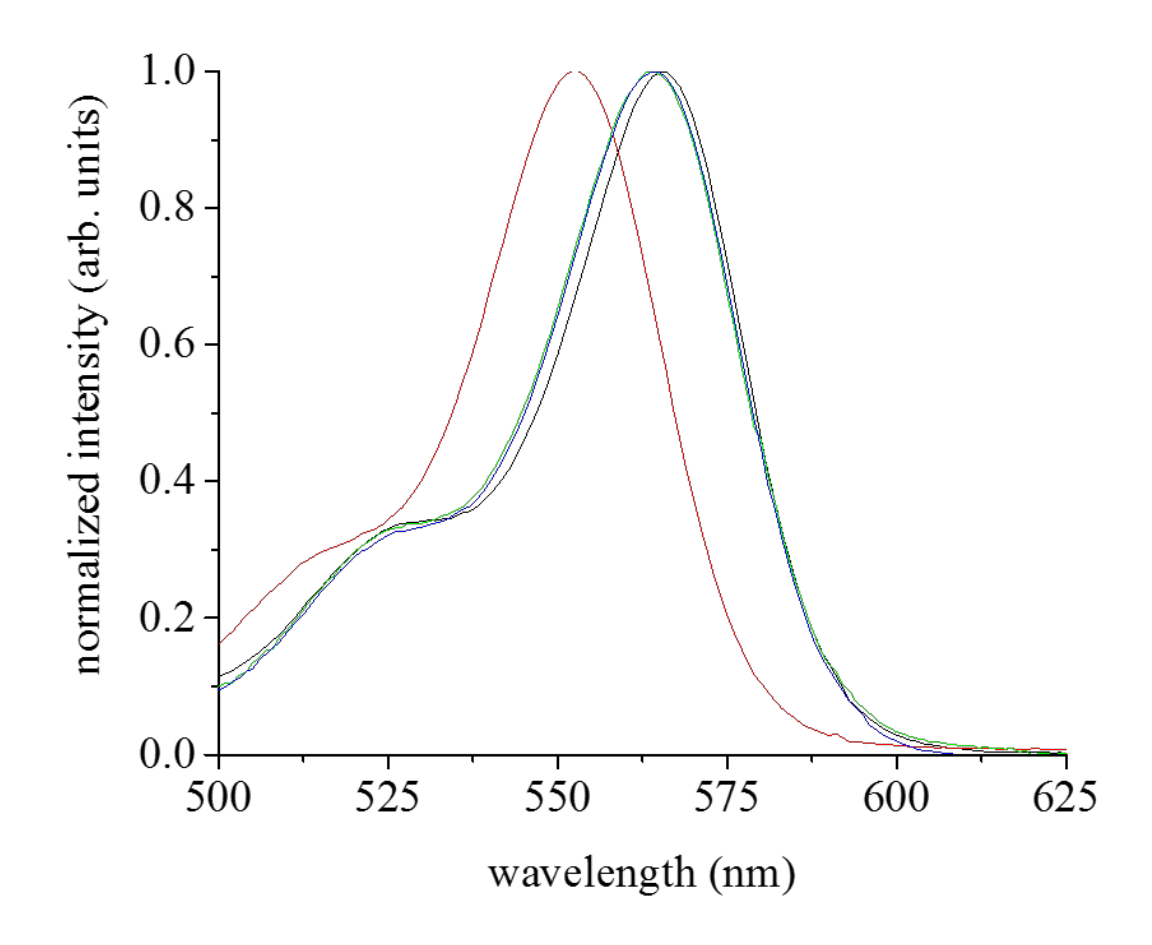


Figure 4.8 Normalized absorption spectra of LRSC in water (black), LRSC in dry NOP (red), LRSC in NOP after equilibration with water (blue), and LRSC in NOP after extraction from water (green).

The second prediction of the model is that, if these data are the result of a water nanoemulsion, there should be detectable droplets present in the solution. We have used DLS to evaluate whether or not this is the case. DLS is a spectroscopic technique used to determine the particle size distribution of a colloidal suspension. A laser light source illuminates the sample and light scattered from the dispersed particles is detected. The intensity of scattered light is recorded as a time-correlation function that is related to movement of the particles via Brownian motion.³³ Particle size distributions are then calculated from the fluctuation in motion of different size particles. We show these results in Fig. 4.9, indicating the presence of species with a diameter of 1.26 ± 0.25 nm in the water-containing NOP solution. An absence of DLS signal is seen in this same size region for dry NOP (Fig. 4.9). For all DLS measurements, no chromophore was present. Comparing these results to those shown in Table 4.1 and Fig. 4.7b, we assert that this represents excellent agreement between experiment and model. We understand the correspondence between the experimental data and predictions of the model as follows. While the results of the model calculation are in agreement with the experimental data to within the experimental uncertainty, the values predicted by the model appear to be consistently higher than those determined by DLS. The DLS measurement samples the bulk solvent system whereas the reorientation data are for the solution near the interface, where the anisotropy decay gradient is observed. Even at a depth of 100 µm, which is our experimental limit with the time-resolved measurement, the trend in size of the chromophore-water entity appears to be decreasing. Thus a bulk (DLS) measurement of the size of the water domains would provide a value that is expected to be smaller than what we observe at and near the glass interface based on the existence of the anisotropy decay gradient.

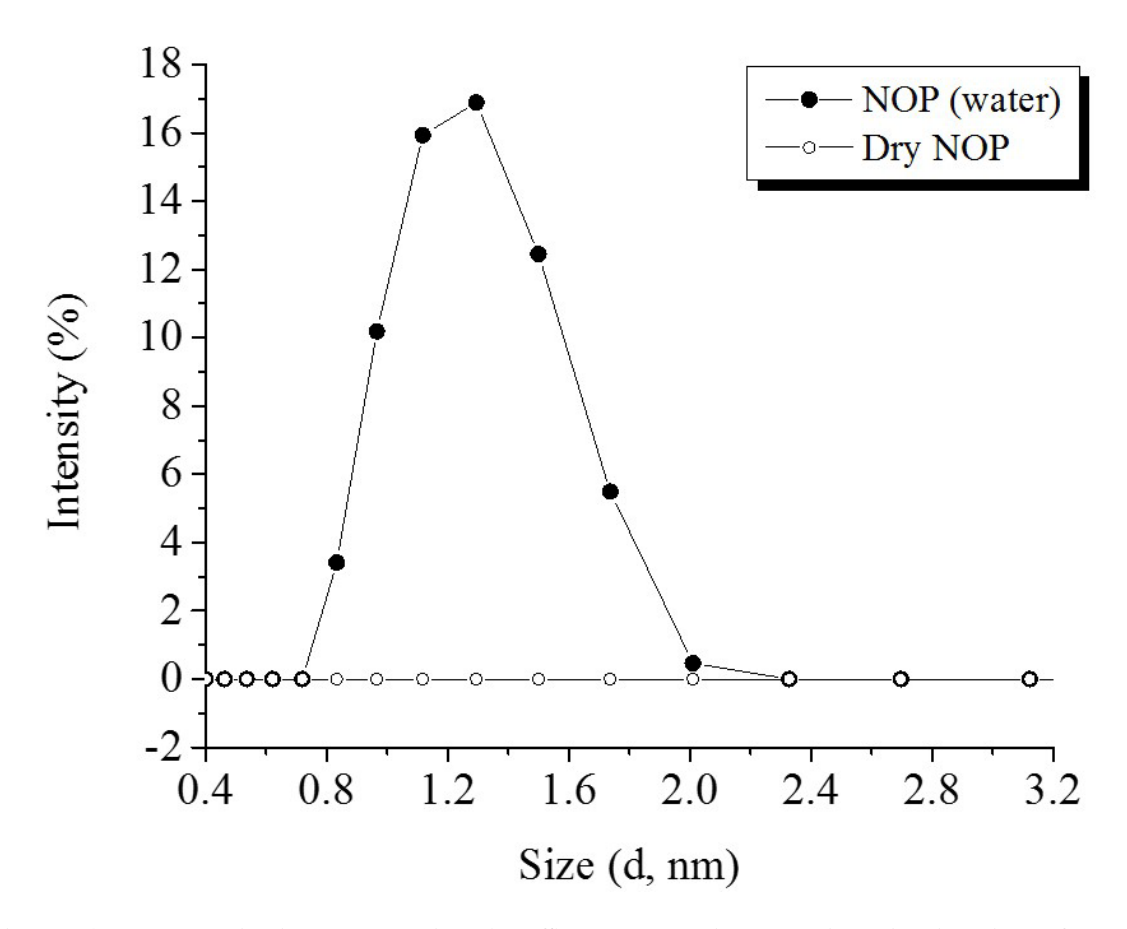


Figure 4.9 Dynamic light scattering (DLS) data showing the size distribution of water nano-droplets present in wet NOP after exposure to water (\bullet) and dry NOP (\circ) , showing the absence of species in the same size range as the water nano-droplets. For all DLS measurements no chromophore was present.

The experimental anisotropy decay data for LRSC in wet NOP are consistent with a gradient in the average size of chromophore-water cluster increasing with proximity to the glass interface and this finding is not expected for a simple solution phase system, such as EG. It is important to consider the implications of this finding. The first implication is that NOP and water, at least up to saturation concentration, exist as a colloidal system. When viewed in this context, it is reasonable to expect there to be a distribution of colloidal "nano-droplets" (i.e. water and water + chromophore) suspended in NOP. In fact, there is precedent for the existence of such nanoscale heterogeneity being induced in liquid crystalline systems by the presence of a small amount of water.³⁴ One possible explanation for the existence of a gradient in the size of the colloidal suspension of water nano-droplets is that there is a difference in the surface energy for the NOP|glass and NOP|water interfaces, and the size gradient in the water nano-droplets represents a gradient in the Laplace pressure of the nano-droplets to compensate for the difference in surface energies of the two interfaces. At the point where the NOP, water nanodroplet and glass are in contact, there is a single Laplace pressure that characterizes the resulting structure, and that Laplace pressure is different than for the water nano-droplet in the NOP phase. Diffusion mediated transport of water nano-droplets occurs and water molecules are "shed" from the nano-droplet to achieve the equilibrium Laplace pressure. This explanation requires that the shedding of water molecules occurs on a time scale similar to that of nanodroplet diffusion, giving rise to a gradient in nano-droplet size over the length scale we observe. A prediction of this explanation is that different interfaces with wet NOP would give rise to different nano-droplet gradients, and that for the NOP|water planar interface there should not be a water nano-droplet size gradient. It is important to keep in mind that the range of the

compositional gradient is on the order of \pm ten water molecules in a cluster, and the use of rotational diffusion allows the resolution of this subtle compositional gradient.

Another issue that is of some significance is that for the NOP|glass system, there is a limited amount of water present in the system and, for thermodynamic reasons, the concentration should be uniform throughout the solution. For this reason, the dielectric constant of the system should be nominally constant, consistent with a depth-independent fluorescence lifetime of the chromophore. This is not expected to be the case under the condition of an excess of water being available to the NOP phase, and we consider this situation in the next chapter.

The issue of hindered Brownian diffusion of nanoscale droplets near a solid surface may play a role in these data as well. Near a solid surface, Brownian diffusion in the liquid phase becomes anisotropic, with motion parallel to the surface remaining more similar to that in the bulk than motion normal to the surface. Interfacially-mediated hindered Brownian diffusion of a nanoparticle near a solid surface can be understood in terms of the surrounding liquid being the source for momentum due to fluctuations in density. As the solid surface is approached, such fluctuations diminish to the level of phonons in the solid, leading to slower diffusion near the surface. While the length scale of this effect (microns) is too short to account for the anisotropy decay gradient we observe (Fig. 4.4), it can play a role in mediating the rate at which nanodroplets diffuse from the surface. Also, to the extent to which translational and rotational diffusional motion are coupled, such interfacial effects could be responsible for the functional form of the anisotropy decay gradient data we see in Fig. 4.4 near the wet NOP|glass interface. This effect is not expected to play a role at the liquid-liquid interface which we consider in the next chapter.

4.4 Conclusions

We have reported on the existence of a gradient in the anisotropy decay time for the chromophore LRSC in NOP that contains water. The anisotropy decay gradient scales with the distance from a glass interface (z), and this gradient is not seen for LRSC in EG in the proximity of a glass interface. We understand these data in the context of a compositional gradient in the wet NOP solvent system, where the species we detect are LRSC solvated by water droplets in the NOP phase. The chromophore-containing water droplets are found to vary in size (hydrodynamic volume) as a function of distance from the glass surface. Anisotropy decay data in conjunction with the modified DSE model point to a progression in the number of water molecules associated with a chromophore molecule with increasing proximity to the glass surface. The size of the water nano-droplets is estimated from these data to be on the order of 1.3 - 1.4 nm in diameter, and dynamic light scattering of the colloidal suspension reveals the presence of nano-droplets that are ca. 1.26 nm diameter, on average. We view this as excellent agreement because the DLS measurements sample all colloidal droplets in the suspension, whereas the anisotropy decay data sample only those droplets in close proximity to the glass surface. The existence of the gradient is consistent with a difference in the surface energies of the wet NOP nano-droplet interface and the NOP glass interface. No analogous organization is found in a solvent system (ethylene glycol) that does not exhibit phase segregation issues. This work points to one possible means of controlling colloidal suspension size in applications where such dimensional issues are important. In the next chapter, we examine the fluorescence lifetimes and anisotropy decays for a NOP|water|glass system.

- 1. Pletcher, D. A First Course in Electrode Processes, 2nd Edition; RSC Publishing: Cambridge, UK, 2009, and references therein.
- 2. Bockris, J. O. M.; Devanathan, M. A. V.; Muller, K. *Journal of the Royal Society, Series A, Mathematical and Physical Sciences* **1963**, 274, 55.
- 3. Helmholtz, H. Annalen der Physik 1853, 165, 211.
- 4. Rosen, M. J.; Zhen, H. Z.; Gu, B.; Murphy, D. S. Langmuir 1988, 4, 1273.
- 5. Lou, A. J.; Pethica, B. A.; Somasundaran, P.; Yu, X. *Journal of Colloid and Interface Science* **2002**, 256, 190.
- 6. Adamy, S. T. Langmuir 1995, 11, 3269.
- 7. Setiawan, I.; Blanchard, G. J. Journal of Physical Chemistry B 2014, 118, 3085.
- 8. Setiawan, I.; Blanchard, G. J. Journal of Physical Chemistry B 2014, 118, 537.
- 9. Rosen, M. J.; Gu, B.; Murphy, D. S.; Zhu, Z. H. *Journal of Colloid and Interface Science* **1989**, *129*, 468.
- 10. Hay, C. E.; Marken, F.; Blanchard, G. J. Journal of Physical Chemistry A 2010, 114, 4957.
- 11. Conway, B. E.; Bockris, J. O. M.; Ammar, I. A. Faraday Transactions 1951, 47, 756.
- 12. Levitz, P.; Elmiri, A.; Keravis, D.; Van Damme, H. *Journal of Colloid and Interface Science* **1984**, *99*, 484.
- 13. Levitz, P.; Van Damme, H.; Keravis, D. *Journal of Physical Chemistry* **1984**, 88, 2228.
- 14. Levitz, P. E. Colloids and Surfaces A: Physicochemical and Engineering Aspects **2002**, 205, 31.
- 15. Cases, J. M. Bulletin De Mineralogie 1979, 102, 684.
- 16. Strom, C.; Hansson, P.; Jonsson, B.; Soderman, O. *Langmuir* **2000**, *16*, 2469.
- 17. Strom, C.; Jonsson, B.; Soderman, O.; Hansson, P. *Colloids and Surfaces A-Physicochemical and Engineering Aspects* **1999**, *159*, 109.
- 18. Paria, S.; Khilar, K. C. Advances in Colloid and Interface Science 2004, 110, 75.

- 19. Zhu, Z. H.; Yang, D.; Rosen, M. J. Journal of the American Oil Chemists Society 1989, 66, 998.
- 20. Chuang, T. J.; Eisenthal, K. B. Journal of Chemical Physics 1972, 57, 5094.
- 21. Dela Cruz, J. L.; Blanchard, G. J. Journal of Physical Chemistry A 2001, 105, 9328.
- 22. Dela Cruz, J. L.; Blanchard, G. J. Journal of Physical Chemistry A 2002, 106, 10718.
- 23. Debye, P. *Polar Molecules* Chemical Catalog Co.: New York 1929.
- 24. Perrin, F. Journal of Physics and Radium 1934 5, 497.
- 25. Edward, J. T. Journal of Chemical Education 1970, 47, 261.
- 26. MacDonald, S. M.; Watkins, J. D.; Bull, S. D.; Davies, I. R.; Gu, Y.; Yunus, K.; Fisher, A. C.; Page, P. C. B.; Chan, Y.; Elliott, C.; Marken, F. *Journal of Physical Organic Chemistry* **2009**, 22, 52.
- 27. MacDonald, S. M.; Watkins, J. D.; Gu, Y.; Yunus, K.; Fisher, A. C.; Shul, G.; Opallo, M.; Marken, F. *Electrochemistry Communications* **2007**, *9*, 2105.
- 28. CRC Handbook of Chemistry and Physics, 71st Edition; Lide, D. R., Ed.; CRC Press: Boca Raton, FL, 1990-1991.
- 29. Beddard, G. S.; Doust, T.; Hudales, J. *Nature* **1981**, 294, 145.
- 30. Dutt, G. B.; Doraiswamy, S. Journal of Chemical Physics 1992, 96, 2475.
- 31. Bhattacharyya, S.; Bagchi, B. Journal of Chemical Physics 2001, 115, 9065.
- 32. Stevenson, S. A.; Blanchard, G. J. Journal of Physical Chemistry A 2006, 110, 3426.
- 33. Berne, B. J.; Pecora, R. *Dynamic Light Scattering With Applications to Chemistry, Biology, and Physics*; General Publishing Company, Ltd: Toronto, 2000.
- 34. Schroder, U.; Wadahawan, J. D.; Compton, R. G.; Marken, F.; Suarez, P. A. Z.; Consorti, C. S.; de Souza, R. F.; Dupont, J. *New Journal of Chemistry* **2000**, *24*, 1009.
- 35. Kihm, K. D.; Banerjee, A.; Choi, C. K.; Takagi, T. Experiments in Fluids 2004, 37, 811.
- 36. Banerjee, A.; Kihm, K. D. *Physical Review E* **2005**, 72, 042101.
- 37. Feitosa, M. I. M.; Mesquita, O. N. Physical Review A 1991, 44, 6677.
- 38. Hosoda, M.; Sakai, K.; Takagi, K. *Physical Review E* **1998**, *58*, 6275.
- 39. Kurban, M. R. *Journal of Chemical Physics* **2011**, *134*, 034503.

Chapter 5

Characterization of Liquid|Liquid|Solid Multi-Interfacial Compositional Gradients

5.1 Introduction

The study of liquid interfaces has garnered interest in industrial, biological, and environmental research because of their broad physical and chemical significance.^{1,2} Interactions between dissimilar molecules and molecular organization at liquid-liquid and liquid-solid interfaces are important for many processes, including chemical separations, extractions, interfacially-mediated polymerization reactions, and drug delivery, for example. Advances in spectroscopic measurement techniques have allowed for greater understanding of the solvation phenomena and intermolecular interactions that occur at liquid interfaces despite the difficulty in selectively probing the liquid-liquid interfacial region (ca. 1 nm thick).³⁻¹² Second order nonlinear optical techniques can provide the requisite interface selectivity, but with these techniques there is little ability to investigate organization and dynamics away from the interface by more than a few nanometers. Understanding and controlling interfacial processes, such as electrochemical phenomena, that occur within a few molecular diameters of liquid-liquid and liquid-solid interfaces requires in-depth knowledge of interfacial composition, organization, and dynamics, which has spurred both experimental studies and theoretical simulations. 13-17 The three-phase boundary, where a liquid-liquid interface comes into contact with a solid surface, has been studied as a reaction center for electrosynthesis and ion transfer in a two-phase flow regime and in microdroplets. 18-22 Liquid interfaces and three phase boundaries have the potential for use in numerous areas. The characterization of these interfaces and their properties, such as the relative surface energies of the interface constituents and the thickness of thin film interfaces, can pose a significant challenge in addition to inherent challenges in differentiating interfacial

and bulk phenomena. Bulk properties are often influenced by thin film geometry and the presence of support materials. For these reasons, we have undertaken the examination of a thin film interface between two liquids using spatially-resolved time-domain fluorescence lifetime and anisotropy decay measurements to gain insight into the physical and chemical properties of such interfaces.

In this work, we utilize the rotational diffusion dynamics of lissamine rhodamine B sulfonyl chloride (LRSC) to characterize a thin film N-octyl-2-pyrrolidone (NOP)|water interface supported on glass. We measure the rotational diffusion behavior of this chromophore as a function of (micron-scale) distance from the interface and as a function of distance from the glass support using time-correlated single photon counting (TCSPC) detection coupled to an inverted confocal microscope to obtain time- and position-resolved fluorescence lifetime and fluorescence anisotropy decay data. Lateral resolution of this system is on the order of the diffraction limit (*ca.* 250 nm) and the depth of focus is less than 1 µm for a 100X objective.

In the previous chapter, we examined a compositional gradient in the size of water nano-droplets that persists for tens of microns from the glass surface into the wet NOP layer. The discovery of the gradient in LRSC rotational diffusion dynamics as a function of distance from the NOP|glass interface was the first report, to our knowledge, of the existence of such a gradient in a nano-emulsion, and this gradient can be understood in the context of the relative surface energies of the NOP|water nano-droplet and the NOP|glass interfaces.²³ In this work, we have constructed a system where there is both a NOP|water interface and a NOP|glass interface, nominally orthogonal to one another, and we have examined the spatial-dependence of the chromophore fluorescence lifetime and anisotropy decay time in the proximity of these interfaces. The data reveal a gradient in the anisotropy decay time constants normal to the

NOP|glass interface consistent with the results from the study in chapter 4 and an absence of the water nano-droplet size gradient normal to a NOP|water interface. We do find evidence for a gradient in the concentration of water nano-droplets normal to the NOP|water interface, and these findings are consistent with the nano-emulsion size being mediated by the surface energies of the NOP|water and NOP|glass interfaces.

5.2 Experimental Methods

The chromophore lissamine rhodamine B sulfonyl chloride (LRSC) (Fig. 4.1a, \geq 99% Acros Organic) and N-octyl-2-pyrrolidone (NOP) (Fig. 4.1b, 98% Aldrich) were used as received. The water for these studies was purified in-house with a Milli-Q filtration system (Millipore). The chromophore concentration was 10^{-4} M in water and in dry NOP. Upon exposure to water the chromophore is likely hydrolyzed to the sulfonic acid. We refer to the chromophore as LRSC throughout because we have not verified the hydrolysis for each system.

For optical measurements, the sample holder was an Attofluor® cell chamber (Molecular Probes) fitted with a round borosilicate glass cover slip (25 mm diameter, No. 1.5 Thomas Scientific). A glass microscope slide (1 mm thick, Globe Scientific) was modified to fit into the Attofluor® cell (inner diameter 18.5 mm) and a hole was bored through the center (inner diameter of 5.1 mm) to form a well to contain liquid samples. The NOP|water interface was formed by adding approximately 150 μL of Milli-Q water to the cell chamber and then depositing ~0.01 μL of NOP containing 10⁻⁴ M LRSC to the well in the center of the microscope slide. A side-by-side interface with a thickness of ~500 μm formed inside the well and was in contact with the surface of the glass coverslip. The glass coverslip and glass microscope slide were cleaned in piranha solution (a 3:1 ratio of concentrated sulfuric acid and 30% hydrogen peroxide – caution *strong oxidizer*!) for 30 minutes prior to each use.

Fluorescence lifetime and anisotropy decay time constants were collected with the time-resolved fluorescence imaging instrument described in section 4.2. Pyrromethene dye (Exciton) was used for sample exication in the range of 550 nm to 595 nm. An oil immersion objective with magnification 100X (Nikon), numerical aperture 1.45, working distance 0.13 mm and depth of field *ca*. 0.45 µm was used for all data acquisition, and the experimental setup is schematized in Fig. 5.1. Depth profiles were generated on the NOP side of the interface by collecting single measurements with the beam parked at a fixed position. Measurements were made in the NOP phase because LRSC preferentially partitions into the NOP phase (Fig. 5.2). The positions along the *x*-axis were fixed using the SPCM galvanometer control and the depth along the *z*-axis was controlled mechanically. Measurements along the *z*-axis were collected in 10 µm increments. Fluorescence lifetime and anisotropy decay time constants were determined using MicroCal Origin Pro v. 9.0.

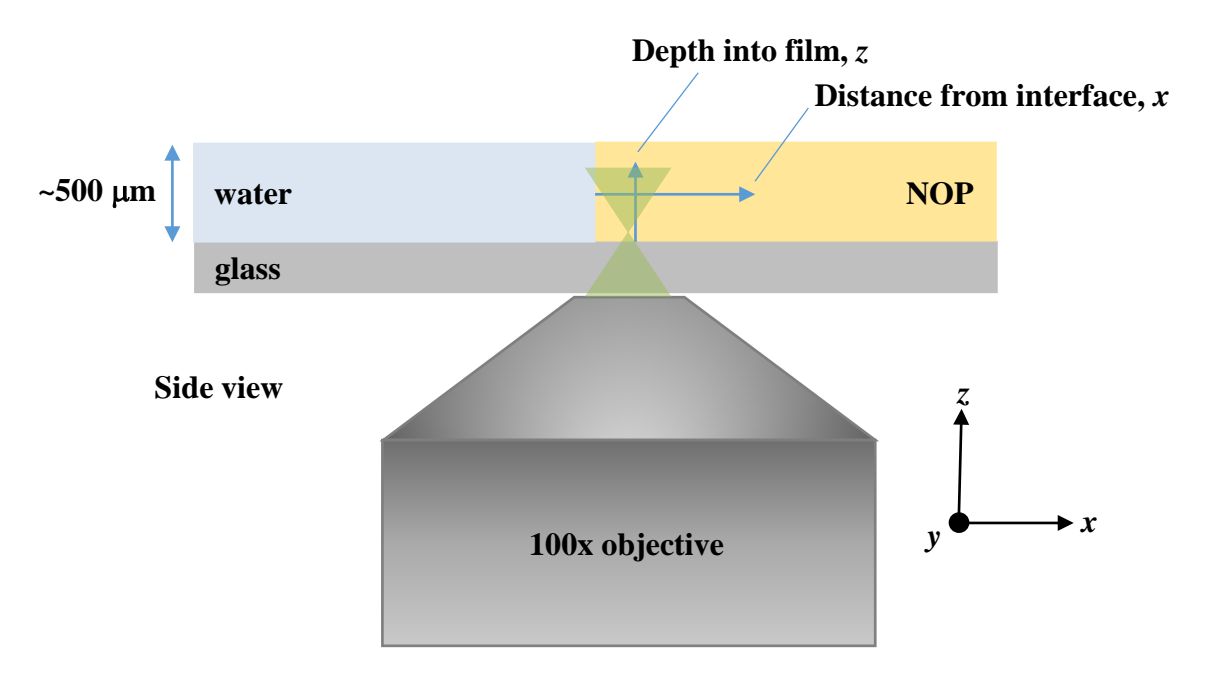


Figure 5.1 Schematic of sample and optical excitation/collection configuration for NOP|water|glass interface.

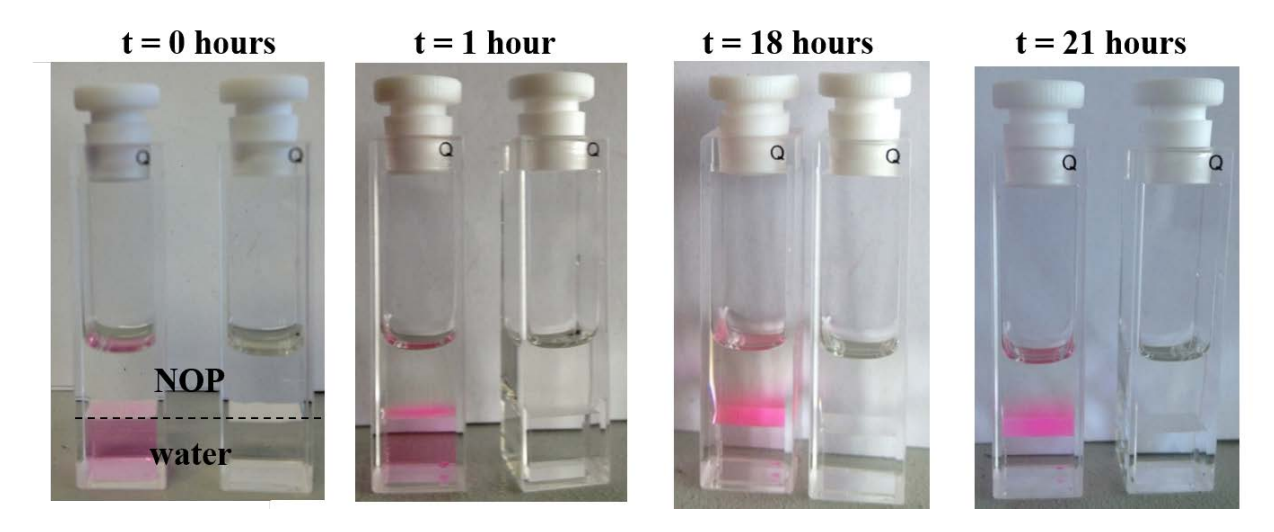


Figure 5.2 Time-resolved images of partitioning of LRSC initially deposited into the aqueous phase (bottom) and migrating into the NOP phase (top). In each image, the cuvette on left contains LRSC and the cuvette on the right is NOP|water with no chromophore to demonstrate the existence of the phase separation.

5.3 Results and Discussion

As noted above, in the preceding chapter we examined a depth-dependent gradient in the anisotropy decay time constant for the chromophore LRSC in a thin film of wet NOP supported on borosilicate glass. Our data were consistent with the depth-dependent anisotropy decay reflecting subtle compositional changes in the micro-scale organization of a water-in-NOP nanoemulsion. In the work presented here, we examine whether or not an analogous gradient can be seen for the liquid-liquid NOP|water interface and within the NOP|water|glass multi-interfacial region.

We have performed fluorescence lifetime and anisotropy decay measurements as a function of depth into the NOP layer (z) (normal to the plane of the glass support) and as a function of distance from the NOP|water interface (x) to resolve the spatial dependence of chromophore reorientation. The complete data sets are tabulated in the appendix (Tables 5.1 and 5.2), while selected data are plotted for illustration purposes. We apply the same treatment to our experimental data that we described in the previous chapter. We find that the anisotropy decay time constant for LRSC in NOP exposed to water is consistent with a reorienting moiety that has a greater volume than that of the chromophore alone. The reorientation data and the steady-state absorbance spectral data point to the chromophore residing in significantly aqueous environment(s) in (wet) NOP, and the reorientation data can be modeled in the context of the LRSC chromophore residing in a nanoscale aqueous region within the NOP. Such a system is described in the context of a nano-emulsion, and in this case the number of water molecules surrounding the chromophore varies in a regular manner, increasing with proximity to the glass support. The experimental anisotropy time constants and the hydrodynamic volume of the reorienting entity were used to estimate the number of water molecules in closest proximity to

the chromophore in the context of the modified Debye-Stokes-Einstein (DSE) equation (Eq. 4.3).²⁴⁻²⁶ We found the number of water molecules to vary in number from ~30–50. The presence and approximate diameters of such nanoscale droplets was consistent with dynamic light scattering (DLS) data for these samples. There is some amount of uncertainty associated with the exact number of water molecules predicted by our model, however, the trends in the time-resolved fluorescence anisotropy and steady-state spectral data are fully valid and consistent with the chromophore sampling an emulsion environment.

Table 5.1 Fluorescence lifetime, τ_{fl} , (ps) of LRSC as a function of depth into the NOP phase of a NOP|water system and distance from the NOP|water interface.

Depth into	Distance from the NOP water interface (μm)					
NOP (μm)	12	23	34	45	56	
0	2964 ± 7	2942 ± 1	2931 ± 3	2919 ± 3	2912 ± 3	
10	2732 ± 19	2745 ± 1	2742 ± 3	2737 ± 3	2730 ± 1	
20	2661 ± 13	2675 ± 3	2689 ± 3	2683 ± 3	2671 ± 3	
30	2618 ± 1	2628 ± 1	2653 ± 1	2656 ± 2	2648 ± 1	
40	2581 ± 3	2594 ± 1	2619 ± 1	2631 ± 2	2630 ± 2	
50	2561 ± 2	2569 ± 1	2588 ± 2	2606 ± 3	2614 ± 2	
60	2545 ± 7	2553 ± 1	2570 ± 3	2591 ± 1	2602 ± 1	
70	2543 ± 3	2544 ± 1	2556 ± 1	2576 ± 2	2590 ± 1	
80	2540 ± 1	2533 ± 3	2543 ± 2	2562 ± 2	2577 ± 3	
90	2539 ± 1	2526 ± 2	2535 ± 1	2548 ± 3	2569 ± 1	
100	2540 ± 5	2522 ± 2	2528 ± 1	2540 ± 3	2560 ± 2	

Table 5.2 Fluorescence anisotropy decay time constants, τ_{OR} , (ps) of LRSC as a function of depth into the NOP phase of a NOP|water system and distance from the NOP|water interface.

Depth into NOP (μm)	Distance from the NOP water interface (μm)					
	12	23	34	45	56	
0	1461 ± 15	1514 ± 17	1594 ± 14	1763 ± 11	1696 ± 12	
10	1596 ± 21	1609 ± 15	1661 ± 5	1695 ± 11	1667 ± 12	
20	1577 ± 17	1603 ± 20	1584 ± 10	1653 ± 14	1668 ± 10	
30	1539 ± 2	1564 ± 15	1527 ± 5	1600 ± 5	1613 ± 11	
40	1517 ± 4	1553 ± 14	1523 ± 5	1561 ± 19	1558 ± 2	
50	1491 ± 15	1534 ± 11	1489 ± 16	1531 ± 1	1516 ± 18	
60	1467 ± 19	1499 ± 13	1469 ± 11	1491 ± 26	1462 ± 8	
70	1478 ± 9	1473 ± 8	1432 ± 5	1472 ± 6	1437 ± 4	
80	1468 ± 14	1463 ± 19	1421 ± 10	1453 ± 11	1409 ± 8	
90	1474 ± 18	1466 ± 18	1402 ± 5	1427 ± 10	1385 ± 18	
100	1477 ± 7	1438 ± 4	1381 ± 19	1385 ± 3	1353 ± 3	

The data we report here, for the NOP|water|glass system are consistent with those reported for the NOP|glass interface, where a gradient in the anisotropy decay time is seen normal to the NOP|glass interface for distances *ca*. 40 µm and greater from the NOP|water interface (Fig. 5.3). In contrast to the gradient normal to the NOP|glass interface, there is not a size gradient in the anisotropy decay data normal to the NOP|water interface (Fig. 5.4). The number of water molecules in closest proximity to LRSC and contributing to the hydrodynamic volume of the reorienting entity is found to vary in number from ~20–30.

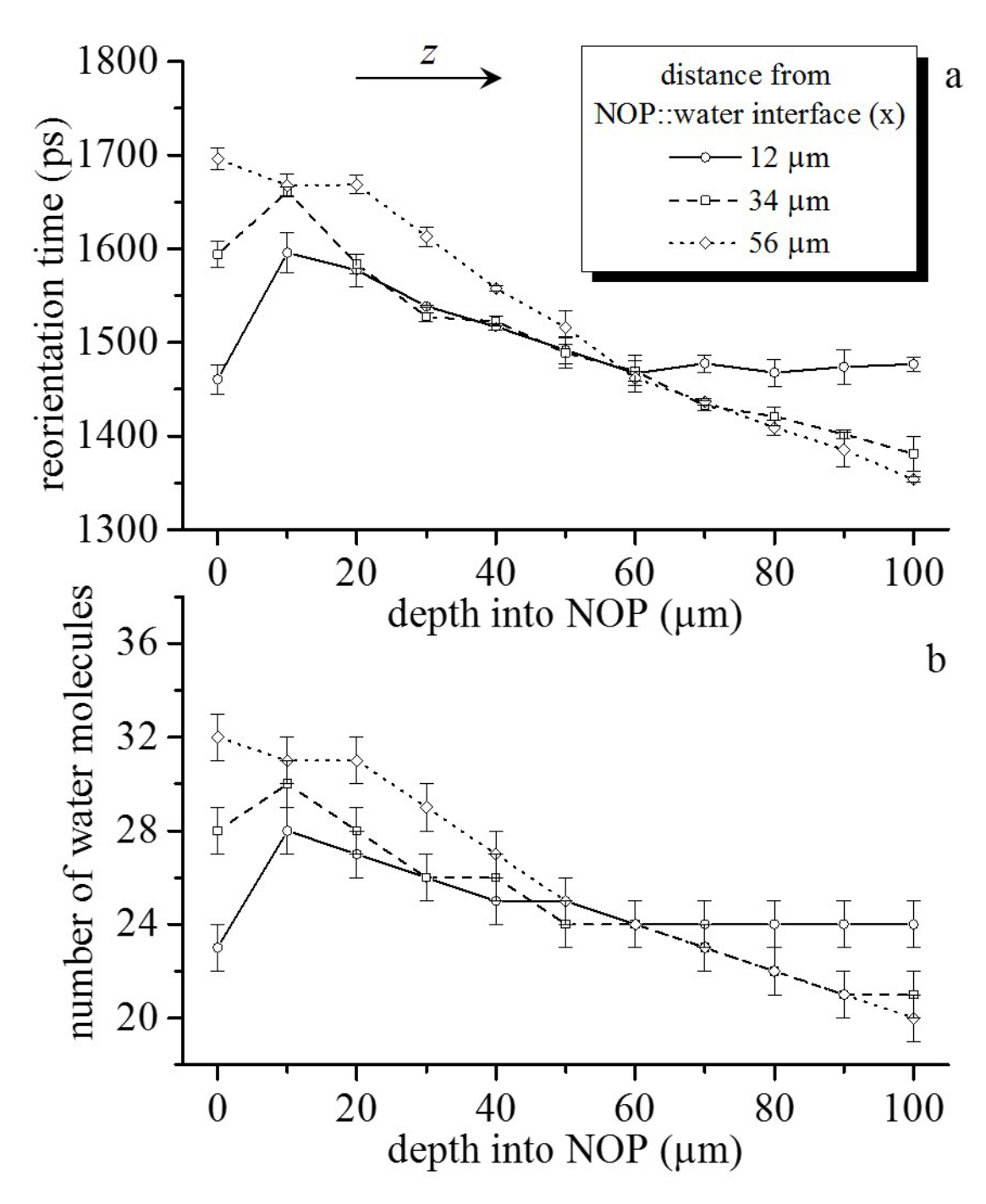


Figure 5.3 (a) Reorientation time and (b) calculated number of water molecules as a function of distance from the NOP|glass interface. Refer to Fig. 5.1 for the experimental configuration and the x, y, z coordinate designation.

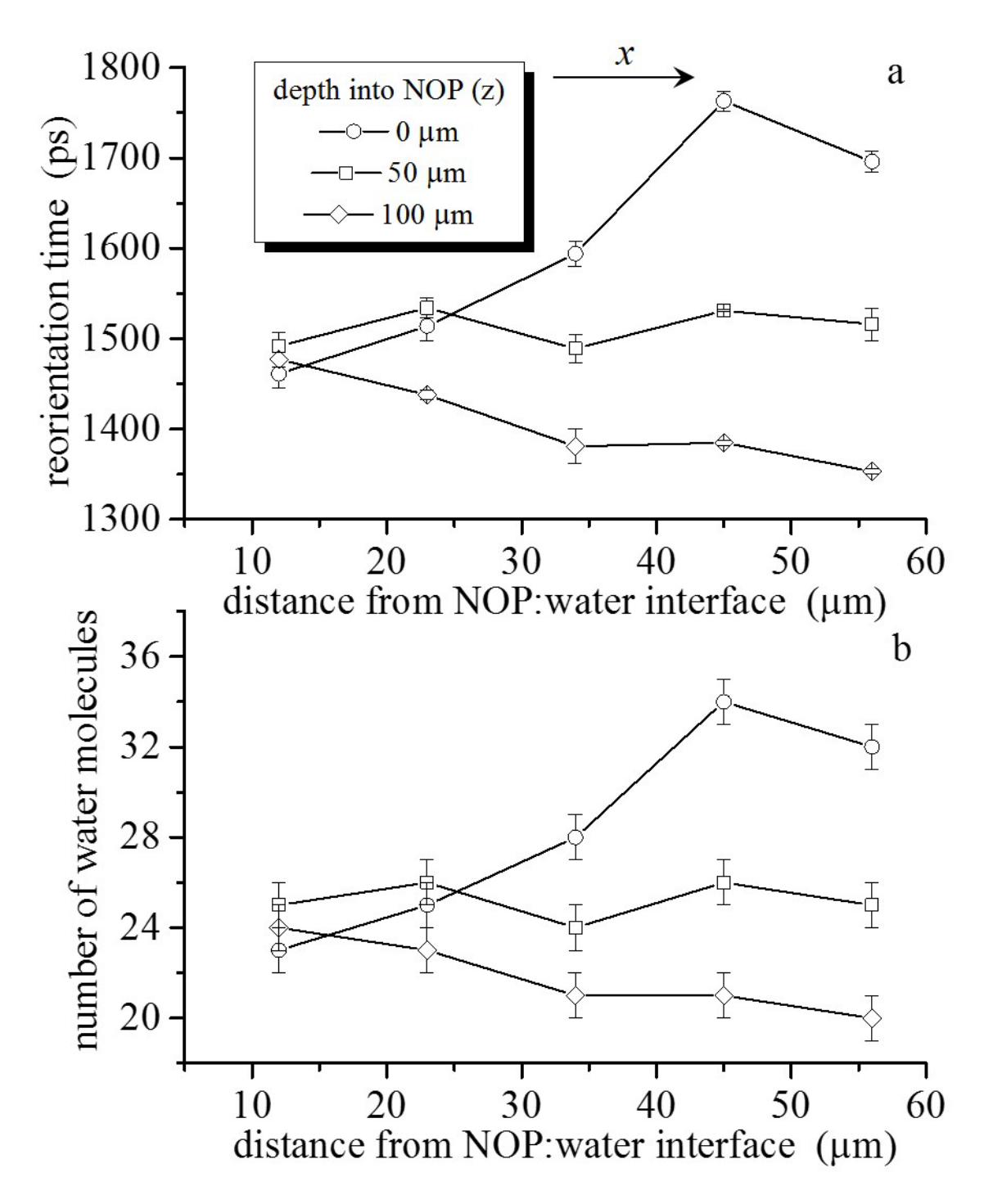


Figure 5.4 (a) Reorientation time and (b) calculated number of water molecules as a function of distance from the NOP|water interface. Refer to Fig. 5.1 for the experimental configuration and the x, y, z coordinate designation.

Given the presence of water in the NOP, it is presumed that the water domains are at least the same size as those seen for the NOP|glass system in the preceding paper, however, we observe smaller water domains. For this reason it may appear anomalous that the anisotropy decay time constants for the NOP|water|glass system are faster than they are for the system with only the NOP|glass interface. This is, however, an expected result for an emulsion. There is a substantial literature on the subject of emulsions and it is known from this literature that the viscosity of the fluid depends inversely on the average size of the emulsion inclusion domains.^{27,28} We would expect this effect to become significant only under conditions where there is a relatively high density of water nano-droplets. Thus the faster reorientation times seen for the system characterized by both water and glass interfaces implies that the average size of the water domains for this system are larger than for the system with only the glass interface.

It is instructive to examine the spatial dependence of the fluorescence lifetime for this system. For the case of the single NOP|glass interface we observed no positional dependence of the fluorescence lifetime save for surface-chromophore interactions. ²³ In contrast, the addition of the NOP|water interface normal to the NOP|glass interface gives rise to position-dependent fluorescence lifetime data in the NOP phase as a function of distance from both interfaces (Fig. 5.5). There is a steep decline in fluorescence lifetime moving away from the glass support while the changes in lifetime as a function of distance away from the NOP|water interface are modest. The fluorescence lifetime of LRSC is sensitive to the polarity of its environment, and spatially resolved lifetime data can be used to infer variations in the dielectric constant (ϵ) of the system. There is a phenomenological relationship between rhodamine fluorescence lifetime and dielectric constant ²⁹ and we use this relationship to estimate the spatial dependence of the dielectric constant (Fig. 5.6). The fact that we observe a spatial dependence to ϵ for this system, with two

distinct interfaces, while we do not observe a corresponding spatial dependence in fluorescence lifetime for the case where there is only the NOP|glass interface is indicative of a compositional gradient in the NOP|water|glass system. We assert the compositional gradient we observe normal to the NOP|water interface is not a gradient in the size of the water nano-drops in NOP, but rather a gradient in the concentration of water nano-droplets in the NOP.

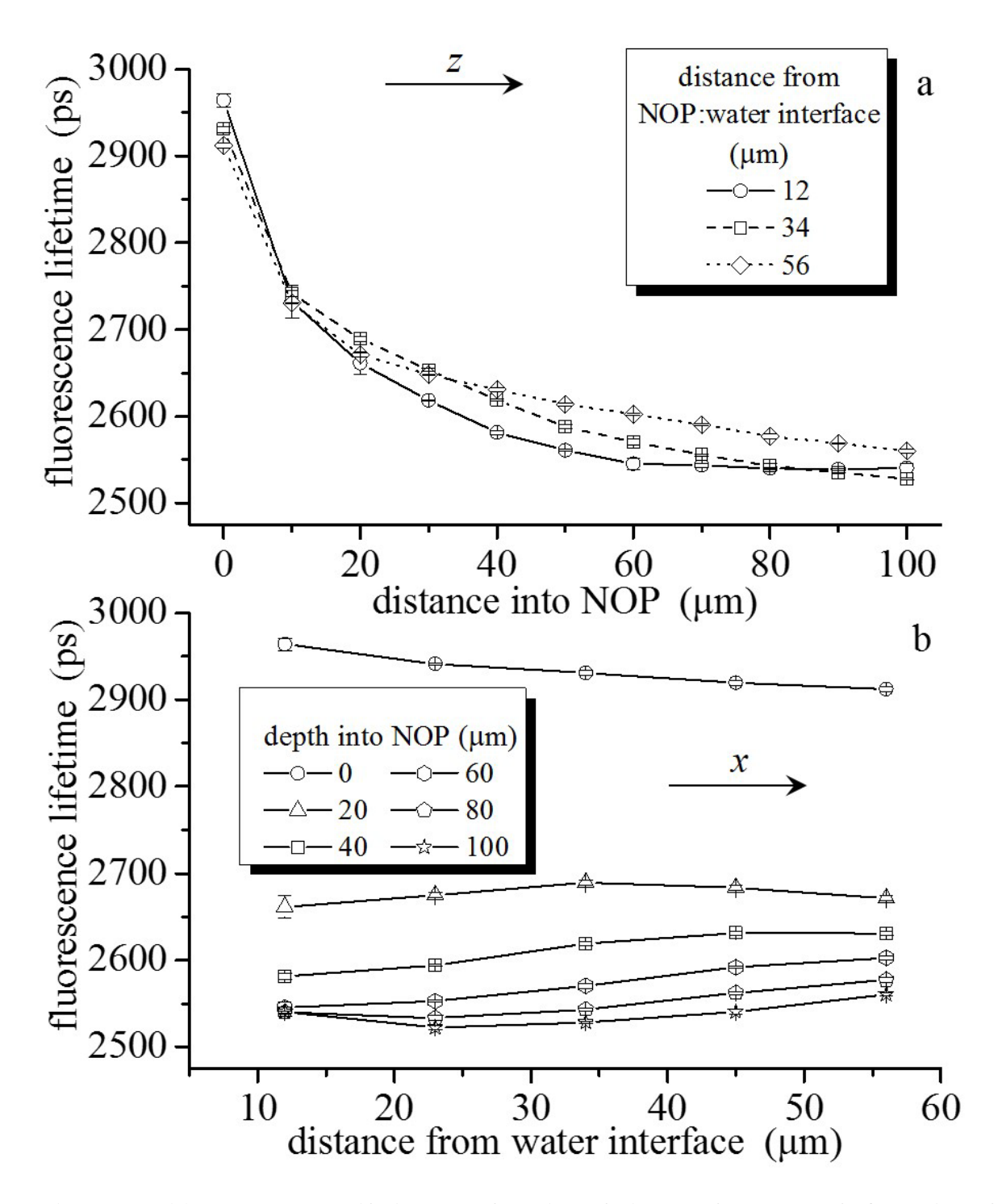


Figure 5.5 (a) Fluorescence lifetime as a function of distance from the NOP|glass interface for three different distances from the water interface. (b) Fluorescence lifetime as a function of distance from the NOP|water interface for six different distances from the NOP|glass interface. Experimental error bars representing the standard deviation are shown for each data point. Refer to Fig. 5.1 for the experimental configuration and the x, y, z coordinate designation.

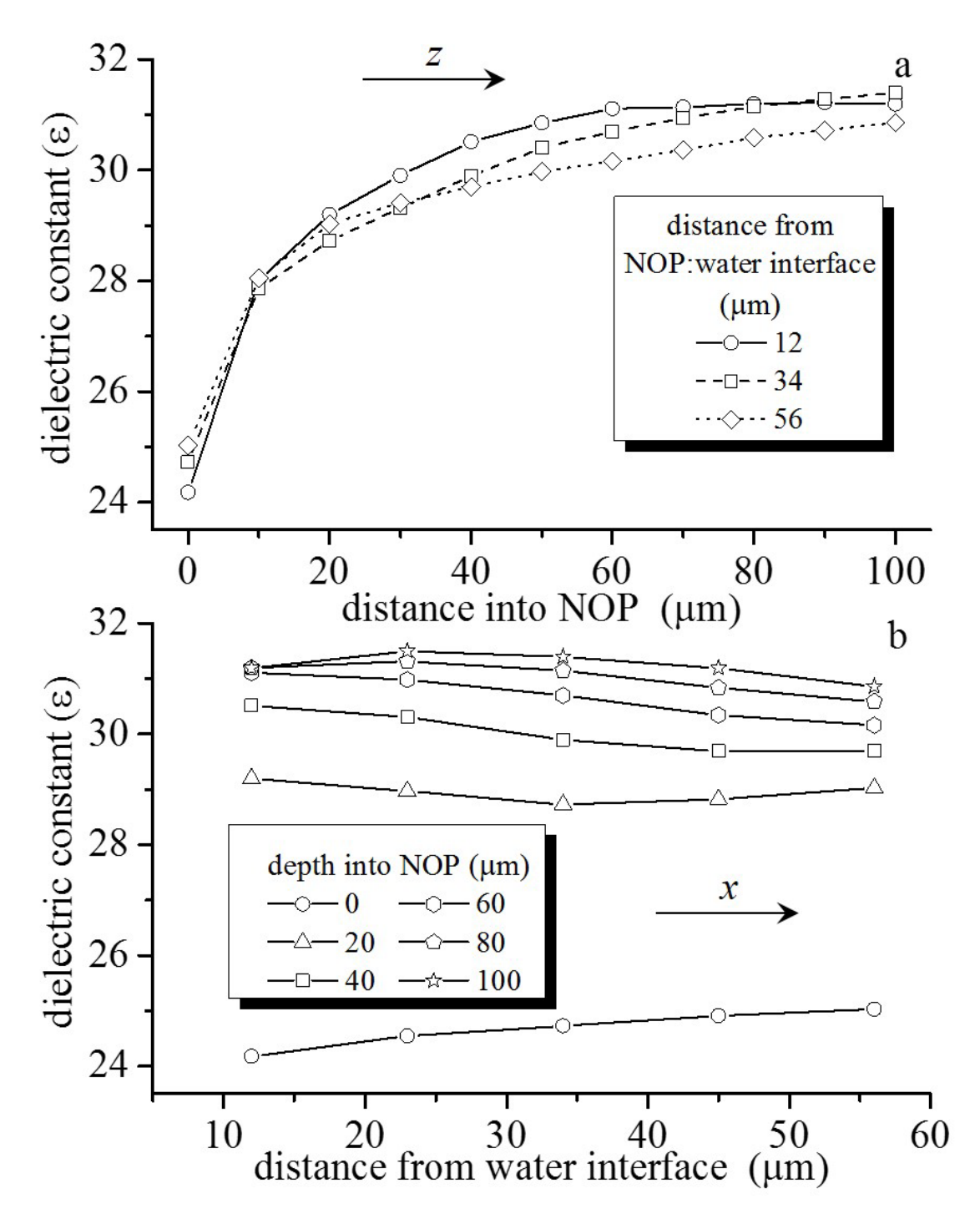


Figure 5.6 (a) Dielectric constant as a function of distance from the NOP|glass interface for three different distances from the water interface. (b) Dielectric constant as a function of distance from the NOP|water interface for six different distances from the NOP|glass interface. Refer to Fig. 5.1 for the experimental configuration and the x, y, z coordinate designation.

It is important to consider the form of the lifetime gradient data and, in particular, to compare it to the absence of a gradient in the two-phase (NOP|glass) system.²³ In that work we did not observe a dielectric constant gradient in the wet NOP liquid phase because there was a fixed concentration of water in the system, determined by exposure of the NOP to water initially and by the amount of adsorbed water at the glass surface. While there is variation in the diameter of the water nano-droplets resulting in a size gradient, for any given region of the sample, the total amount of water present remains nominally the same. For this reason, there is no expectation of a dielectric gradient in the NOP|glass system studied in chapter 4. For the three phase system, where (excess) water is in contact with both the NOP and glass phases, it is possible for there to be not only a size gradient, but also a water nano-droplet concentration gradient. Close to the NOP|water interface, the size of the water nano-droplets will be the same as those that are distant from the interface because the NOP|water surface energy is the same in both cases. The region of the intersection of the two interfaces is the meniscus of the NOP|water|glass system formed as the denser and hydrophilic water molecules make contact with the glass surface near the three phase boundary. While we do not have a ready means of evaluating the profile on this meniscus, the water forming the meniscus may contribute to the effects we observe. Near the NOP|glass interface, the water nano-droplet size is different than the droplet size for distances greater than 10 µm for the reasons discussed in association with the anisotropy data, but due to the presence of a meniscus in the NOP|water|glass system, the total amount of water accessible to this interface is not limited. Thus, there can be a relatively higher concentration of large water droplets near the NOP|glass interface, leading to a dielectric gradient along the z-axis that is more pronounced than the gradient for the NOP|water interface along the x-axis, and this is precisely the situation we observe experimentally (Figs. 5.5 and 5.6). Taken collectively, the lifetime and anisotropy decay time constant data indicate that there is infiltration of water into NOP resulting from the presence of the NOP|water interface.

The water concentration gradient exists normal to the NOP|water interface as is indicated from the fluorescence lifetime data, but there is not a gradient in the anisotropy decay data to support a size gradient. The nano-emulsion we observe normal to the NOP|water interface is comprised of a distribution of water nano-droplets that maintain a constant average size. This is an expected result based on surface energy considerations, where the NOP|water interface is characterized by a surface energy essentially the same as that of the water nano-droplets in bulk NOP. Normal to the NOP|glass interface and parallel to the NOP|water interface there is a gradient in the size of the water nano-droplets, manifested in the anisotropy decay gradient, which can also be understood in terms of interfacial surface energies.

5.4 Conclusions

We have investigated a system comprised of two interfaces, a NOP|water interface and a NOP|glass interface, nominally perpendicular to one another using the fluorescent probe molecule LRSC. Characterizing this two-interface system by means of spatial variations in the fluorescence lifetime and anisotropy decay constant has shown that the (wet) NOP phase exists as a nano-emulsion and that there are different compositional gradients, with one perpendicular to the NOP|glass interface and one perpendicular to the NOP|water interface. Normal to the NOP|water interface is a gradient in the concentration of water nano-droplets of constant average size, and normal to the NOP|glass interface there exists a gradient in the average size of the water nano-droplets. We understand the reason for different types of water nano-droplet gradients in the context of differences in the surface tension for the NOP|glass and NOP|water interfaces. A

clear implication of these findings is that nano-emulsion size gradients can be controlled through the identity of the solid support with which the nano-emulsion is in contact.

- 1. Interfacial Nanochemistry: Molecular Science and Engineering at Liquid-Liquid Interfaces; Watarai, H.; Teramae, N.; Sawada, T., Eds.; Kluwer Academic/Plenum Publishers: New York, 2005.
- 2. Perera, J. M.; Stevens, G. W. Analytical and Bioanalytical Chemistry 2009, 395, 1019.
- 3. Kovaleski, J. M.; Wirth, M. J. Journal of Physical Chemistry 1995, 99, 4091.
- 4. Burbage, J. D.; Wirth, M. J. Journal of Physical Chemistry 1992, 96, 5943.
- 5. Wirth, M. J.; Burbage, J. D. Journal of Physical Chemistry 1992, 96, 9022.
- 6. Watarai, H.; Funaki, F. Langmuir 1996, 12, 6717.
- 7. Ishizaka, S.; Kim, H. B.; Kitamura, N. Analytical Chemistry 2001, 73, 2421.
- 8. Walker, D. S.; Richmond, G. L. Journal of Physical Chemistry C 2008, 112, 201.
- 9. Walker, D. S.; Brown, M.; McFearin, C. L.; Richmond, G. L. *Journal of Physical Chemistry* B **2004**, *108*, 2111.
- 10. Steel, W. H.; Walker, R. A. Nature 2003, 424, 296.
- 11. Messmer, M. C.; Conboy, J. C.; Richmond, G. L. *Journal of the American Chemical Society* **1995**, *117*, 8039.
- 12. Fedoseeva, M.; Richert, S.; Vauthey, E. *Langmuir* **2012**, 28, 11291.
- 13. Nagatani, H.; Fermin, D. J.; Girault, H. H. Journal of Physical Chemistry B 2001, 105, 9463.
- 14. Dryfe, R. A. W.; Ding, Z. F.; Wellington, R. G.; Brevet, P. F.; Kuznetzov, A. M.; Girault, H. H. *Journal of Physical Chemistry A* **1997**, *101*, 2519.
- 15. Reymond, F.; Fermin, D.; Lee, H. J.; Girault, H. H. Electrochimica Acta 2000, 45, 2647.
- 16. Benjamin, I. Chemical Physics **1994**, 180, 287.
- 17. Benjamin, I. Chemical Reviews **1996**, 96, 1449.
- 18. MacDonald, S. M.; Watkins, J. D.; Gu, Y.; Yunus, K.; Fisher, A. C.; Shul, G.; Opallo, M.; Marken, F. *Electrochemistry Communications* **2007**, *9*, 2105.

- 19. MacDonald, S. M.; Watkins, J. D.; Bull, S. D.; Davies, I. R.; Gu, Y.; Yunus, K.; Fisher, A. C.; Page, P. C. B.; Chan, Y.; Elliott, C.; Marken, F. *Journal of Physical Organic Chemistry* **2009**, 22, 52.
- 20. Collins, A. M.; Zhang, X. H.; Scragg, J. J.; Blanchard, G. J.; Marken, F. *ChemPhysChem* **2010**, *11*, 2862.
- 21. Collins, A. M.; Blanchard, G. J.; Hawkett, J.; Collison, D.; Marken, F. Langmuir 2011, 27, 6471.
- 22. Collins, A. M.; Blanchard, G. J.; Marken, F. Electroanalysis 2012, 24, 246.
- 23. Hay, C. E.; Marken, F.; Blanchard, G. J. Langmuir 2014, 30, 9951.
- 24. Chuang, T. J.; Eisenthal, K. B. Journal of Chemical Physics 1972, 57, 5094.
- 25. Perrin, F. Journal of Physics and Radium 1934 5, 497.
- 26. Hu, C. M.; Zwanzig, R. Journal of Chemical Physics 1974, 60, 4354.
- 27. Pal, R. AIChE Journal 1996, 42, 3181.
- 28. Chanamai, R.; McClements, D. J. Colloids and Surfaces A: Physicochemical and Engineering Aspects **2000**, 172, 79.
- 29. Snare, M. J.; Treloar, F. E.; Ghiggino, K. P.; Thistlethwaite, P. J. *Journal of Photochemistry* **1982**, *18*, 335.

Chapter 6

Conclusions

6.1 Conclusions

Throughout this research we sought to gain a better fundamental understanding of the molecular structure and organization in liquid solutions and in proximity to liquid interfaces. We utilized time-correlated single photon counting (TCSPC) to measure the fluorescence lifetime and anisotropy decay of fluorescent probe molecules in the solvents, water and N-octyl-2-pyrrolidone (NOP), separately, with addition of electrolyte, and in combination with each other. Our results have enhanced our knowledge of the solvation properties of NOP and have implications in the utilization of NOP|water systems in interfacial transport processes.

In chapter 2, we reported on the rotational diffusion dynamics of two structurally distinct, polar chromophores in water and in NOP. Initial steady-state absorption and emission results showed that resorufin and 6-[N-(7-nitrobenz-2-oxa-1,3-diazol-4-yl)amino] hexanoic acid (NBDHA) exhibit different solute-solvent interactions in NOP. Resorufin underwent a change in dipole moment upon excitation, while no analogous change was observed for NBDHA indicating different solvation environments. The fluorescence anisotropy of each of these probe molecules provided more information on the local solvation environment. Both probe molecules were found to reorient as prolate rotors in water exhibiting one-component anisotropy decays and as oblate rotors in NOP exhibiting two-component anisotropy decays. This change in rotor shape indicates the rotational motion changes from out-of-plane rotation in water to in-plane rotation in NOP. The more restrictive in-plane rotation occurring in NOP was attributed to solvent-solvent interactions, as well as the size of the solvent relative to the solute. The similar behavior of the two structurally different chromophores in water and in NOP is evidence that the solvent-solvent

interactions in NOP mediate the rotational motion and play a more significant role than the solute-solvent interactions.

In chapter 3, we assessed the effect of electrolyte on the rotational diffusion dynamics of resorufin in water and in NOP. The addition of a quarternary ammonium electrolyte to NOP disrupted the solvent-solvent interactions discussed in the previous study. We arrived at this conclusion through the observation that resorufin exhibited a change in rotor shape from oblate in pure NOP to prolate in NOP containing tetrabutyl ammonium bromide (TBAB) or tetraoctyl ammonium bromide (TOAB). The reorientation times of the anionic chromophore were concentration dependent, which points to ion pair formation between the resorufin anion and the ammonium cations. Equilibrium constants for complex formation (2 ± 1 for TOAB and 11 ± 8 for TBAB) were consistent with a stronger complex forming between TBAB and resorufin compared to the TOAB-resorufin complex, which is expected due to steric hindrance issues associated complex formation with the tetraoctyl ammonium cation.

In aqueous electrolyte solutions of lithium perchlorate (LiClO₄), resorufin exhibited inplane rotation as was the case in pure water and concentration dependent reorientation times
were observed. The complex formation between the resorufin anion and a Li cation, which is
relatively small, does not make a significant impact on the rotational dynamics of resorufin.

These results showed the solute-electrolyte interactions have an influence on rotational motion
that can disrupt solvent-solvent interactions. The solute-solvent and solvent-solvent interactions
studied in water and in NOP set the stage for the next step of the research which was forming
NOP|water interfaces.

In chapter 4, we utilized a TCSPC fluorescence anisotropy and lifetime confocal imaging instrument to generate depth profiles as a function of distance from a NOP|glass interface. Using

lissamine rhodamine B sulfonyl chloride (LRSC) as a probe molecule in wet NOP, a fluorescence anisotropy decay gradient was revealed. This anisotropy decay gradient, which showed decreasing reorientation times with increasing distance from the glass surface, was determined to result from a compositional gradient due to the presence of water nano-droplets in the NOP phase. In this study, NOP was exposed to water prior to the analysis and some mutual solubility allowed for water to infiltrate the NOP phase. The decreasing trend in reorientation times as a function of distance from the NOP|glass interface corresponds to the changing molecular environment experienced by the LRSC as the size of the water inclusion decreases. Absorbance spectra of LRSC in water, NOP, and NOP exposed to water support our theory that LRSC resides in an aqueous environment, while dynamic light scattering data (DLS) confirmed the approximate particle size of the nano-droplets (ca. 1.26 nm diameter). Depth profiles collected as a function of distance from an ethylene glycol (EG)|glass interface showed no analogous anisotropy gradient. The absence of a gradient in EG, which is miscible with water in all proportions, is significant because it rules out other possible phenomena and supports the theory of a compositional gradient in NOP. These findings demonstrated that the properties of NOP allow for uptake of small amounts of water and the water contained in the nano-emulsion varies in size based on proximity to a liquid-solid interface. The results of this study allowed for the interpretation of findings in a phase separated system of NOP|water.

In chapter 5, we measure the rotational diffusion dynamics of LRSC in a two interface system composed of NOP and water on a glass support. Fluorescence anisotropy and lifetime were collected in the NOP phase as a function of distance from a NOP water interface and a NOP glass interface. The two interfaces situated normal to one another formed a three phase liquid liquid solid boundary and both exhibited fluorescence lifetime gradients as a function of

distance from the interfaces, while a fluorescence anisotropy gradient was only recorded normal to the NOP|glass interface. The anisotropy gradient confirms the result of the previous study, which reported the presence of a compositional gradient resulting from water nano-droplets of decreasing size in the NOP phase. The lifetime gradients indicate dielectric gradients emanating from each interface. A slight lifetime gradient exists normal to the NOP|glass, while the gradient normal to the NOP|water interface is more pronounced. The presence of a lifetime gradient normal to NOP|water, where no anisotropy gradient exists, is taken to be a sign that the water nano-droplets remain a constant average size, but are present in different concentrations with a greater concentration near the NOP|water interface. The constant average size extending from the NOP|water interface is an expected result because the surface tension between water and NOP should remain constant from the NOP|water interface to the water nano-droplets in the bulk NOP.

The results of this research have given us a more in depth understanding of the solvent systems, water and NOP, and their interactions in a liquid-liquid system. Rotational diffusion measurements have allowed us to establish the organization surrounding chromophores in neat liquids and in nano-emulsions. The discovery of water nano-droplets in NOP with size and concentration gradients has implications in containment and transport of polar molecules through nonpolar barriers.

6.2 Future Directions

This research has laid the groundwork for future studies on the unique properties of NOP|water interfaces and emulsions. The discovery of water nano-droplets present in the NOP phase is influential in the direction of future work on NOP containing systems. Our measurements were performed on borosilicate glass cleaned with oxidizing agents making the

surfaces hydrophilic. An interesting follow-up would be to change the character of the solid support by siliconization of glass, for example, to make the surface hydrophobic in order to assess the effect of surface character on droplet formation and size. In our studies, the hydrophilic glass support essentially acted as a reservoir for water to move into the NOP phase, so it is expected a hydrophobic surface would limit the availability of water in a wet NOP|glass system.

The polar rhodamine chromophore used in the studies of NOP|glass and NOP|water|glass systems in chapters 4 and 5 was solvated in an aqueous environment that was surrounded by NOP molecules. The presence of water in NOP necessitates that the amphiphilic NOP molecules likely surround the water by forming inverse micelle-like structures. Incorporation of a nonpolar chromophore in the acyl chains of the NOP secondary structures would provide another perspective on the local environment in a binary system. Alternately, a study could be done on the oil-in-water structures that may be present in the water phase of the NOP|water|glass system. The solubility of NOP in water is documented (0.12% (v/v) (20 °C))¹ and, therefore, the water phase of the three phase system is likely to contain NOP. The secondary structures formed by the amphiphilic NOP molecules is not known. Although no data were collected, observations were made of fluorescent droplets in the water phase of the three phase system. We know from our measurements in the wet NOP presented in chapter 4 that the polar rhodamine molecules partition into an aqueous environment leading to the possibility of multilayer micellar structures of NOP in the water phase of the NOP|water|glass system. Obtaining rotational diffusion data on a polar chromophore within one of these droplets would provide information on the local environment of the secondary structure.

At the end of chapter 4, we alluded to a phenomenon in which particles near solid surfaces exhibit slower diffusion due to hindered Brownian motion. Delving deeper into this phenomenon in the wet NOP|glass system would provide more information about the formation and movement of the water nano-droplets near the solid support. Confocal laser scanning microscopy has been used for imaging optical slices of microtubes containing water previously.² Park et al. exploited the lateral and depth resolution of confocal microscopy to scan at different depths and create a 3D map of particle velocities. In our confocal imaging system, we have a high magnification oil immersion objective (100X, NA 1.45) capable of adequate depth resolution for imaging different focal planes of a colloidal suspension.

Beyond altering the current system to gain new information, there are additional avenues to take this research which include studying transfer processes. Marken et al. showed coupled ion and electron transfer occurs at the three phase boundaries using electrochemical techniques.³⁻⁵ Our confocal imaging setup could enhance what is known about the local environment during these processes by coupling spectroscopic and electrochemical techniques. In chapter 5, we showed fluorescence lifetime and anisotropy gradients in a three phase NOP|water|glass system. The replacement of glass with a conductive and optically transparent solid support, such as fluorine tin oxide (FTO) and incorporation of a redox couple would be the first steps for making simultaneous electrochemical and spectroscopic measurements.

This work as a whole has characterized the local organization of NOP from strong solvent-solvent interactions in neat solution to accommodation of water droplets and formation of two phases with water. Our studies on the properties of NOP will be a resource for future work on NOP and its inclusion in new industrial formulations. Additionally, it is our hope that the research presented here on depth profiles using the fluorescence lifetime and anisotropy

confocal imaging instrument will be applied to gain fundamental understanding of new interfacial systems.

- 1. Login, R. B. Journal of the American Oil Chemists Society 1995, 72, 759.
- 2. Park, J. S.; Choi, C. K.; Kihm, K. D. Experiments in Fluids 2004, 37, 105.
- 3. Marken, F.; Webster, R. D.; Bull, S. D.; Davies, S. G. *Journal of Electroanalytical Chemistry* **1997**, *437*, 209.
- 4. Wadhawan, J. D.; Compton, R. G.; Marken, F.; Bull, S. D.; Davies, S. G. *Journal of Solid State Electrochemistry* **2001**, *5*, 301.
- 5. MacDonald, S. M.; Watkins, J. D.; Gu, Y.; Yunus, K.; Fisher, A. C.; Shul, G.; Opallo, M.; Marken, F. *Electrochemistry Communications* **2007**, *9*, 2105.